THE IMPACT OF DEVELOPMENTAL AGE AND LOADING RATE ON THE PATTERNS OF BONE FRACTURE UNDER TORSION AND BENDING USING EITHER IMMATURE PORCINE OR OVINE FEMURS

By

Patrick E. Vaughan

A THESIS

Submitted to
Michigan State University
in partial fulfillment of the requirements
for the degree of

Engineering Mechanics – Master of Science

2017

ABSTRACT

THE IMPACT OF DEVELOPMENTAL AGE AND LOADING RATE ON THE PATTERNS OF BONE FRACTURE UNDER TORSION AND BENDING USING EITHER IMMATURE PORCINE OR OVINE FEMURS

By

Patrick E. Vaughan

The determination of whether pediatric long bone fracture is based on accidental trauma or an abusive act is a major question in forensics. A recent clinical study has suggested that the mechanisms of long bone fracture can be determined based on the fracture pattern. While human pediatric bone is difficult to obtain, immature animal models, like porcine and ovine models, can act as adequate surrogates for scientific studies. The first research topic explored in this thesis is the influence of specimen age and loading rate on whole-bone fracture patterns. Under femoral torsion, the spiral fracture pattern (fracture ratio) was shown to increase with porcine age and rate of twist, bringing into question results of the clinical study. The second research topic explored direction-specific tensile and shear test data versus specimen age and loading rate in the immature porcine model. Results showed that both porcine age and loading rate can affect transverse and longitudinal shear stress components, altering the torsional fracture pattern. In another study the immature ovine femur was used in concentrated four-point bending tests, and was shown to produce transverse fractures, while mature specimens produced compressive wedge fractures. Preliminary evidence suggested that at higher test rates, a tensile wedge pattern is produced for mature specimens. As impact direction is currently cited by tensile wedges, consistent generation of compression wedges muddle this practice. The compilation of this work demonstrates that loading rate and developmental age affect fracture patterns in immature femora, highlighting that caution needs to be taken when analyzing pediatric long-bone fractures.

ACKNOWLEDGEMENTS

I would like to first and foremost like to thank Dr. Roger C. Haut for taking the chance on me four years ago and for providing me with the opportunity to study under his mentorship. I appreciate how he has always pushed me to strive for more, how he has taught me what the “re” in research means, and how he has taught me to always keep sight of the ‘story’. I would like to thank Dr. Feng Wei for aiding me in my time here and for always providing an ear to listen to me. I would also like to sincerely thank Clifford Beckett for drilling the principles of hard work into me and for teaching me some of the technical skills required by an engineer. I would like to thank Dr. Todd Fenton for providing me with the opportunity to expand my studies in cranial trauma and for the inter-disciplinary collaborations he provided with his team of forensic anthropologists. Thank you to Kevin Turner and Chris Rosenbom in the Porcine Research Laboratories at MSU and to Dr. Tammy Haut Donahue from Colorado State University for providing me with specimens to test in this research. Finally, I would like to thank my twin brother, Ryan F. Vaughan, for being my inspiration in this pursuit as well as my parents for supporting me on this eventful journey. I would also like to thank all of the friends that have supported me on this journey: Alli Harju, Alex Goots, Mari Isa, Elena Watson, Paul Snyder, Caitlin Vogelsberg, and Jen Vollner.

TABLE OF CONTENTS

LIST OF TABLES

LIST OF FIGURES

CHAPTER ONE: INTRODUCTION AND BACKGROUND

FEMORAL BONE COMPOSITION

Bone is an optimized geometrical structure that possesses an ideal combination of properties, namely high stiffness, strength, fracture toughness, and low weight (Tadano et al., 2011). At the whole bone level, the femur is composed of a tough cortical outside and a pliable trabecular inside. The cortical bone sheathing is composed of osteons, which are generally oriented along the long-axis of the bone. The osteons themselves are composed of collagen fibers with a boundary of collagen fibers acting as a tough "cement line". Between osteons exist a lamellar interface consisting of collagen molecules and a mineralized layer of collagen fibrils that acts as a "glue" and a sacrificial "stretch" layer (Figure 1.1).

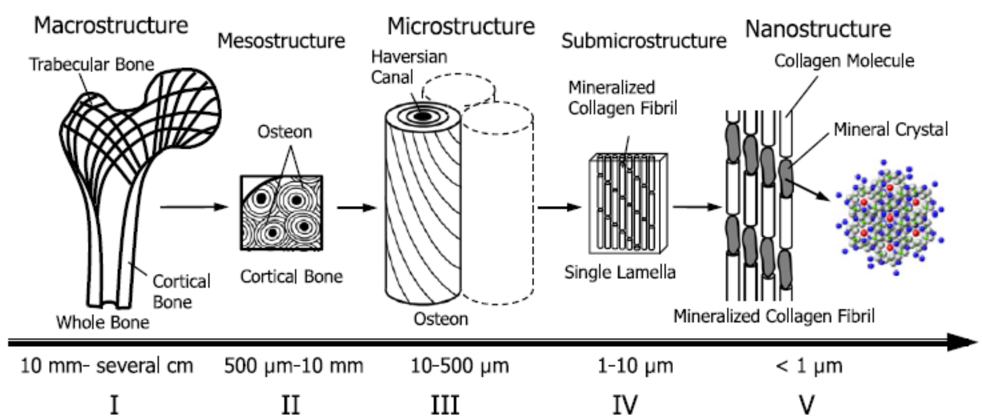

Figure 1.1 *Depiction of bone composition from the macroscale to the microscale, adapted from Tadano et al., 2011.*

The beauty of this molecular make-up is that upon tension loosely packed interlamellar collagen fibrils stretch apart breaking at predetermined sacrificial locations and releasing more hidden length. This mechanism becomes advantageous by dissipating a significant amount of energy allowing for small deformations between lamellae. This pre-determined failure method allows osteons to withstand various modes of micro-deformation without the need to dissipate strain energy by means of cracking, but instead, allows bone to dissipate energy via a reversible mechanism (Katsamenis et al., 2013).

FORENSIC RELEVANCE OF THE FEMUR

The femur is the largest bone in the human body, and it is also the strongest bone. Femoral fracture therefore requires a large amount of mechanical energy. Despite this, femur fractures are common childhood injuries. Between 10 and 20 people out of 100,000 sustain femoral shaft fractures annually (Rewers et al., 2005). The most common causes of fracture are high speed trauma, motor-vehicle accidents, a fall from a high place, injury during an extreme or a contact sport, and cases of child abuse (Hunter, 2005). Femoral shaft fractures are the most common pediatric fracture site, accounting for 62% of all femur fractures (Rewers et al., 2005). These fractures can be spiral, oblique, transverse, comminuted, or wedge-types (Shrader et al., 2011). Femoral shaft fractures in children, however, are typically spiral and occur in 52% of cases (Shrader et al., 2011).

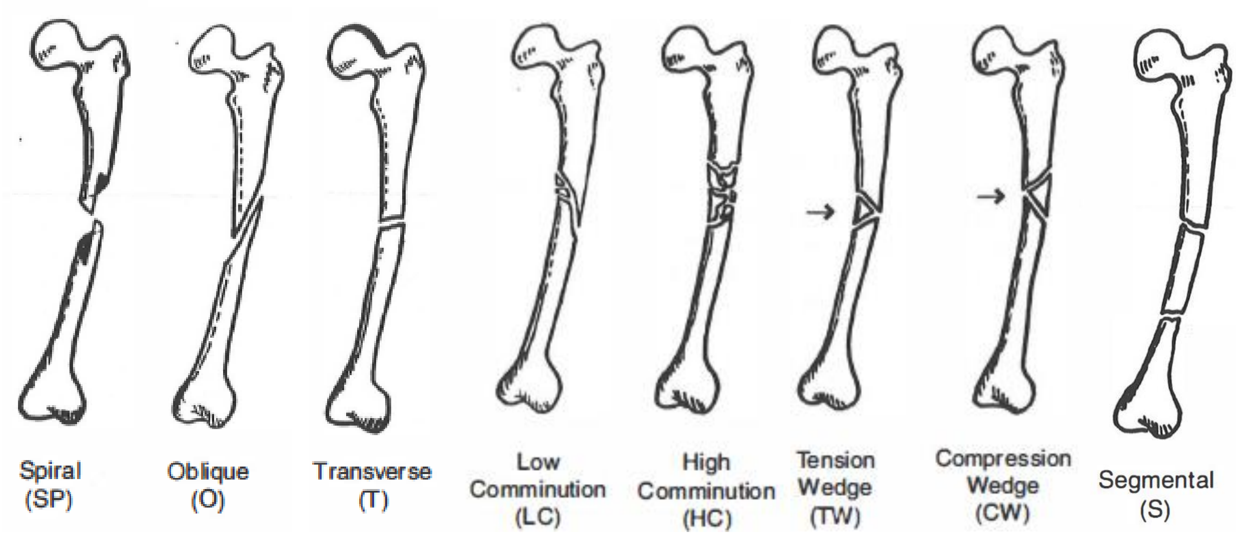

Figure 1.2 *Common fracture patterns and their forensic description, adapted from Kress et al., 1996.*

As shown in Figure 1.2, spiral fractures consist of a helical pattern around the shaft of the bone. Oblique patterns are defined as an angled break across the bone. Transverse fractures are described as perpendicular to the long-axis of the bone. Comminuted fractures are identified through multiple breakages. Wedge patterns, on the other hand, resemble a Y-shape either in line with or opposed to the direction of loading. Segmental patterns result in the bone being split into three fragments.

PEDIATRIC DEVELOPMENT AND FEMUR FRACTURE

Specific fracture patterns are a result of the orientation and type of loading applied to the bone. For example, it is known that torsional loading generates spiral fractures (Kress et al., 1996). However, as bone is an anisotropic composite structure fracture propagation can also be influenced by the material structure of the bone itself (Taylor et al., 2003). Therefore, when considering fracture patterns in children it is imperative to consider how whole-bone geometry, microstructural progression and mechanically relevant material properties change with age. Gosman et al., 2013 has documented that in human children from neonatal to 18 years of age young bone has greater circularity, while more mature bone becomes increasingly asymmetric (Figure 1.3). Mechanically, this is relevant because circular cross-sectional areas tend to have more uniform stress distributions under loading, while asymmetric cross-sections will have non-uniform stress distributions under loading. Additionally, Torzillia et al., 1982 have shown that material properties of bone, such as the ultimate tensile strength and modulus positively correlate with age. While the literature highlights such developmental changes with age, however, there is limited data on how fracture patterns themselves may be affected by these changes.

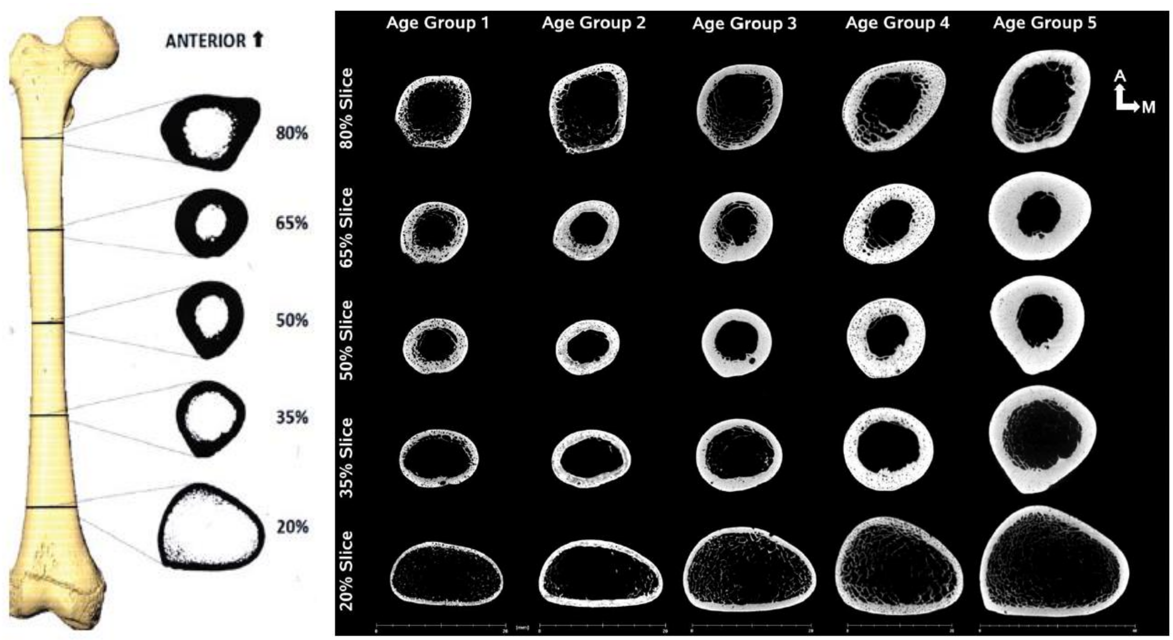

Figure 1.3 *(left figure) slice location to whole bone representative. (right figure) Young age group (left) to old age group (right) femoral cross-sections at various bone locations {A – Anterior, M – Medial directions}, adapted from Gosman et al., 2013.*

TORSION AND PEDIATRIC FRACTURE

In the current forensic literature differentiation between an abusive and accidental trauma (AT) in children under three years of age remains challenging. It is assumed that any trauma incurred by children under three years of age is frequently non-accidental trauma (NAT/abuse), and that any trauma in children less than one year is always NAT (Carty, 1993). Furthermore, spiral long-bone fractures in young children are challenging cases because there are limited 'ground truth' studies to help forensic investigators determine whether these fractures are from an abusive act or accidental trauma, as both situations can produce spiral fractures under torsional loads. A recent clinical-based study, however, has proposed to document fracture ratio, defined as the fracture length in a lateral radiograph over the diameter of the bone, to help distinguish NAT from AT. The study associates small fracture ratios (≈1.6) with NAT and large ratios (≈2.8) with AT (Murphy et al., 2015). Another study, using an immature canine model, indicates that fracture ratio is increased for a high versus low rate of bone twist (Theobald et al., 2012). The authors of this study likely assume AT occurs at a high rate of twist while NAT occurs at a low rate. While the study of Murphy et al., 2015 did document a slightly younger age for the NAT population than the AT population, the age effect was not statistically significant. Thus, it remains somewhat unclear if age is a covariate of facture ratio generated under torsional loads.

TORSIONAL FAILURE

Torsion is typically defined using an isotropic cylindrical shaft, keeping one end fixed and applying a torque to the free end. If observing a singular point on the free end of the beam ab (Figure 1.4a), this point would rotate at some angle theta ab'. This rotation generates shear stress that will vary linearly from the origin, as demonstrated by the triangular stress distribution in the cross-section of Figure 1.4a (Gere and Goodno, 2008). Therefore, if some arbitrary plane (*abcd*) was selected, analyzed in the cross-sectional plane (Figure 1.4b), and then represented as a 2D stress element; taking the radial direction (r) as the direction of displacement (Figure 1.4c), it can easily be seen that both transverse and longitudinal shear stresses are generated.

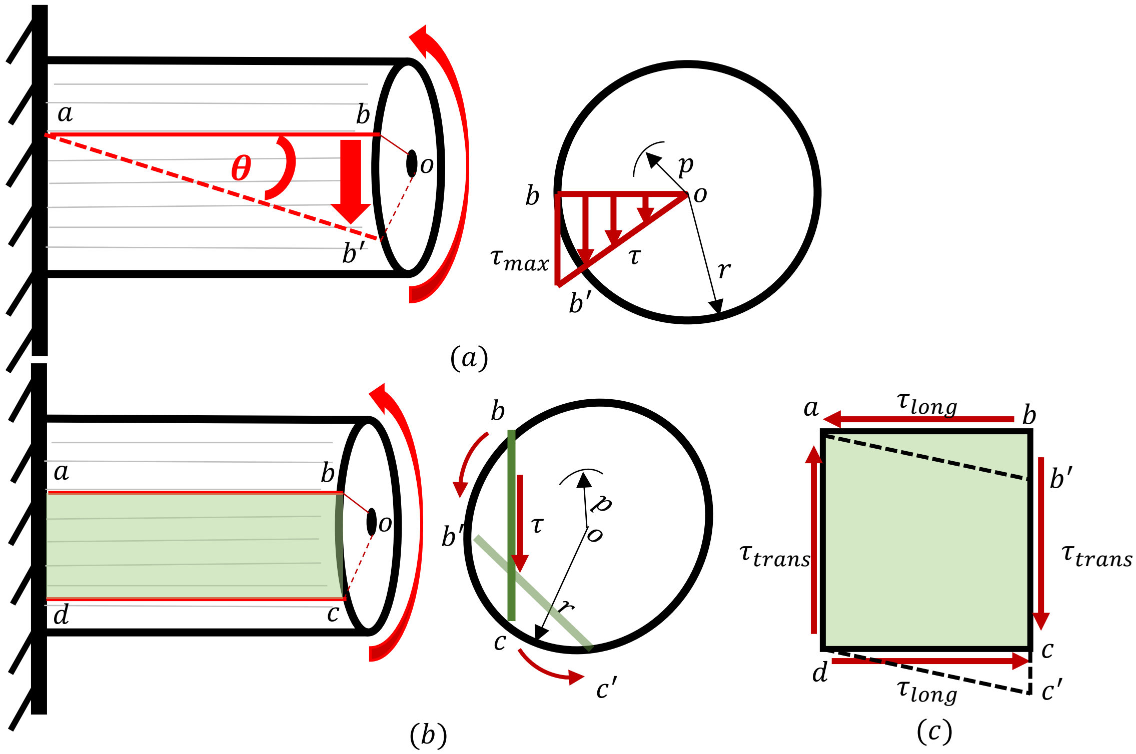

Figure 1.4 *Torsion and its deconstruction into longitudinal and transverse shear components.*

Furthermore, if the same stress element were to be rotated forty-five degrees to align with the direction of maximum principal stress, and were to experience the same shear-type deformation, then there were would be an extension (tensile stress) in one direction, and a contraction (compressive stress) in the other direction (Özkaya et al., 2017) (Figure 1.5).

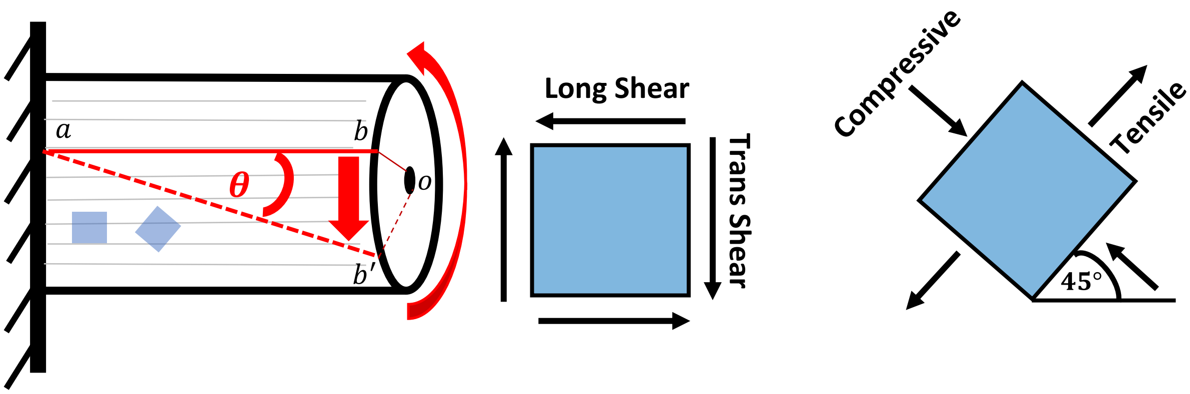

Figure 1.5 *Shear stress element (left), description of maximum shear direction (central), and generalized stress transformation into maximum shear plane (right).*

BENDING FAILURE AND FEMUR FRACTURE

Case studies and the medical literature associate long bone failure by bending with butterfly fractures. It is expected these occur in a tension wedge configuration, with fracture initiating as a transverse crack at the tensile surface of the bent bone and branching toward the compressed or impact surface (Kress, 1996, Fenton, 2012, Isa, 2015), supposedly due to shear failure on the compressive side of the bone (Figure 1.6).

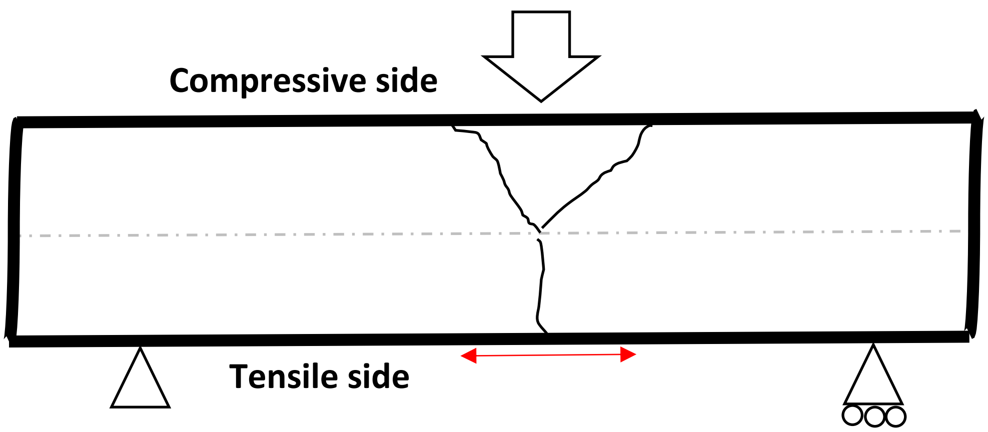

Figure 1.6 *Typical tensile wedge pattern under three-point bending.*

A wedge configuration is forensically significant because analysts often cite the presence and orientation of butterfly fractures as diagnostic of impact direction (Kress, 1996, Fenton, 2012, Isa, 2015). Experimental research indicates this practice is problematic as Martens et al., 1986 and Reber and Simmons, 2015 have demonstrated that under specific loading configurations, butterfly fractures may occur in a reversed pattern on the compressive side of the bone, such that the transverse crack is on the impact surface as opposed to the tensile surface (Figure 1.7). Most recently, Reber and Simmons, 2015 produced a study reporting 40% of complete wedge patterns as reverse tensile wedges, and Martens et al., 1986 demonstrated near-exclusive reverse tensile wedge failure when loading the bone at a slow rate, under a specific, concentrated four-point bending scenario.

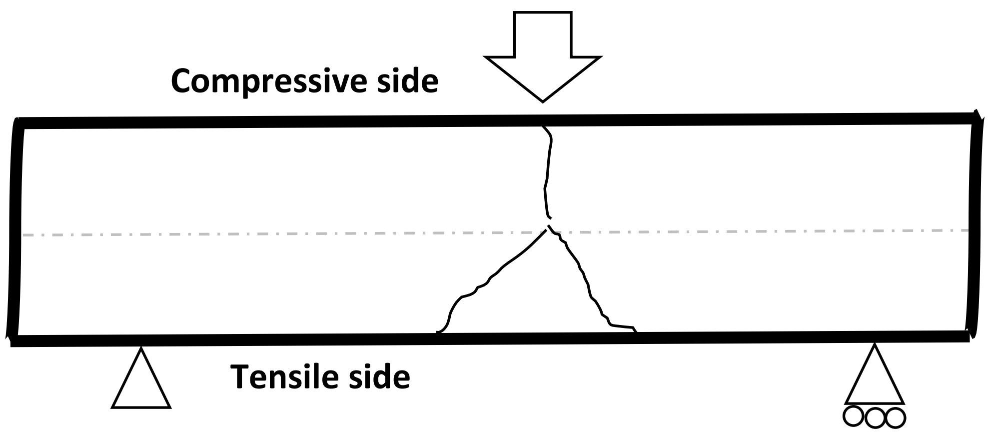

Figure 1.7 *Simplified reverse tensile wedge 'compression wedge' pattern, showing the direction of loading and the compressive and tensile sides of the bone. Note: the pattern is most consistently generated under four-point bending. However, large impact surfaces such as a flat plate (Reber and Simmons, 2015) or a large curved impactor (Kress et al., 1996) have also been shown to generate this fracture type.*

Thus, it is forensically relevant to prove the replicability of the work of Martens et al., 1986 to investigate if the authors configuration can exclusively produce ‘compression wedge’ failures; a mode of failure Kress et al., 1996 has deemed unlikely to be produced consistently. Additionally, as no research has yet been performed to test immature bone under Martens-type loading conditions, it is also forensically relevant to investigate if there is an age-effect associated with this reverse wedge, or ‘compressive wedge’ pattern.

SUMMARY AND OBJECTIVES

Pediatric studies are difficult to perform due to the costs involved and the relative scarcity of bones specimens. For such reasons, most trauma-based studies have been performed on mature bone, leaving pediatric trauma analysis to be, in large part, speculated from studies on mature bone specimens. Since human bone is difficult to obtain immature animal models, like the porcine or ovine models, act can act as surrogates to investigate questions on developing bone. While animal test data is not directly applicable to the pediatric subject, researchers can supplement knowledge acquired from such laboratory-controlled experiments to form and standardize practices and develop a scientific basis for fracture mechanics.

Since the mechanical properties of bone may depend on age (Torzilli et al., 1982) and rate of loading (Theobald et al., 2012) and since spiral fractures occur by the combination of tensile and shear failure of the bone (Turner et al., 2001), altered tensile and shear properties with specimen age and rate of loading may then in turn influence the location and direction of crack propagation within the bone during torsion (Norman et al., 1996). The first hypothesis of the study was that when using the immature porcine model, the previously introduced fracture ratio would increase with specimen age, as osteon strength has been noted to increase with age, allowing the fracture to fail more along the line of maximum principal stress, as opposed to through osteons, which would result in a larger fracture ratio. The second hypothesis of the study was that the fracture ratio would systematically increase with an increased rate of twist in the immature porcine bone model, based on the previous work of Theobald et al., 2012.

As suggested above, the underlying failure mechanisms and resulting fracture patterns of whole bone under torsion is not yet fully understood. As spiral fracture is considered a combination of both transverse and longitudinal shear failure (Vashishth et al., 2005), it is theorized that a pre-disposed weakness to a given shear-type will be evident in the spiral fracture pattern of the bone. In example, if bone is weaker in transverse shear than in longitudinal shear, then this type of shear failure will become a viable alternative fracture path to the preferred mode of failure under tension, and vice versa. Another hypothesis of the current study was that when using the immature porcine model and testing the intrinsic material property values, the transverse and longitudinal shear strengths would fluctuate with specimen age. If at younger ages the bone was weaker in transverse shear than in longitudinal shear, then shearing across osteons would become a viable failure path, resulting in lower fracture ratios and vice versa. Another hypothesis of the current study on the intrinsic properties of bone was that when conducting tests using the immature porcine model an increased loading rate would result in stronger property values at lower ages, which would in turn impact the fracture ratio, as depicted by the work of Theobald et al., 2012.

Finally, as suggested above, the current forensic practice of denoting impact direction based on the transverse fracture of a butterfly wedge-type pattern may be problematic. The studies of Reber and Simmons, 2015 and Martens et al., 1986 have demonstrated that there is a significant prevalence of reverse tensile wedge ‘compressive wedge’ fractures produced under experimental settings, providing evidence that these types of fracture patterns are not as unlikely as Kress et al., 1996 infer them to be. Therefore, in another set of experiments a hypothesis was that when using the mature ovine model, the work of Martens et al., 1986 would be replicable, and that near-exclusive ‘compressive wedge’ patterns would be produced. Furthermore, when using the immature ovine specimen under the Martens-type experimental set-up, the fracture pattern produced would not be a ‘compression wedge’ and will instead be a transverse failure. The transverse pattern would be more likely produced in the immature bone as the bone has not yet strengthened in the medial-posterior directions from increased geometric asymmetry which takes place with maturation, and because the osteon strength of the bone in the immature specimen may not yet be strong enough to inhibit crack growth through osteons.

REFERENCES

REFERENCES

Carty HM. Fractures caused by child abuse. *J Bone Joint Surg Br*. 1993; 75(6):849-57.

Fenton TW, Kendell AE, DeLand TS, Haut RC. Determination of impact direction based on fracture patterns in human long bones. Proceedings of the American Academy of Forensic Sciences; Atlanta, GA. *American Academy of Forensic Sciences*, 2012; H72.

Gere, James M., and Goodno, Barry J. *Mechanics of Materials*. Cernage Learning, 2008.

Gosman JH, Hubbell ZR, Shaw CN, and Ryan TM. Development of cortical bone geometry in the human femoral and tibial diaphysis. *Anat Rec*. 2013; 296: 774-787.

Hunter JB. Femoral shaft fractures in children. *Injury, Int. J. Care Injured*. 2005; 36: S-A86-S-A93.

Isa MI, Fenton TW, DeLand TS, Haut RC. Fracture Characteristics of Fresh Human Femora Under Controlled Three-Point Bending. Proceedings of the 67th Annual Meeting of the American Academy of Forensic Sciences; Orlando, FL. *American Academy of Forensic Sciences*, 2015; A96.

Katsamenis OL, Chong HMH, Andriotis OG, and Thurner PJ. Load-bearing in cortical bone microstructure: Selective stiffening and heterogeneous strain distribution at the lamellar level. *J Mech Behav Biomed Mater*. 2013; 17:152-165.

Kress TA. Impact biomechanics of the human body [dissertation]. Knoxville (TN): Univ. of Tennessee, 1996.

Martens M, Van Audekercke R, DeMeester P, Mulier JC. Mechanical behavior of femoral bones in bending loading. *J Biomechanics*. 1986:19(6):443-54.

Murphy R, Kelly DM, Moisan A, Thompson NB, Warner WC Jr, Beaty JH, Sawyer JR. Transverse fractures of the femoral shaft are a better predictor of nonaccidental trauma in young children than spiral fractures are. *J Bone Joint Surg Am*. 2015; 97(2):106-11.

Norman TL, Nivargikar SV, and Burr DB. Resistance to crack growth in human cortical bone is greater in shear than in tension, *J Biomech*. 29(8) (1996) 1023-31.

Özkaya, Nihat, Dawn Leger, David Goldsheyder, and Margareta Nordin. *Fundamentals of Biomechanics: Equilibrium, Motion, and Deformation*. 2017.

Reber SL, and Simmons T. Interpreting injury mechanisms of blunt force trauma from butterfly fracture formation. *J Forensic Sci*. 2015; 60(6):1401-1411.

Rewers A, Hedegaard H, Lezotte D, Meng K, Battan K, Emery K, and Hammen RF. Childhood femur fractures, associated injuries, and sociodemographic risk factors: a population-based study. *Pediatrics*. 2005; 115(5): e543-e552.

Shrader WM, Bernat NM, and Segal LS. Suspected non-accidental trauma and femoral shaft fractures in children. *Orthopedics*. 2011; 34(5): E70-E74.

Tadano S, and Giri B. X-ray diffraction as a promising tool to characterize bone nanocomposites. *Sci. Technol. Adv. Mater*. 2011; 12(064708): 1-11.

Taylor D, O'Reilly P, Vallet L, and Lee TC. The fatigue strength of compact bone in torsion. *J Biomech*. 2003; 36: 1103-1109.

Theobald PS, Qureshi A, Jones MD. Biomechanical investigation into the torsional failure of immature long bone. *J Clin Orthop Trauma*. 2012; 3(1):24–7.

Torzilli PA, Takebe K, Burstein AH, Zika JM, and Heiple KG. The material properties of immature bone. *J Biomech Eng*. 1982; 104(1) (1982) 12-20.

Vashishth WT. "Damage mechanisms and failure modes of cortical bone under components of physiological loading". *J. Orthop. Res*. 2005; 23:1047-1053.

CHAPTER TWO: SPECIMEN AGE AND TORSIONAL RATE OF TWIST INFLUENCE HELICAL FRACTURE PATTERNS OF THE IMMATURE PORCINE FEMUR

ABSTRACT

In the current forensic literature differentiation between abusive (NAT) and accidental trauma (AT) in children under three years of age remains challenging. Currently, it is assumed that any trauma incurred by children under three years of age is frequently non-accidental trauma (NAT), and that any trauma in children less than one year is always NAT. Furthermore, spiral long-bone fractures in young children are challenging cases because there are limited 'ground truth' data to help forensic investigators determine abuse from accidental trauma of torsional long-bone fracture. A recent case study separates pediatric abusive trauma from accidental trauma based on fracture pattern in which the length of torsional fracture divided by bone diameter, namely fracture ratio, was found to be low in cases of abuse (≈1.6) and higher in cases of documented accidental injury (≈2.8). In the case study, there was a reported difference in the mean ages between accidental and abuse populations, where NAT possessed slightly younger victims. This age effect while noted, was not statistically significant in the case study. In the current study, the immature porcine femoral model has been used to study the effects of age and rate of twist on a redefined fracture ratio. Results of the study showed that both specimen age and rate of twist were significant factors influencing fracture ratio in the immature porcine long bone specimen. At younger ages the fracture ratio was low, and it was seen to statistically increase with specimen age in both the low rate and high rate tests. Correspondingly, at lower rates the fracture pattern transitioned from a high-angle fracture in the young group to a combination of both low-angle and longitudinal failure segments in the older group, when measured with respect to the longitudinal axis. At higher rates the fracture pattern rapidly transitioned from low-angle failure

to very low angle tensile failure with longitudinal elements, and specimen comminution occurred as specimen age increased. Notably, the fracture ratio was consistently higher for all ages when tested at high rates of twist.

INTRODUCTION

Femur fractures are the second most common long bone injury in child abuse cases, after the humerus (Baldwin et al., 2011), with spiral fractures being the most frequently occurring fracture pattern in children younger than 15 months of age (Kemp et al., 2008, Worlock et al., 1986). Spiral fractures, which suggest a twisting action, currently incite forensic practitioners to suspect non-accidental trauma in children younger than 3 years of age (Carty et al., 1993). This is especially true for children who are not yet walking, as spiral fractures may well occur more often accidentally in the femur once the child begins to walk (Baldwin et al., 2011, Flaherty et al., 2014). For example, a child could trip down a flight of stairs resulting in a twist of the leg, or the child could fall into a split-legged position while running (Baldwin et al., 2011). Often it is the job of the forensic practitioner to comment if the injury is accidental or due to an abusive act by gathering testimony, studying familial history, assessing the time to report the injury, and utilizing relevant biomechanical data in case evaluations. These types of injury parameters, as described by Pierce et al., 2005, can be utilized to objectively comment on the probability that an injury was the result of an abusive action on a case by case basis.

Forensic anthropologists and biomechanists currently have no way of discerning between accidental injury and an injury resulting from an abusive act, as both produce spiral fractures under torsional loading. This is problematic for medicolegal investigators. Potentially, a recent case study suggests a method to separate abusive from accidental trauma based on the long bone fracture pattern (Murphy et al., 2015). The quantitative tool, developed in the study, is called the fracture ratio and it is defined as the length of torsional fracture in a radiological view of the bone divided by bone diameter. The study shows that patterns of bone fracture generally have a low fracture ratio for cases found to be due to abusive acts, as opposed to a high fracture ratio in cases of documented accidental injury (Murphy et al., 2015). A potential limitation of the study may be that there was a slight but statistically insignificant age effect biasing the results, as the abuse population of victims was slightly younger. Secondly, the material properties of bone, such as the ultimate tensile strength and modulus, have been shown to positively correlate with age (Torzilli et al., 1982). This may then influence the pattern of torsional fracture, as a spiral fracture occurs from the combination of tensile and shear failure of the bone (Turner et al., 2001). A long bone under torsional loading experiences maximum shear stresses on planes perpendicular and parallel to its longitudinal axis, while maximum tensile stresses are generated 45 degrees to the long-axis of the bone. This in turn influences the location and direction of crack propagation within the bone that produces a spiral fracture under torsional loads (Norman et al., 1996). Another potential limitation of the Murphy et al., 2015 study was that there was not a stratification of the speed of each traumatic event, especially those separating the abuse from accidental groups. A study by Theobald et al., 2012, using 7-day old calf femurs, has shown that an increase in the rate of twist generates a corresponding increase in fracture ratio (decrease in fracture angle).

Due to the lack of infant and child cadavers for controlled biomechanical experiments, investigators have largely had to use surrogate animal models. Pearce et al., 2007, for example, has shown similarities in bone mineral density of porcine bone to that of human bone. Similarities have also been documented in the femoral cross-sectional area between humans and pigs (Pearce et al., 2007). Our laboratory has also used the immature porcine model in studies of cranial fracture (Baumer et al., 2009, Deland et al., 2016, Vaughan et al., 2016). This is because Baumer et al., 2010 has shown a direct correlation in bending rigidity of the infant human parietal bone in months to that of the infant porcine bone in days of age. Cheong et al., 2017 recently has also recently suggested that one week in development of the porcine femur is approximately equivalent to 1 year of development of the human femur.

In the current study immature porcine femurs were used to study the effects of age and rate of twist on bone fracture ratio. A hypothesis of the study was that the fracture ratio would increase with age, since the tensile strength of bone has been shown to increase with age in humans (Vinz et al., 1975). Second, it was also hypothesized that fracture ratio would increase with rate of twist in the immature porcine bone model, based on the previous work of Theobald et al., 2012

METHODS

Fifteen pairs of porcine femur specimens aged 1-26 days old were collected from a local farm and frozen within 12 hours of death at -20°C. Prior to testing the specimens were thawed at ambient temperature for 24 hours. After the tissues thawed, the femurs were dissected, cleaned of soft tissue and immediately wrapped in a gauze-soaked phosphate buffered solution (PBS) to prevent the bones from drying and changing their material properties (Kim et al., 2004). Each specimen was inserted into a custom-built, laser alignment fixture (Figure 2.1).

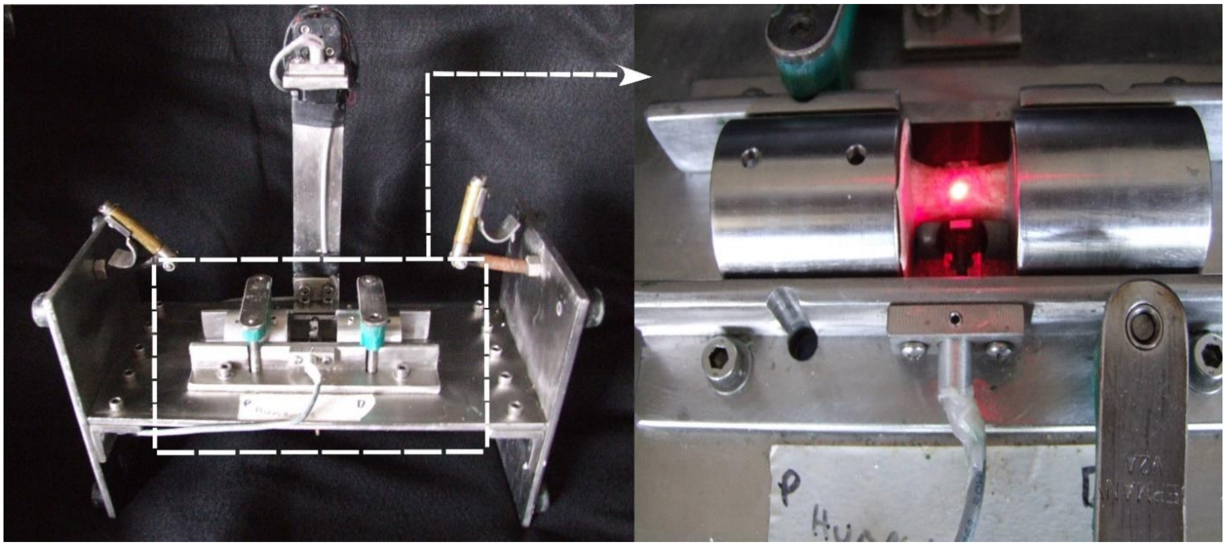

Figure 2.1 *Photograph of the custom-built laser alignment fixture and the process of centering the bone.*

A liquid resin hardener purchased from technovit (J-61Lb, J-61pb, Jorgensen Laboratories Inc., Loveland, CO) was used to pot the bones in cylindrical cups to provide a gripping surface during these torsion experiments (Figure 2.2). After potting, the specimens were maintained in a refrigerator at 0°C while wrapped with saline-moistened gauze until testing. All tests were performed within 24 hours of thawing.

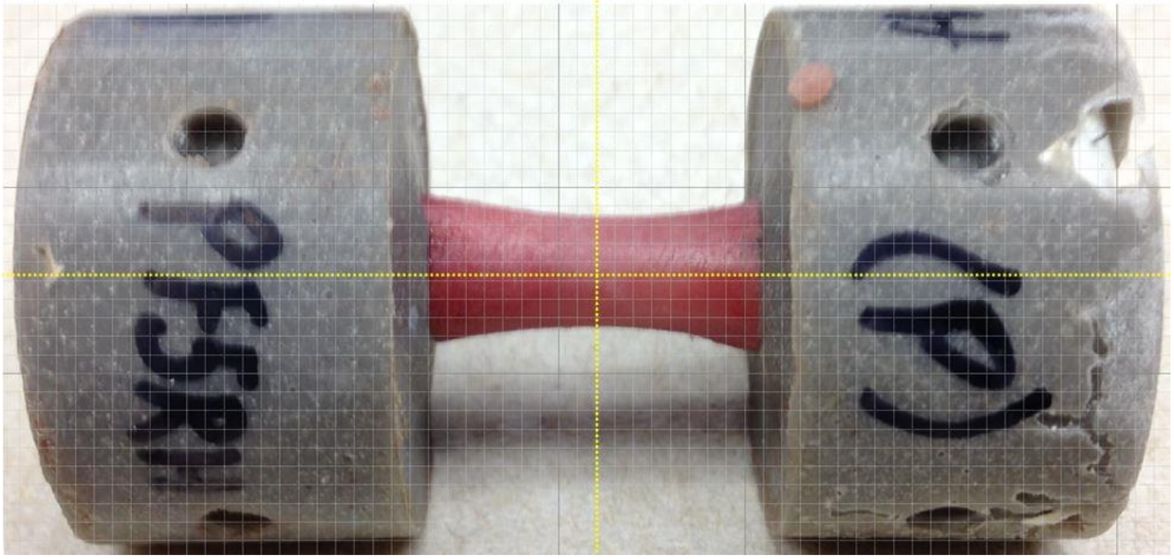

Figure 2.2 *Example of a potted bone specimen using the fast technovit liquid resin hardener formed to the cylindrical shape of the potting cups.*

Each specimen was twisted until observable failure in a servo-hydraulic testing machine (model 1331, Instron Corporation; Norwood, MA), using a custom-built torsion fixture (Figure 2.3). The linear actuator of the servo-hydraulic testing machine provided linear displacement to a rack and pinion assembly to provide controlled torsion of each specimen. To secure the specimen in the fixture, set screws were inserted through the potting cups into holes in the potting material (Figures 2.2 and 2.3). In preliminary tests it was decided to maintain an average gauge or test length of 3 times the smallest mid-shaft bone diameter for each specimen, regardless of specimen age. The test length was selected to provide the maximal exposed bone length, while retaining a sufficient length of potting to secure the specimen in the test fixture.

Specimens were rotated until failure under external rotation for each leg pair, recording the torque and the angle of rotation at a sampling rate of 10,000 Hz. The angle of rotation was measured with a rotary encoder (model BHW 16.05A72000-BP-A, Baumer Electric, Frauenfield, Switzerland) attached to the moving cup, while the torque was recorded using a 200 in-lb. torsion transducer (model TRT-200, Transducer Techniques; Temecula, CA) attached to the fixed cup.

In this study the left femur of each pair was twisted to failure at a rate of 3 degree/sec, while the right femur was twisted at a rate of 90 degree/sec. The fracture ratio was defined as total fracture length / bone diameter (Figure 2.4). Additionally, while not the target focus of the study, a composite fracture angle was also measured and recorded with respect to the longitudinal axis to more easily compare the current results to angles reported in a previous study.

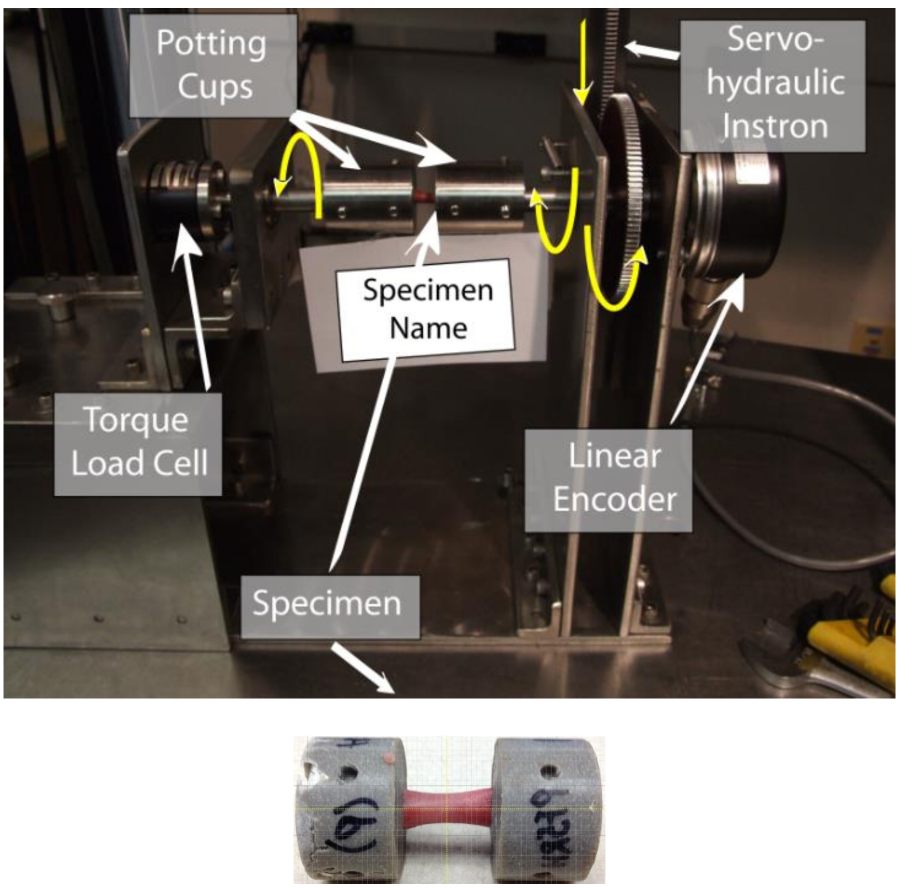

Figure 2.3 *Set-up: custom-built torsion fixture and servohydraulic hydraulic testing machine.*

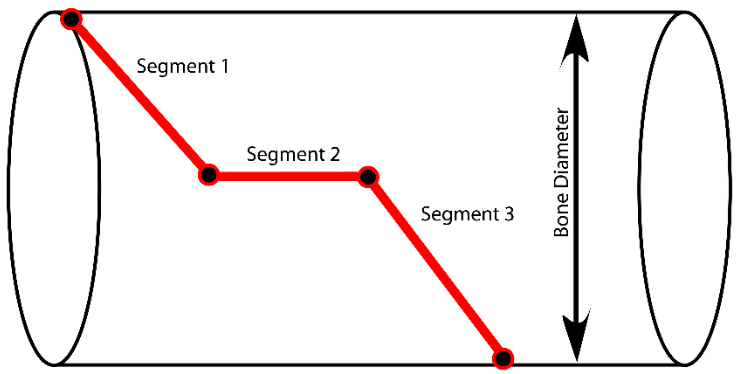

Figure 2.4 *Example of measuring the total fracture length using fracture segments in a single 2-dimensional plane of view.*

The total fracture length was defined as the summation of each fracture segment in a single plane of view, and the bone diameter was the smallest diameter of the bone measured pre-failure in the same 2-dimensional plane.

Photographs of each failed specimen were taken in both the anteroposterior and mediolateral planes of the bone (Figure 2.5). A reference scale was placed in the same plane as the specimen diameter and fracture ratio to measure these parameters directly from the photographs.

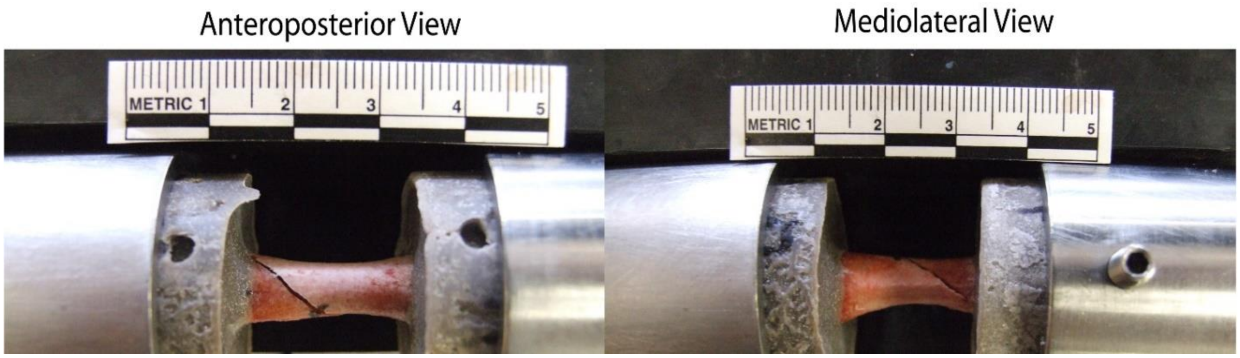

Figure 2.5 *2-dimmensional measurement technique of a mediolateral and anteroposterior view, shown for a low-rate specimen.*

Statistical tests to compare differences in some test parameters between groups were performed using a two-way ANOVA in Minitab 16 (State College, PA). The parameters examined here were the effects of specimen age and rate of twist on fracture ratio. This statistical test was utilized for the low and high rates of twist when compared against specimen age. A linear regression analysis was performed on the above parameters as well as the total angled (e.g. segment 1 and segment 3 in Figure 2.4) and longitudinal (e.g. segment 2 in Figure 2.4) components of the fracture surface versus specimen age using SPSS (SPSS Inc., Chicago, IL) to determine if the slopes and intercepts of the regression lines were significantly different from zero. If the slope of the lines was not significantly different from zero, an average value was computed and a one-sample t-test was performed between test groups using Minitab 16 (State College, PA). All statistical analyses used a criterion alpha level of 0.05.

RESULTS

Fifteen specimens were tested, ranging from 1-26 days of age. From the youngest to oldest specimen the total bone length increased from approximately 20 to 60 mm, and the bone diameter increased from approximately 6 to 9 mm. The average exposed bone length after potting was 3.0 ± 0.2 times the smallest bone diameter for each specimen in the current study. Spiral fracture patterns were produced in all specimens. Fracture comminution was only observed in some of the high rate of twist experiments.

It was noted that the fracture ratio increased with specimen age in both mediolateral and anteroposterior planes, with the low rate of twist yielding a consistently lower fracture ratio than the high rate of twist (Figure 2.6 and 2.7). A polynomial curve was fit to the dataset to highlight the rapid increase in the fracture ratio from (1-9 days), plateauing after about 10 days of age. Mediolateral specimens showed incomplete fracture patterns in the low and high rate pairings (did not fracture completely across the bone diameter) for specimen ages 2,5,9, and 13, so these pairs were eliminated from the mediolateral data set. This reduced the sample size to 11 paired specimens. Specimen age and rate of twist were significant factors influencing the anteroposterior fracture ratio with $p=0.031$ and $p=0.0001$, respectively (Figure 2.6). Specimen age and rate of twist were also significant factors influencing the mediolateral fracture ratio with $p=0.026$ and $p=0.0001$, respectively (Figure 2.7).

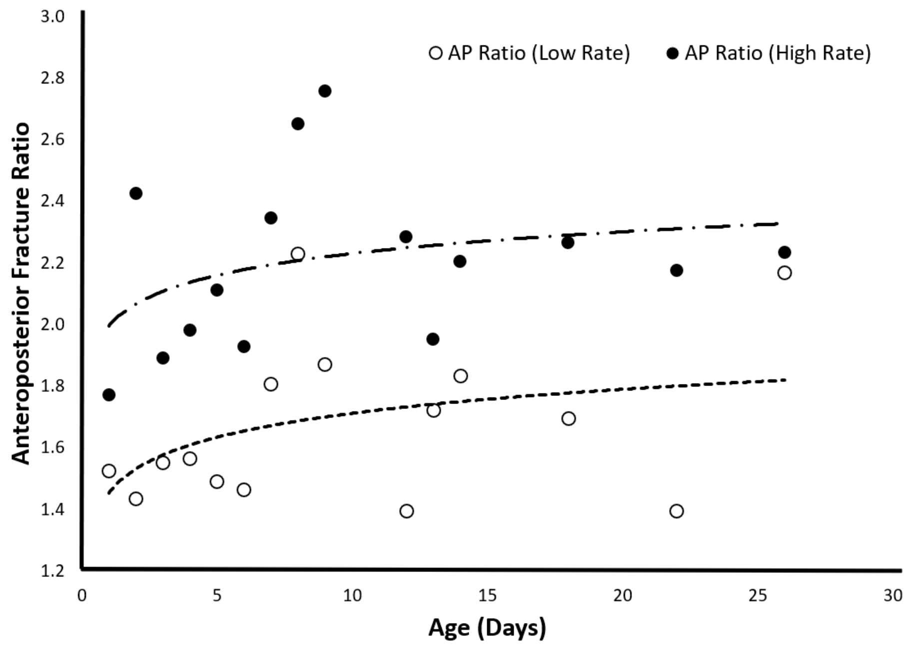

Figure 2.6 *Plot of anteroposterior fracture ratio with respect to twist rate and specimen age (measured on anterior side of bone), n = 15.*

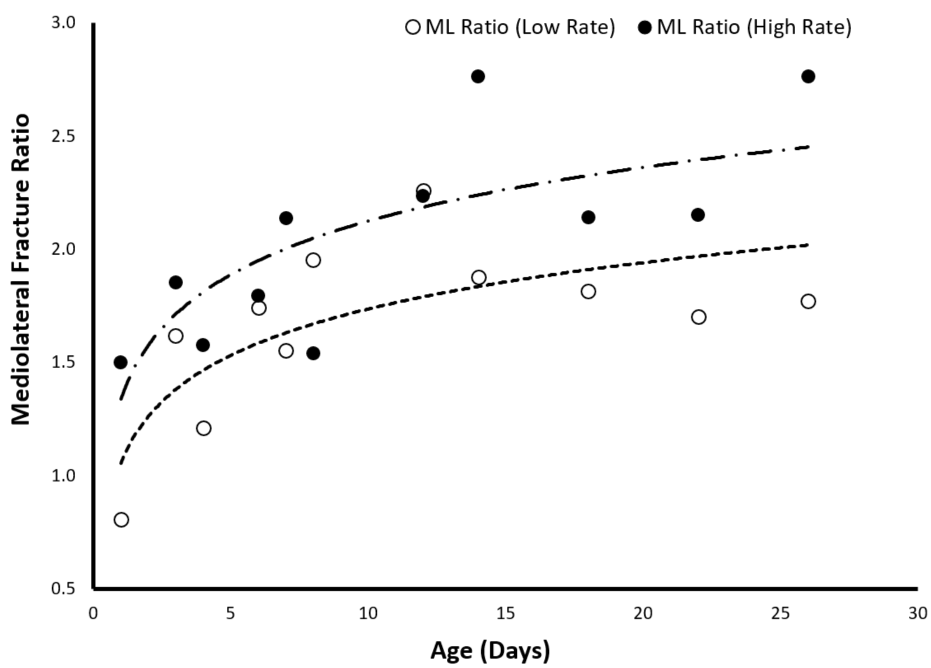

Figure 2.7 *Plot of mediolateral fracture ratio with respect to twist rate and specimen age (measured on medial side of bone), n = 11.*

Upon a detailed inspection of the fracture segments, the total length of longitudinal, segment type-2, fracture and the total length of angled, segment 1 and 3-type fracture, followed consistent trends. In low rate experiments for specimens 1 to 9 days of age, there was no observable segment type-2 failure in either the ML or AP views. For specimens aged 10 to 26 days of age in the AP view, the length of segment type-2 failure increased with age (Figure 2.8). In the AP view, the linear regression slope and intercept was significantly different than zero for the old group (p=0.033). In the ML view the length of longitudinal fractures remained constant, becoming visible after 10 days of age, with no significant age effect 3.48 ± 0.49 mm.

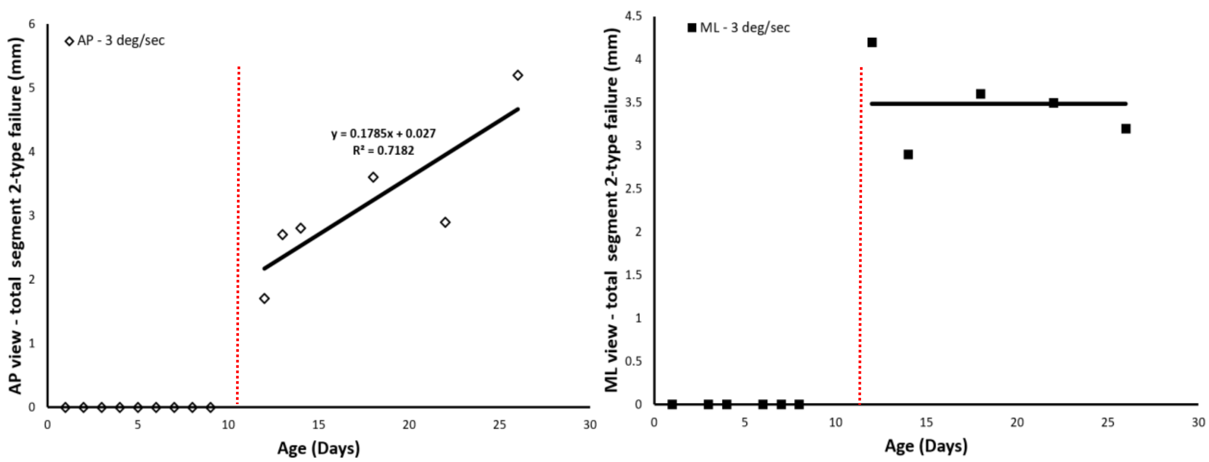

Figure 2.8 *Plots of the low-rate total longitudinal (element 2) fracture length versus specimen age (AP ratio left (n=15), ML ratio right (n=11)).*

In the higher rate experiments the longitudinal component of fracture appeared earlier with age, between approximately 3 and 5 days for ML and AP views, respectively (Figure 2.9). For all non-zero length of longitudinal fracturing there was no significant age effect observed in both views 4.62 ± 0.69 mm and 4.29 ± 1.96 mm for ML and AP, respectively.

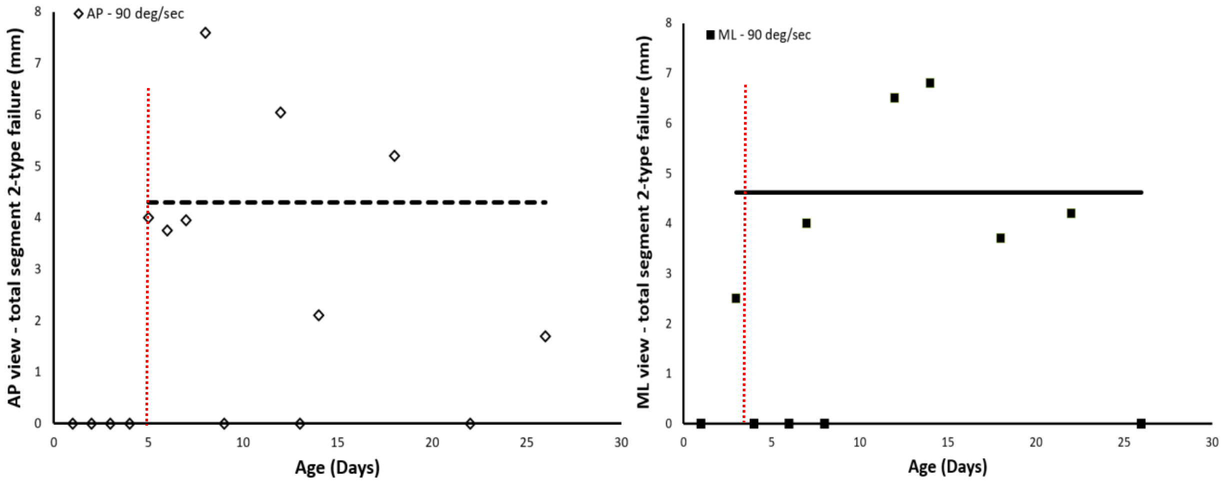

Figure 2.9 *Plots of the high-rate total longitudinal fracture component versus specimen age (AP ratio left (n=15), ML ratio right (n=11)).*

In contrast, the length of the angled failure components, taken as fracture lines that propagated at some angle theta to the longitudinal axis, increased rapidly for early ages, reaching a critical value between 10 and 12 days of age, where the total angled fracture component became relatively constant for the low-rate experiments (Figure 2.10). This was true in both the ML and AP views.

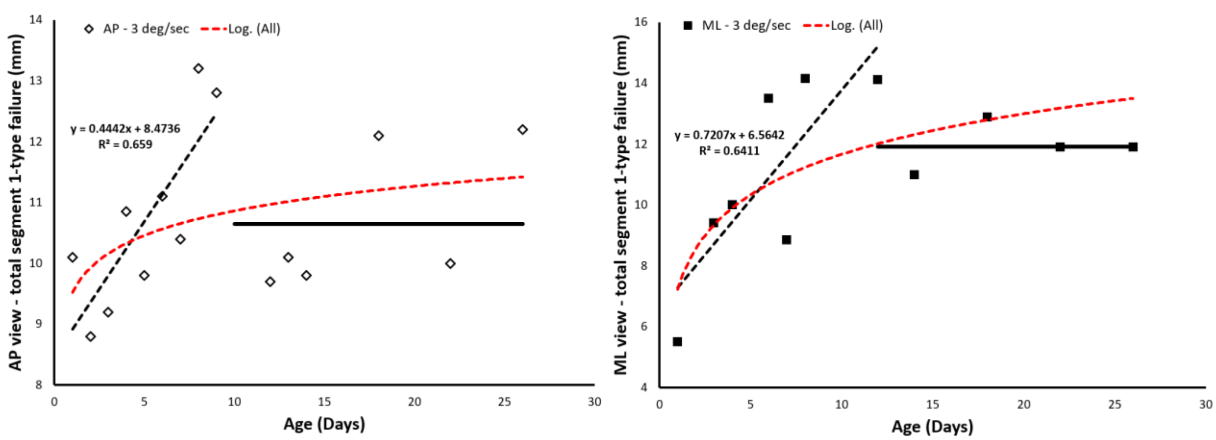

Figure 2.10 *Plots of the low-rate total angled fracture components versus specimen age (AP ratio left (n=15), ML ratio right (n=11)).*

In low-rate tests the linear regression slope was only significantly different than zero at younger ages, with (p=0.008) and (p=0.030) for AP and ML views respectively.

Interestingly, the high-rate of twist experiments revealed a significant age effect, with (p = 0.025) and (p=0.002) over all ages tested in AP and ML views, respectively. The measured length of the angled fracture segments was shown to increase with specimen age (Figure 2.11). Additionally, for the higher rate of twist experiments there was a noted increase in the number of fracture lines in addition to the main break, with specimen age. These additional fracture lines were not measured by fracture ratio, but are instead additional evidence of a high-speed bone fracture event for older bone specimens.

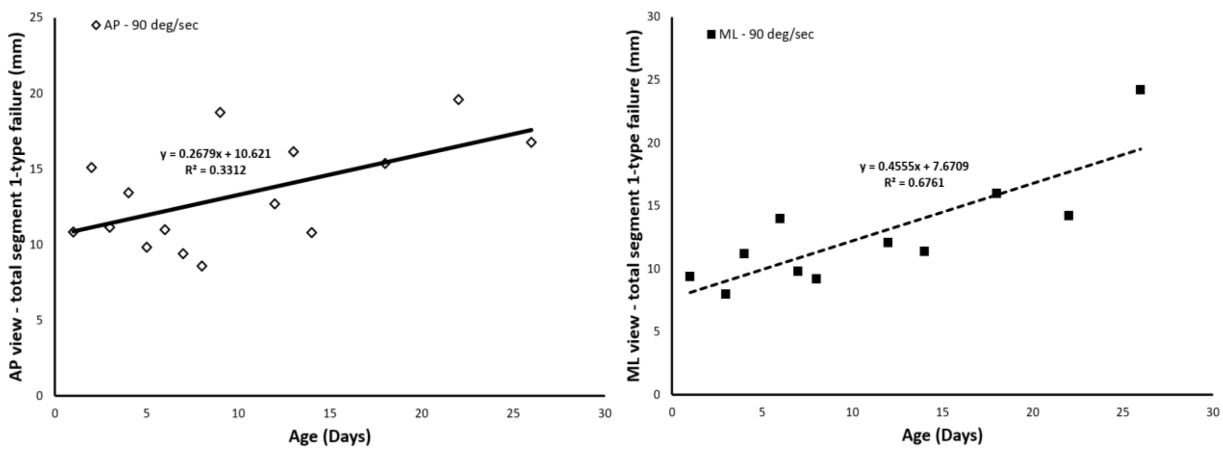

Figure 2.11 *Plots of the high-rate total angled fracture components versus specimen age (AP ratio left (n=15), ML ratio right (n=11)).*

DISCUSSION

The current study was performed to determine if the parameters of age and rate of twist would influence the fracture pattern of immature porcine femora under torsional loading. The study generated biomechanical data supporting this first hypothesis. It was shown that the fracture ratio began low and significantly increased with specimen age. Additionally, the study supported the second hypothesis that fracture ratio was significantly greater in the high rate of twist experiments than in the low rate tests, which had been suggested by the previous work of Theobald et al.

Interestingly at low rates of twist as age increased the length of the type-1 and type-3 angled segments increased, with the angle of the fracture decreasing to 30 degrees from the long axis of the bone (Figure 2.12a). At an age of 10 days and beyond, the fracture pattern began to fail with an increasing length of segment type-2 failure (Figure 2.12b). The length of segment type-2 failure was proportionally smaller than the combined type-1 and type-3 failure, which is supported by Norman et al., 1996 who demonstrated that cracks are more likely to grow in tension than in shear, even when the longitudinal shear stresses are significantly high enough to cause fracture (Jepsen et al., 1999).

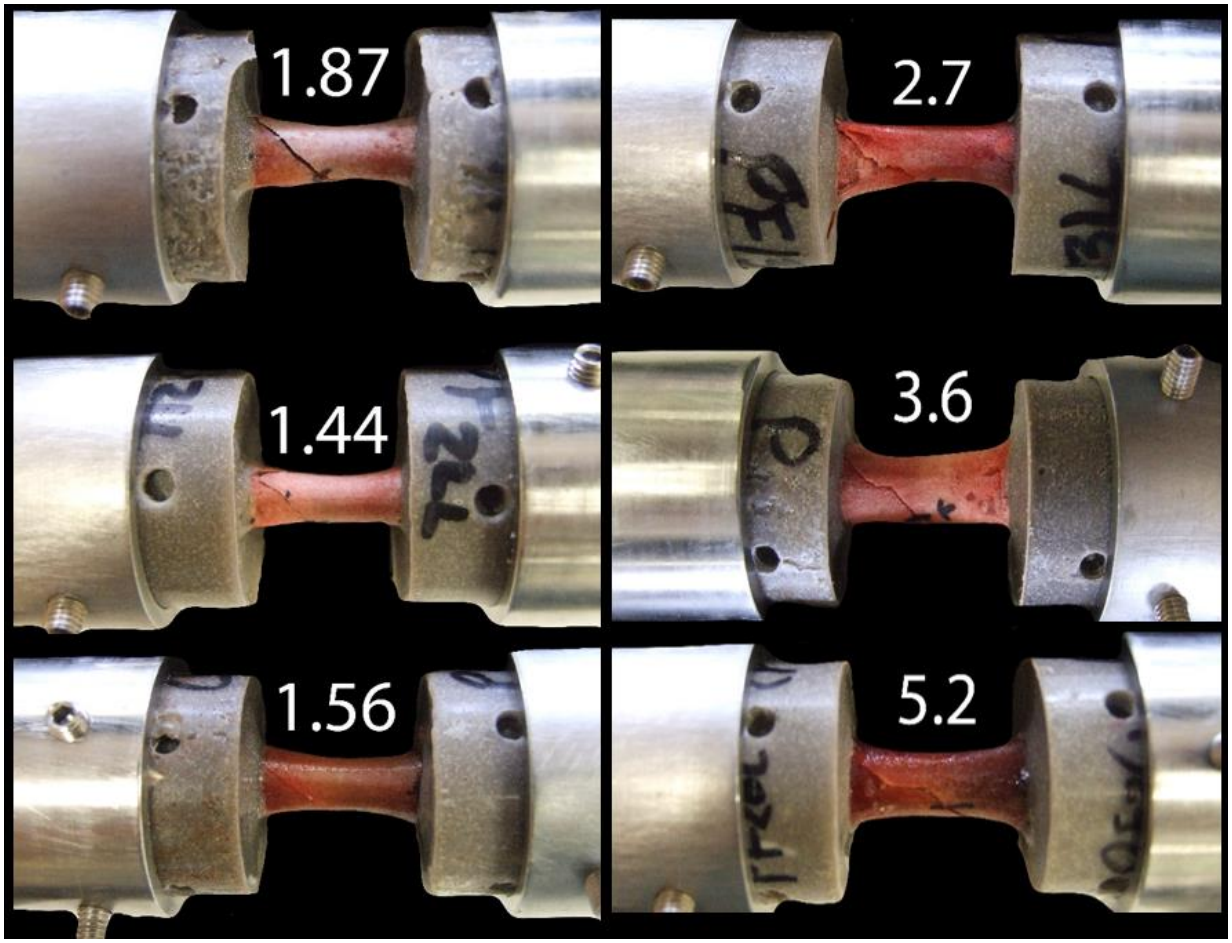

(a) **(b)**

Figure 2.12 *Photographs of low-rate tests, showing the increase in angled fracture lengths in mm for specimens (2,4,9 days) top-bottom, and its effect on the AP fracture ratio (column a). Photographs showing the increase in length of the longitudinal fracture element in mm for specimens (13,18,26 days) top-bottom, and its effect on the AP fracture ratio (column b).*

In the higher rate experiments the overall fracture pattern transitioned from low-angle failure (approximately 35 degrees), to very low angle failure (approximately 25 degrees), with longitudinal elements and increased comminution as specimen age increased (figure 2.13).

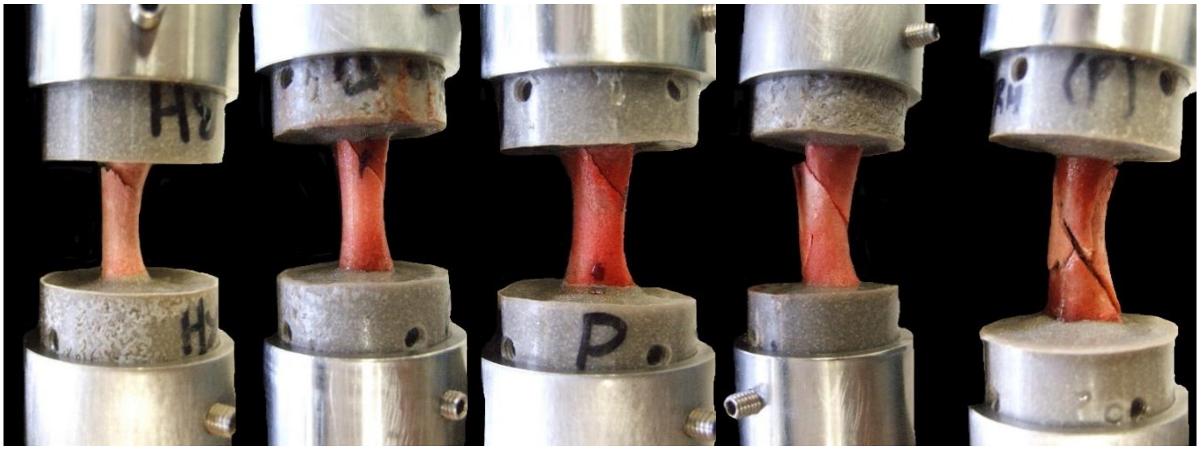

Figure 2.13 *Photographs showing changes in the fracture pattern under a high rate of twist. Specimen age (1,6,12,18,26 days) left to right at mediolateral view.*

Upon closer inspection of the bone for the higher rate experiments, the helical fracture pattern appeared to vary with specimen age and failed under differing mechanisms. At one day of age the helical fracture appeared more jagged, suggesting that the fracture was continuously shearing through osteons. At as early as six days the helical pattern became smooth with no apparent deflections. After 10 days of age the helical pattern became more step-like, failing successively in the longitudinal direction, directly increasing the crack length and fracture ratio (Figure 2.14).

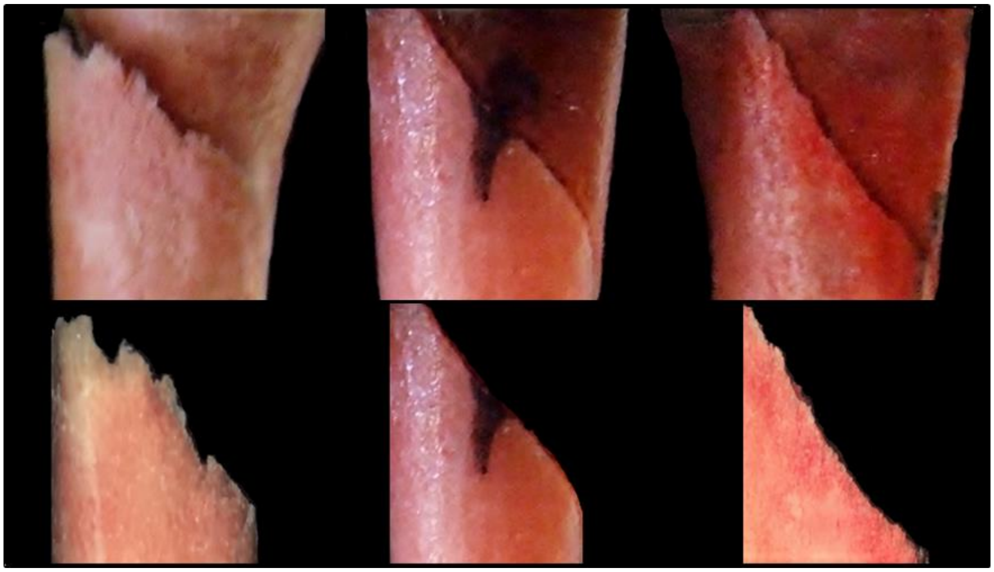

Figure 2.14 *Enlarged photographs of high-rate test specimens 1,6,12, from Figure 2.13 (top) and a single enhanced surface view from the same specimen (bottom). Showing a jagged shallow helical pattern for 1-day old specimen (left), a "smooth" helical pattern for a 6-day old specimen (center), and showing a step-like helical pattern at 12 days of age (right).*

The studies by Turner et al.,2001 and Saha, 1977 previously indicate that cortical bone is weak in both tension and shear, particularly in the longitudinal shear plane. Additionally, using compact bone tissue from the adult human femurs of different ages, Vinz et al., 1975 has shown that the tensile strength of bone increases with age. This increase in tensile strength has been correlated with an increased number of osteons in the bone with increasing age (Evans et al., 1967, Frassica et al., 1997). Furthermore, a high number of osteons has been shown to help inhibit crack propagation (Norman et al., 1996). This could imply that as the bone properties strengthen with age, due to an increase in the number of osteons, relatively more shear failure occurs between osteons as opposed to through osteons. This hypothesis, to help explain the increase in longitudinal shear failure with age, will need further investigation.

For an infant porcine femur twisted at a low rate, 10 days appears to be a critical age where below this threshold the fracture is transverse shear and tensile fracture dominate, whereas past this threshold age longitudinal shear becomes a more significant failure mode, as evidenced in Figures 2.8, 2.9, 2.10, 2.11, 2.12a. and 2.12b. This possible semi-maturation age of approximately 10 days for a porcine bone (tested under low-rate) was also shown to be a critical age in previous studies from our laboratory that investigated the patterns of porcine cranial fracture in relation to porcine growth and development (Baumer et al., 2010, Powell et al., 2012). In contrast, for the high rate of twist experiments this transition occurred much earlier between 3 and 5 days of age, more likely due to relative stiffness increases, as the bone responded to the faster loading.

In contrast to the study by Murphy et al., 2015, that the fracture ratio can be utilized to differentiate between accidental and abusive acts, the current study may suggest that age and speed of twisting may have influenced the results of this clinical-based study. Using the immature porcine model, the current study has also shown that the newly defined fracture ratio is increased with rate of twist. It might be suggested then that accidental traumas, especially those from automobile accidents, may generate a high fracture ratio due to a potentially high rate of twist. While not mentioned in the Murphy et al., 2015 study, based on a personal communication between the authors of the current study and those of Murphy et al., 2015, all the known accidental cases in that study were motor vehicle accidents or falls from heights. As a result, these cases may have potentially involved high rates of twist that, based on the results of the current study, produce a high fracture ratio, therefore leading to the correlation between the high fracture ratio and accidental trauma. Furthermore, the current study showed age was an influencing parameter on the fracture ratio. While age was not shown to be a significant statistical factor in the Murphy et al., 2015 study, explaining the lower fracture ratio for abuse cases, the power of the Murphy et al., 2015 study was not clearly defined. As such the current study, while limited to using the infant porcine model, might suggest additional clinical studies utilizing more specimens and stratification by rate of loading may be needed before fracture ratio alone should be utilized for the determination of accidental versus abusive pediatric trauma.

In summary the current study has documented that fracture ratio was significantly dependent on both specimen age and rate of twist, using the infant porcine femur model, with low rates of twist consistently producing lower fracture ratios than those shown under high rates of twist. While both an accidental and abusive act may produce spiral fractures, the results of the current study cannot aid in the interpretation of intent. This study does, however, provide experimental ‘ground-truth data’ that may help forensic biomechanists and anthropologists draw conclusions surrounding the circumstances of an injury that may help in the evaluation of truth in testimony during criminal litigations.

REFERENCES

REFERENCES

Baldwin K, Pandya NK, Wolfgruber H, Drummond DS, and Hosalkar HS. Femur fractures in the pediatric population: abuse or accidental trauma?, *Clin Orthop Relat Res.* 469(3) (2011) 798-804.

Baumer TG, Powell BJ, Fenton TW, and R.C. Haut. Age dependent mechanical properties of the infant porcine parietal bone and a correlation to the human, *J Biomech Eng.* 131(11) (2009) 111006.

Baumer TG, Passalacqua NV, Powell BJ, Newberry WN, Fenton TW, and Haut RC. Age-dependent fracture characteristics of rigid and compliant surface impacts on the infant skull - a porcine model, *J Forensic Sci*. 55(4) (2010) 993-7.

Carty HM. Fractures caused by child abuse, *J Bone Joint Surg Br.* 75(6) (1993) 849-57.

Cheong VS, Karunaratne A, Amis AA, and Bull AMJ. Strain rate dependency of fractures of immature bone. *J Mech Behav Biomed Mater*. 2017; 66:68-76.

Deland TS, Niespodziewanski E, Fenton TW, and Haut RC. The Role of Interface on the Impact Characteristics and Cranial Fracture Patterns Using the Immature Porcine Head Model, *J Forensic Sci*. 61 Suppl 1 (2016) S53-9.

Evans FG, and Bang S. Differences and relationships between the physical properties and the microscopic structure of human femoral, tibial and fibular cortical bone, *American Journal of Anatomy.* 120(1) (1967) 79-88.

Flaherty EG, Perez-Rossello JM, Levine MA, and Hennrikus WL. A.A.o.P.C.o.C.A.a. Neglect, A.e.A.o.P. Section on Radiology, A.e.A.o.P. Section on Endocrinology, A.e.A.o.P. Section on Orthopaedics, S.f.P. Radiology, Evaluating children with fractures for child physical abuse, *Pediatrics.* 133(2) (2014) e477-89.

Frassica FJ, Inoue N, Virolainen P, and Chao EY. Skeletal system: biomechanical concepts and relationships to normal and abnormal conditions, *Semin Nucl Med*. 27(4) (1997) 321-7.

Kemp AM, Dunstan F, Harrison S, Morris S, Mann M, Rolfe K, Datta S, Thomas DP, Sibert JR, and Maguire S. Patterns of skeletal fractures in child abuse: systematic review, BMJ 337 (2008).

Kim WK, Donalson LM, Herrera P, Woodward CL, Kubena LF, Nisbet DJ, and Ricke SC. Research note: Effects of different bone preparation methods (fresh, dry, and fat-free dry) on bone parameters and the correlations between bone breaking strength and the other bone parameters, *Poult Sci.* 83(10) (2004) 1663-6.

Murphy R, Kelly DM, Moisan A, Thompson NB, Warner WC, Beaty JH, and Sawyer JR. Transverse fractures of the femoral shaft are a better predictor of nonaccidental trauma in young children than spiral fractures are, *J Bone Joint Surg Am*. 97(2) (2015) 106-11.

Norman TL, Nivargikar SV, and Burr DB. Resistance to crack growth in human cortical bone is greater in shear than in tension, *J Biomech*. 29(8) (1996) 1023-31.

Pearce AI, Richards RG, Milz S, Schneider E, and Pearce SG. Animal models for implant biomaterial research in bone: a review, *Eur Cell Mater.* 13 (2007) 1-10.

Pierce MC, Bertocci GE, Janosky JE, Aguel F, Deemer E, Moreland M, Boal DK, Garcia S, Herr S, Zuckerbraun N, and Vogeley E. Femur fractures resulting from stair falls among children: an injury plausibility model, *Pediatrics.* 115(6) (2005) 1712-22.

Powell BJ, Passalacqua NV, Baumer TG, Fenton TW, and Haut RC. Fracture patterns on the infant porcine skull following severe blunt impact, *J Forensic Sci.* 57(2) (2012) 312-7.

Saha S. Longitudinal shear properties of human compact bone and its constituents, and the associated failure mechanisms, *Journal of Materials Science*. 12(9) (1977) 1798-1806.

Theobald PS, Qureshi A, and Jones MD. Biomechanical investigation into the torsional failure of immature long bone, *J Clin Orthop Trauma*. 3(1) (2012) 24-7.

Torzilli PA, Takebe K, Burstein AH, Zika JM, and Heiple KG. The material properties of immature bone, *J Biomech Eng*. 104(1) (1982) 12-20.

Turner CH, Wang T, and Burr DB. Shear strength and fatigue properties of human cortical bone determined from pure shear tests, *Calcif Tissue Int.* 69(6) (2001) 373-8.

Vaughan PE, Vogelsberg CC, Vollner JM, Fenton TW, and Haut RC. The Role of Interface Shape on the Impact Characteristics and Cranial Fracture Patterns Using the Immature Porcine Head Model, *J Forensic Sci.* 61(5) (2016) 1190-7.

Vinz H. Change in the mechanical properties of human compact bone tissue upon aging, *Polymer Mechanics.* 11(4) (1975) 568-571.

Worlock P, Stower M, and Barbor P. Patterns of fractures in accidental and non-accidental injury in children: a comparative study, *Br Med J (Clin Res Ed).* 293(6539) (1986) 100-2.

CHAPTER THREE: THE EFFECT OF SPECIMEN AGE AND LOADING RATE ON INTRINSIC MATERIAL PARAMTERS OF THE IMAMTURE PORCINE FEMORA

ABSTRACT

The underlying failure mechanisms and resulting fracture patterns of whole bone under torsion is not fully understood. From torsional testing conducted previously by this lab, it was discovered that the spiral fracture's surface changes with specimen age and rate of twist, and that this change in the fracture pattern is measurable via a fracture ratio, where the spiral fracture length is divided by the bone diameter when measured under a single radiographic view. Under close examination the fracture surface was seen to transition from a jagged surface (high angle failure) at a young age, to a smooth break, and then to a step-like fracture surface (low angle failure), as measured from the longitudinal axis of the bone. It was theorized that a pre-disposed weakness to a given shear-type, namely low fracture strength of the bone under longitudinal or transverse shear, is what causes deviation in the spiral fracture surface from an idealized 'smooth' fracture surface resulting from failure under tension. For example, if bone is weaker in transverse shear than in longitudinal shear, then this type of shear failure will become a viable alternative fracture path to the preferred mode of failure under tension, and vice versa. Results of this study indicated that at low rates the longitudinal shear strength from birth was initially stronger than the transverse shear strength, becoming weaker than the transverse shear strength after approximately 7 days of development. A similar trend was also noted at a high rate of loading, with approximately 4.5 days of development acting as the critical transition age for failure strength of the bone. This information supports the notion that there are three modes of spiral bone fracture. Below the critical transition ages reported above for each respective rate of testing, a combined transverse shear and tensile failure mode is likely to occur, resulting in a low fracture

ratio due to increased transverse failure through osteons. At and perhaps a few days before and after the critical age, which from herein will be defined as the critical region where the transverse and longitudinal shear strengths are approximately equal, a purely tensile mode of failure is likely to be seen in the spiral failure, generating a smooth fracture surface, increasing the fracture ratio. After the reported critical age, a combined tensile and longitudinal mode of failure is likely to be generated, further increasing the fracture ratio due to increased failure between osteons cement lines.

INTRODUCTION

The underlying failure mechanisms and resulting fracture patterns of whole bone under torsion is not fully understood. Currently forensic biomechanists and anthropologists only report is that a spiral fracture pattern is evidence that the bone was twisted, and in which direction the bone had been twisted (Kress et al., 1996). This may not provide evidence whether the injury was due to an accident or an abuse-type scenario. The only comment forensic practitioners often are willing to make is that for children under the age of walking to acquire a spiral fracture of the femur is by non-accidental trauma or abuse (Carty, 1993, Pierce et al., 2004).

As bone is an anisotropic material, it has differing properties in different directions. This is largely a result of its underlying microstructure (Pierce et al., 2004). The femur is composed of longitudinally-oriented osteons which are composed of a stretchable fibrous protein collagen and a brittle mineral phase hydroxyapatite, which results in a very strong and tough material (Tadano et al., 2011). Osteons are interconnected by a cement lining and a weak lamellar interface (Katsamenis et al., 2012). For purposes of this thesis the longitudinal direction will be taken as the long-axis of the femur, and the transverse direction will be taken as perpendicular to the long-axis.

Indirect measures of the aggregate properties of the osteon and lamellar interface can be found through material testing techniques, such as tensile and shear tests. In bone the longitudinal tensile strength and the transverse shear strength can be considered as indirect measures of the aggregate strength of the bone. The transverse tensile strength and the longitudinal shear strength of the bone can be considered as indirect measures of the cement-lining and matrix interface between osteons. Understanding how these properties are influenced by both specimen age and loading rate are pivotal in the understanding of whole bone failure mechanisms, like twisting-fracture.

As noted by Turner et al., 2001, shear strength is typically reported as the torsional shear strength of whole bone while there is limited data on ‘pure’ shear values in either the longitudinal or transverse directions. Furthermore, there is limited data presented on immature bone, as more mature ‘adult’ bone is typically available for study. It has been generally assumed in the literature that immature bone will produce fracture patterns and fail under similar mechanisms to those of mature bone, with limited supporting data at this time.

The aim of the current study was to collect ‘pure’ shear and tension data from immature porcine femora in both the longitudinal and transverse directions over a range of ages and two rates of loading that parallels the study in Chapter 2. As spiral fracture is considered a combination of both transverse and longitudinal shear failure (Vashishth et al., 2005), it is theorized that a predispositional weakness to a given shear-type will be evident in the spiral fracture pattern of the bone as a function of specimen age and rate of loading. For example, if bone is weaker in transverse shear than in longitudinal shear then this type of shear failure will become a viable alternative fracture path to the preferred mode of failure under tension, and vice versa.

METHODS

Forty paired porcine specimens aged 1-24 days old were collected from the MSU swine research facilities and frozen within 12 hours of death at -20°C. All specimens that were collected perished of natural causes. Prior to testing specimens were brought to room-temperature and dissected from the limb, cleaned of excess muscular tissue, and immediately wrapped in saline-moistened gauze to prevent drying-out of the bone. The mid-section of the right and left leg pairs was then removed with a bone saw from the anterior plane of the bone. The anterior plane was selected, as Chapter 2 Figure 2.6 showed that the greatest rate effect occurred on the anterior plane. Specimens were then wet-cut by hand into tensile and shear testing shapes (Figure 3.1). After shaping and prior to testing specimens were maintained in a refrigerator at 0°C while wrapped in saline-soaked gauze. Prior to testing, the specimens were brought back to ambient temperature. Tests were performed within 48 hours of initial thawing.

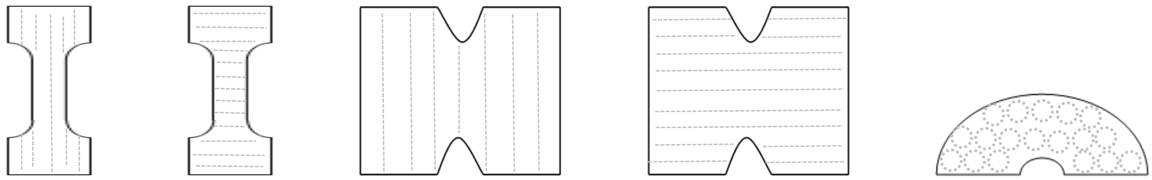

(a) (b) (c) (d) (e)

Figure 3.1 *Longitudinal tensile testing representation (a), transverse tensile testing representation (b) longitudinal shear testing representation (c), transverse shear testing representation (d) natural curvature of the bone (e). For all pictures the direction of osteons is represented by a gray dotted line.*

Each specimen was tested until failure in a servo-hydraulic testing machine (model 1331, Instron Corporation; Norwood, MA) using a custom-built tensile and shear test fixture (Figure 3.2). The linear actuator provided a measurable vertical displacement which resulted in controlled shear or tensile deformation. To help reduce bending forces on the bone from direct clamping of a curved surface, a small curvature was set into the clamp itself to mimic the natural curvature of the bone surface (Figure 3.3).

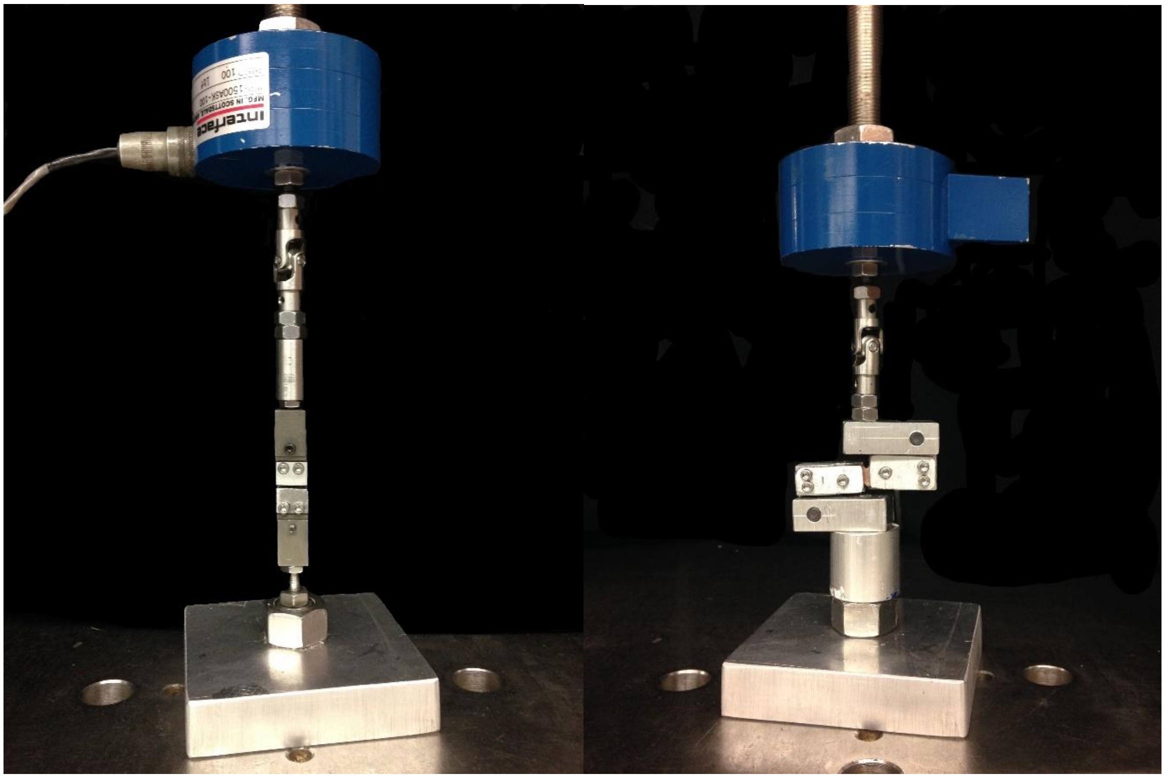

Figure 3.2 *Photograph of tensile testing fixture (left), photograph of the shear testing fixture (right)*

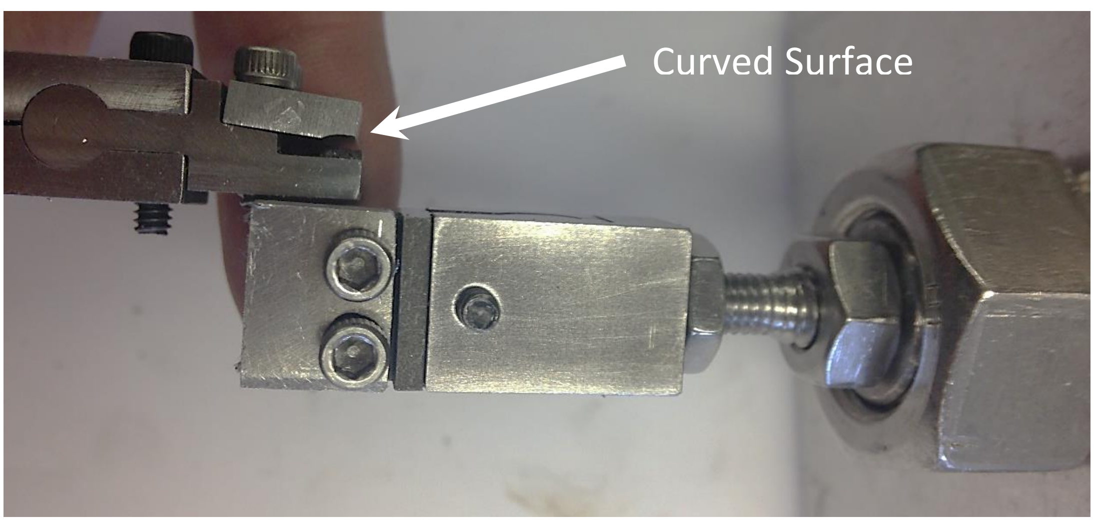

Figure 3.3 *Photograph of the curvature designed into the clamp*

As the load-displacement rate in tension and shear could not be directly resolved from the tests performed in Chapter 2, it was decided to match the failure time of the tensile test specimen in both directions to that of the failure time recorded at 3 degree/sec and 90 degree/sec under torsion. This was selected because bone is claimed to fail in torsion primarily under tension, as opposed to shear (Kress et al.,1996, Turner et al., 2001), and shear failure under torsion is theorized to only act as a secondary alternative failure mode for crack energy dissipation of propagating helical cracks. In preliminary tests the rate of displacement that fit this criterion was a low rate of 0.065 mm/sec to match failure time at 3 degree/sec, and a high displacement rate of 1.61 mm/sec to match the failure time at 90 degree/sec.

Force-time data was collected with a 100 lb load cell (model 1500ASK-100, Interface; Scottsdale, AZ) at a sampling rate of 5000 Hz for the high rate tests, and a sampling rate of 2500 Hz for the low rate tests. A pre-load of 2N was applied for both tests to take slack out of a joint which was added to the fixture to reduce bending loads and promote ‘pure’ axial loading of the specimens. The pre-load of 2N was then held for three seconds before a haversine load at the previously given rates was applied for a total displacement of 1 mm and 2 mm in the low and high rate tests, respectively.

Traditional engineering mechanics equations were utilized in the study (Sukla, 2014). The ultimate tensile strength of the bone was calculated using the expression

$$\sigma = \frac{F_{fail}}{w*t} \tag{3.1}$$

where σ is the ultimate tensile strength in megapascals, F_{fail} is the failure force required to break the specimen in Newtons, w is the width of the test specimen in millimeters, and t is the cortical bone thickness in millimeters. The tensile strain was calculated using the expression

$$\varepsilon_{tensile} = \frac{\Delta x}{L_{effective}} \tag{3.2}$$

where $\varepsilon_{tensile}$ is the tensile strain in either the longitudinal or transverse directions, Δx is the measured displacement of the Instron machine in millimeters, and $L_{effective}$ is the effective length of the test section of the specimen in millimeters. The Young's modulus was calculated using the expression

$$E = \frac{\sigma}{\varepsilon_{tensile}} \tag{3.3}$$

where E is the Young's modulus of elasticity in megapascals. The modulus was taken as a linear regression over the elastic portion of the stress-strain curve (Figure 3.4 left).

For shear tests the ultimate shear strength of the bone was calculated using the expression

$$\tau = \frac{F_{fail}}{h*t} \tag{3.4}$$

where τ was the ultimate shear strength in megapascals in either the longitudinal or transverse direction, h was the notch height of the specimen in millimeters, and t was the cortical bone thickness in millimeters. The shear strain was taken as

$$\varepsilon_{shear} = \frac{\Delta x}{h} \tag{3.5}$$

where ε_{shear} was the shear strain, Δx was the measured displacement of the Instron in millimeters, and h was the effective length of the specimen minus the notch dimensions in millimeters. The shear modulus was given by the expression

$$G = \frac{\tau}{\varepsilon_{shear}} \tag{3.6}$$

where G is the shear modulus in megapascals. The shear modulus was taken as a linear regression over the elastic portion of the stress-strain curve, as performed for the Young's modulus (Figure 3.4 right).

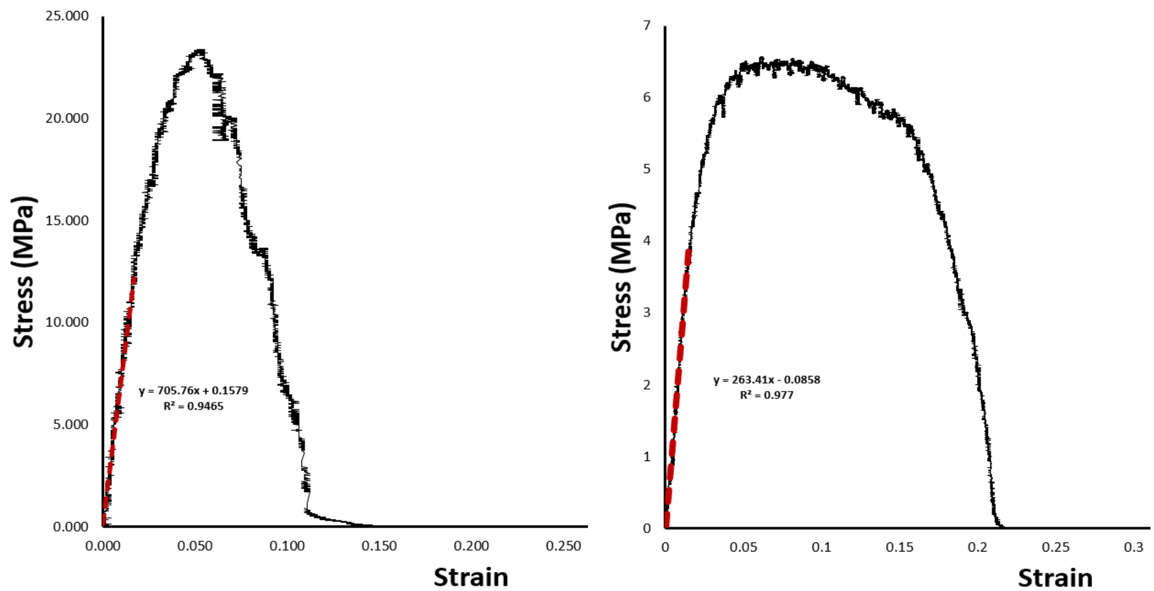

Figure 3.4 Young's *modulus determination for an 8-day old, low rate longitudinal tensile specimen (left), shear modulus determination for a 7-day old, low rate longitudinal shear specimen (right).*

STATISTICAL METHODS

A two-way ANOVA was performed in Minitab 18 (State College, PA) to compare the effects of specimen age (1-24) and specimen loading rate (low and high) on various factors such as ultimate strength, tensile and shear moduli, time to failure, and failure strain. A linear regression analysis was performed on all parameters to determine if the slope and intercepts were significantly different from zero. If the slopes of the lines were not significantly different from zero, and average value was computed for the dataset, and a one-sample t-test was performed to produce the confidence range of that data, using Minitab 18 (State College, PA). All statistical analyses used an alpha-criterion of 0.05.

RESULTS

Forty specimen pairs were tested at both low and high loading rates, ranging from 1-24 days of age. 10 specimens were tested at low and high rates for longitudinal tensile tests, transverse tensile tests, longitudinal shear tests, and transverse shear tests. A sample size of (n=10) was recorded for each test, excluding the longitudinal tensile test where (n=9) as a paired specimen broke while loading into the clamps.

FAILURE STRENGTH RESULTS

It was noted in low rate tests that the longitudinal shear strength decreased with specimen age. Interestingly, the longitudinal shear strength from birth was initially stronger than the transverse shear strength, becoming weaker than the transverse shear strength after 7 days of development. For these low rate tests 7 days appeared to be a critical age, where the transverse and longitudinal shear strengths were equal (Figure 3.5). A similar trend was also noted in high rate tests where 4.5 days of development appeared to be the critical age (Figure 3.6).

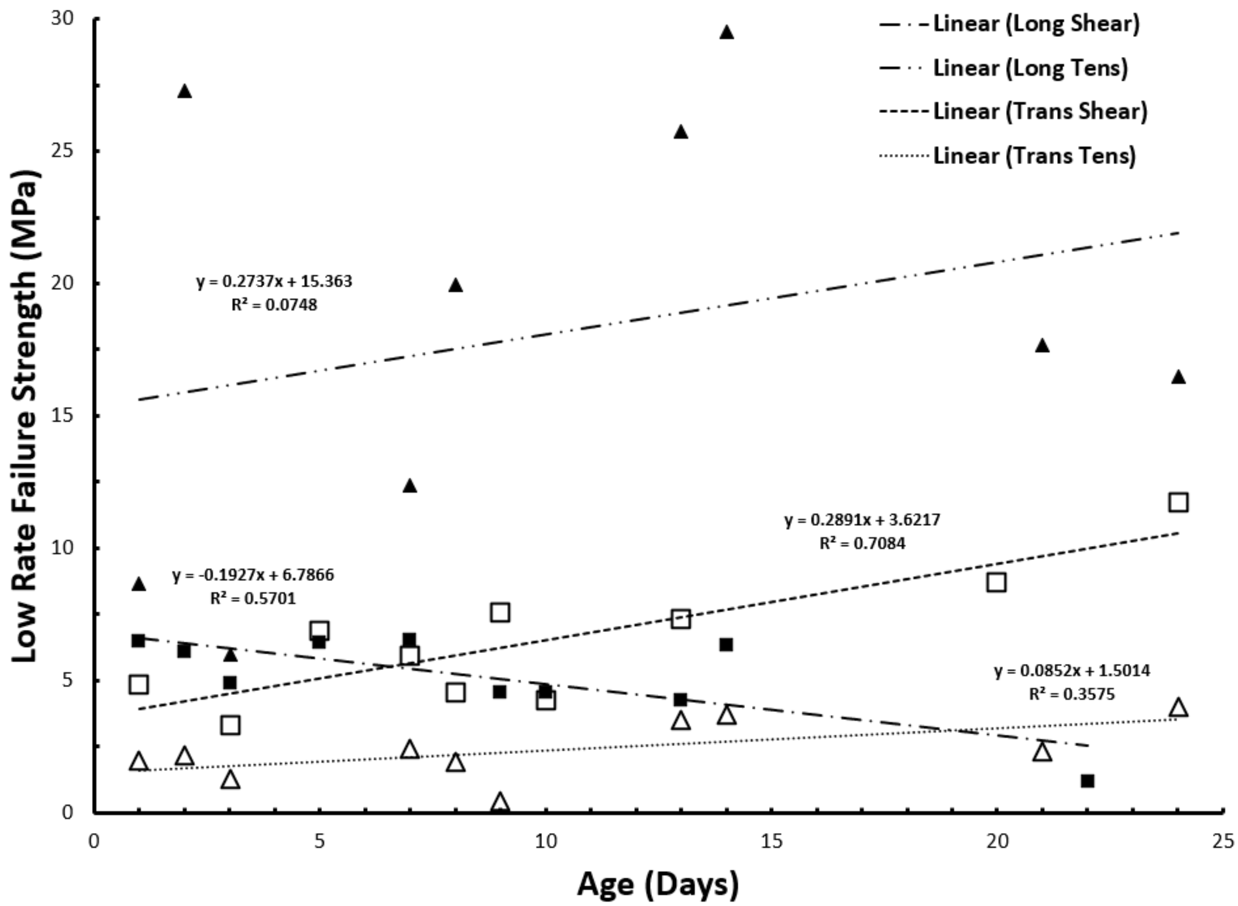

Figure 3.5 *Plot of low rate failure strength values. Closed triangles are longitudinal tensile data points (n=9), open triangles are transverse tensile data points (n=10), closed squares are longitudinal shear data points (n=10), and open squares are transverse shear data points (n=10).*

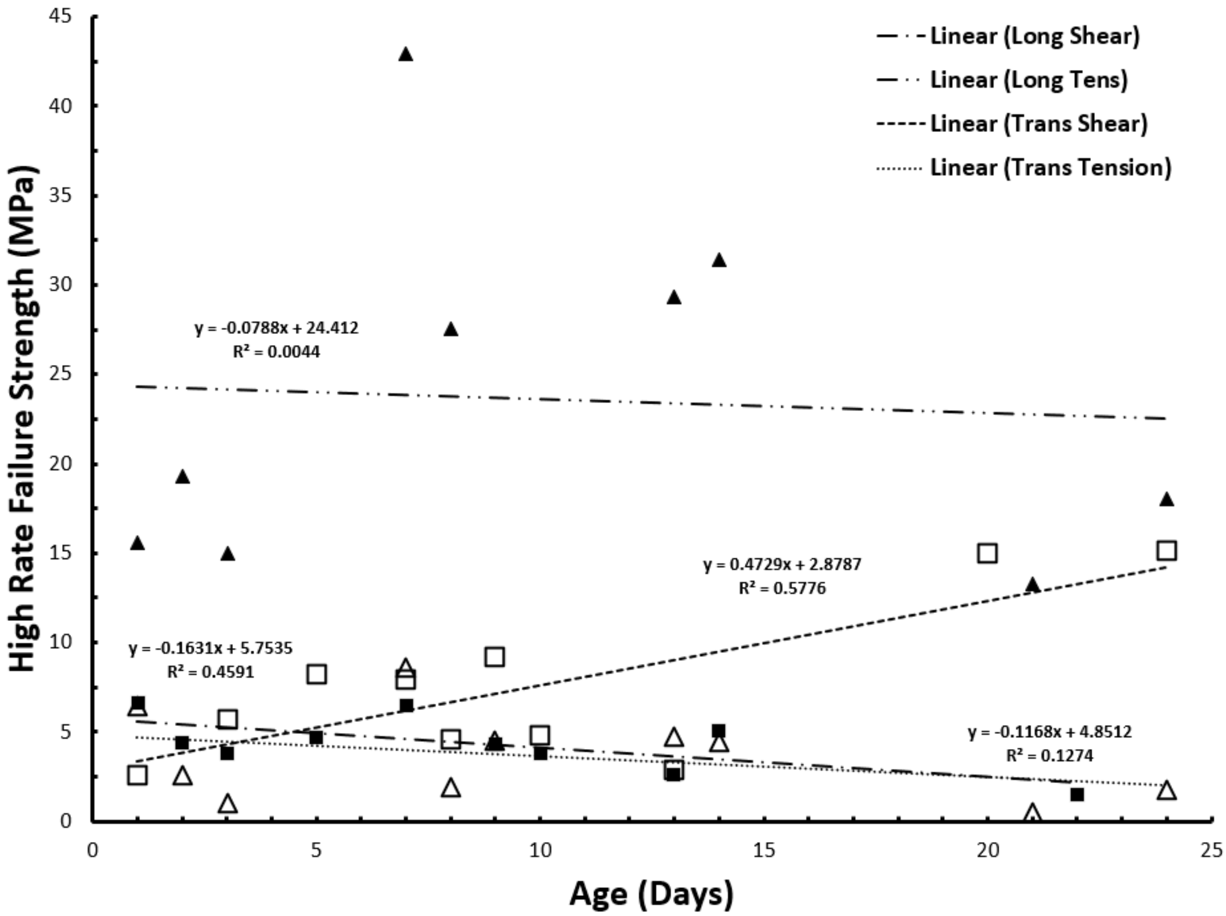

Figure 3.6 *Plot of high rate failure strength values. Closed triangles are longitudinal tensile data points (n=9), open triangles are transverse tensile data points (n=10), closed squares are longitudinal shear data points (n=10), and open squares are transverse shear data points (n=10).*

The longitudinal shear strength had an age ($p = 0.0001$) and rate effect ($p = 0.012$) with the high rate tests yielding lower longitudinal shear strength values than the low rate tests. For both high and low rates the longitudinal shear strength decreased with increasing age. The transverse shear strength also had an age effect ($p = 0.014$), but no discernable rate effect. The transverse shear strength was shown to increase with increasing specimen age. The longitudinal tensile strength and the transverse shear strength were neither rate nor age dependent.

YOUNG'S MODULUS AND SHEAR MODULUS RESULTS

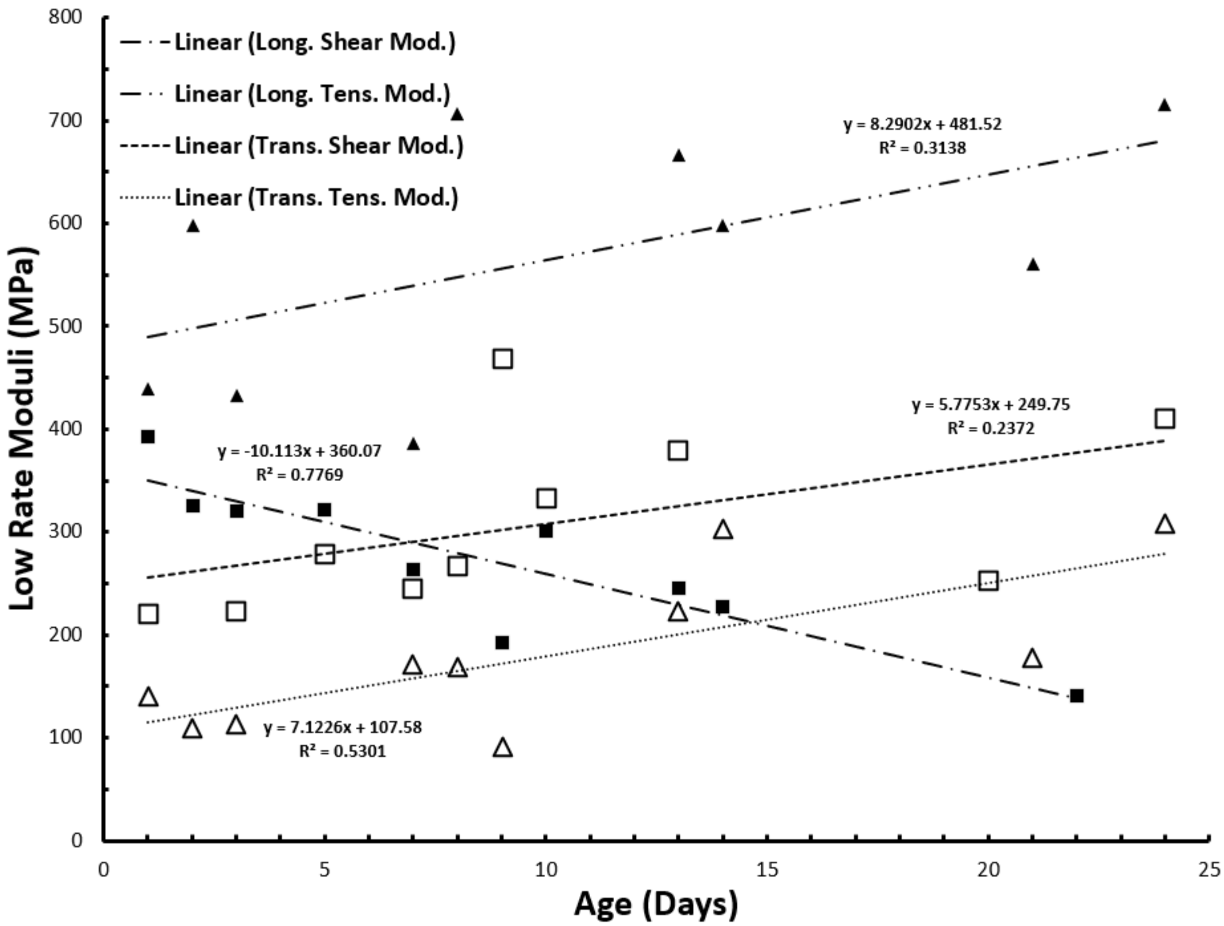

Figure 3.7 *Plot of low rate shear and tensile moduli. Closed triangles are longitudinal tensile data points (n=9), open triangles are transverse tensile data points (n=10), closed squares are longitudinal shear data points (n=10), and open squares are transverse shear data points (n=10).*

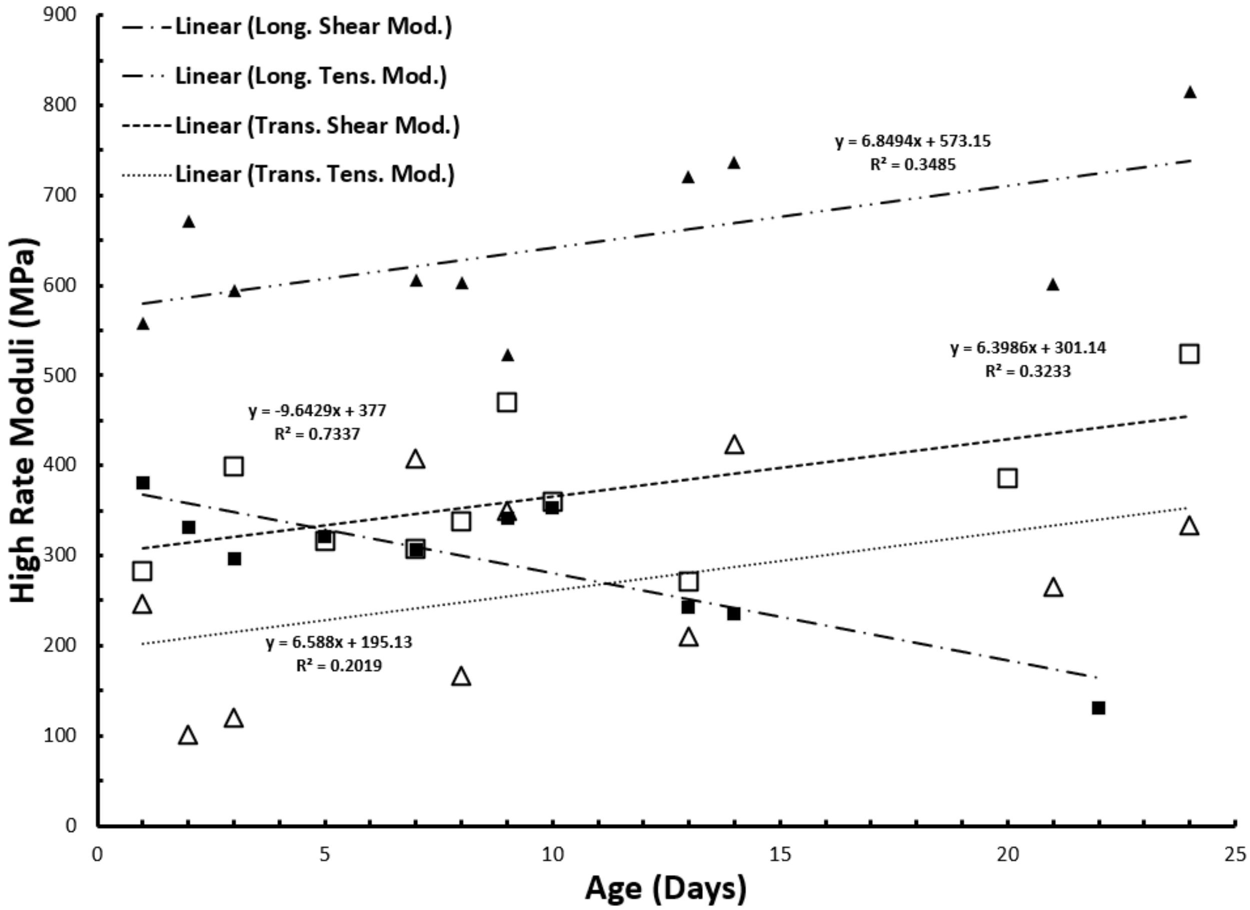

Figure 3.8 *Plot of high rate shear and tensile moduli. Closed triangles are longitudinal tensile data points (n=9), open triangles are transverse tensile data points (n=10), closed squares are longitudinal shear data points (n=10), and open squares are transverse shear data points (n=10).*

Similar trends to that of the failure strength were also noted for the shear and tensile moduli of the bone at the two rates (Figure 3.7 and Figure 3.8). The longitudinal shear modulus had an age effect ($p = 0.003$), but there was no statistically significant difference between the low and high rate data. For both high and low rate tests the longitudinal shear modulus decreased with increasing age. The transverse shear modulus had both an age ($p = 0.035$) and a rate effect ($p = 0.045$) with the high rate transverse shear moduli possessing a higher value for all ages when compared to the low rate data. The transverse shear modulus was shown to increase with increasing specimen age. The longitudinal tensile modulus was also both age ($p = 0.025$) and rate-sensitive ($p = 0.018$) with the high rate Young's modulus yielding higher values for all ages compared to the low rate test data. The longitudinal tensile modulus increased with increasing specimen age. The transverse tensile modulus was only age-dependent ($p = 0.004$). The transverse Young's modulus increased with increasing specimen age.

TIME TO FAILURE

The low rate test of 0.065 mm/sec over a 1mm displacement and the high rate test of 1.61 mm/sec over a 2mm displacement in these experiments were selected to be loading rates representative of the 3 degree/sec and 90 degree/sec torsional tests, based upon recorded time at bone fracture. All low rate and high rate test data fell within a range that was not statistically different from the torsional tests, except for the transverse shear tests. At the same failure rate as the longitudinal shear, longitudinal tensile, and transverse tensile tests, it took significantly more time for the transverse shear tests to achieve total failure (Figure 3.9 and Figure 3.10).

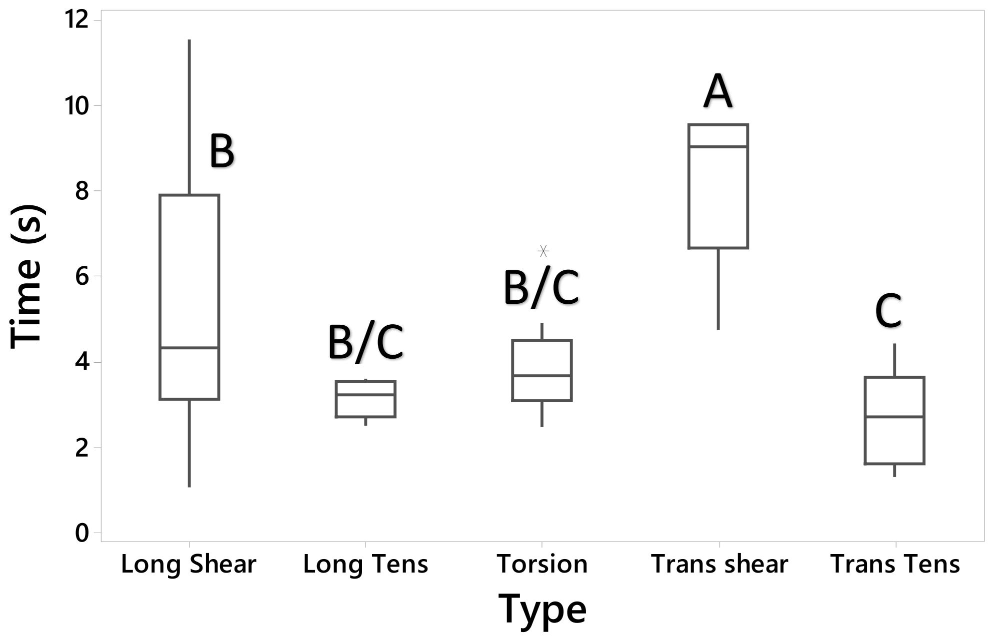

Figure 3.9 *Plot of the various test data and the time (in seconds) it took to reach bone fracture for low rate tests.*

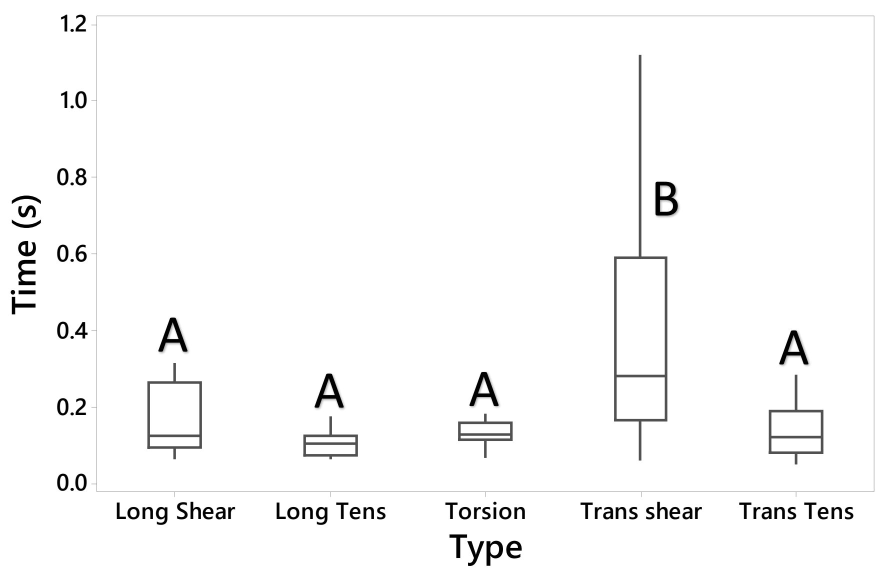

Figure 3.10 *Plot of the various data and the time (in seconds) it took to reach bone fracture in the high rate tests.*

DISCUSSION

The current study was performed to assess the effects of specimen age and loading rate on the intrinsic material properties of the immature porcine femur in both the longitudinal and transverse directions. From torsional testing conducted in Chapter 2 of this thesis, it was discovered that the spiral fracture surface changed with specimen age, transitioning from a low fracture ratio (large-angle failure from long-axis) to a high fracture ratio (low-angle failure from long-axis). The fracture surface transitioned from a jagged surface at a young age, to a smooth break, and then to a step-like fracture surface with increasing age of specimen (Figure 3.11).

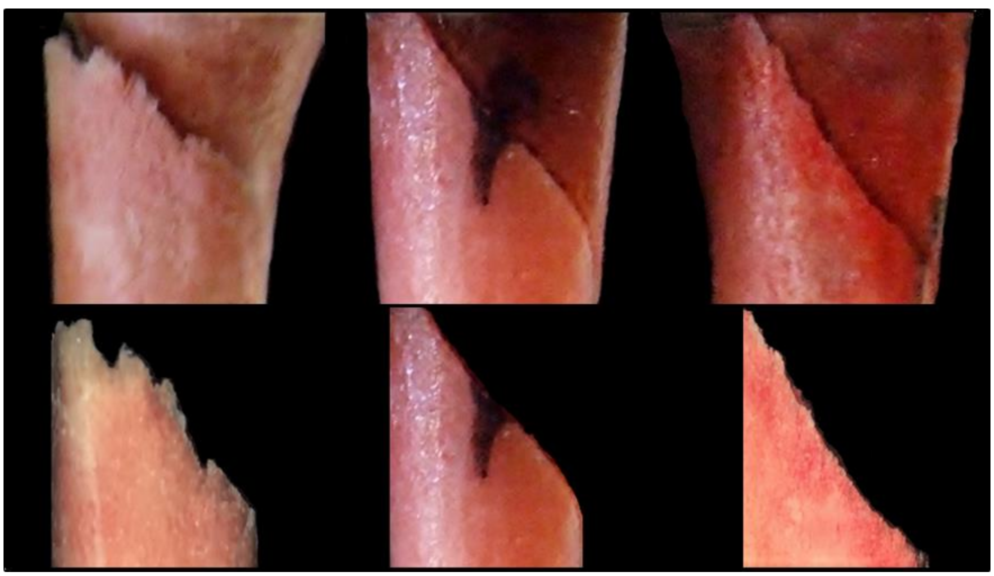

Figure 3.11 *Enlarged photographs of high-rate test specimens 1,6,12, from Figure 2.13 (top three photos) and a single enhanced surface view from the same specimen (bottom three photos). Showing a jagged shallow helical pattern for 1-day old specimen (left, column 1), a "smooth" helical pattern for a 6-day old specimen (center, column 2), and showing a step-like helical pattern at 12 days of age (right, column 3). Adapted from Figure 2.14.*

It was therefore theorized that a pre-disposed weakness to a given shear-type or tensile-type would be evident in the spiral fracture pattern of the bone, and that this weakness would allow the crack to either propagate transversely though osteons, or longitudinal along osteons, as an alternative crack path from the preferred mode of failure along the line of maximum tension. Therefore, if bone is weaker in transverse shear than in longitudinal shear, then transverse shear failure through osteons will become a viable alternative fracture path to the preferred mode of failure under tension, reducing the fracture ratio (increasing the angle of fracture from the long-axis and vice versa if longitudinal shear is the viable alternative fracture pathway, resulting in an increase in the fracture ratio (decreasing the angle of fracture from the long-axis). The study generated biomechanical data supporting this hypothesis.

Treating the transverse and longitudinal shear strength as a ratio of the fitted curves from Figures 3.5 and 3.6, the point where the shear strengths are equal (a ratio value of one) was approximately 4.5 days for high-rate tests and approximately 7 days for low-rate tests (Figure 3.12). Taken as the mean critical transition point, it is likely that a few days before and after the critical value will possess similar fracture properties, and is defined here as the critical region. While not a direct finding of Chapter 2, composite fracture angles were measured of the spiral fractures produced for all ages, for convenience when comparing the fracture ratio to the fracture angles that are commonly reported in the literature. In this critical region it appeared the bone failed purely in tension at an angle of approximately 45 degrees. This is the most commonly reported mode of spiral fracture (Porta et al., 2005). Prior to this critical range the transverse shear strength is weaker than the longitudinal shear strength, allowing for deviations from the mechanically preferred mode of failure by tension, and allowing energy to be dissipated by crack failure through osteons (resulting in a low fracture ratio/high fracture angle). After this critical region the longitudinal shear strength was weaker than the transverse shear strength, allowing for deviations from the mechanically preferred mode of failure in tension, and allowing energy to be dissipated by crack failure along the cement line, longitudinally (resulting in a high fracture ratio/low fracture angle).

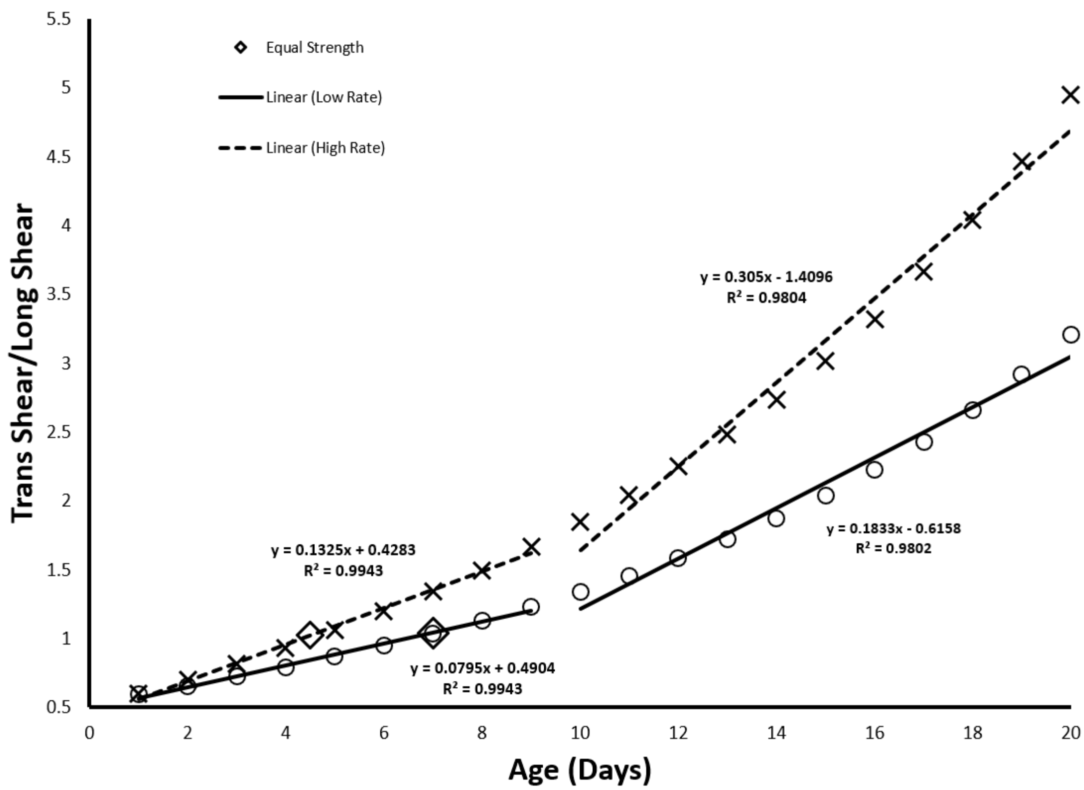

Figure 3.12 *Plot of the ratio of transverse shear strength over the longitudinal shear strength against specimen age.*

Nalla et al., 2005 used notched human bone specimens to demonstrate that bone is tougher in the transverse direction than in the longitudinal direction. When bone fails under transverse shear, not only does it break through osteons, but the crack is also deflected along cement lines as it propagates generating a highly torturous crack (Koester et al., 2008, Nalla et al., 2005 and Vashishth et al., 2005). This pattern-type in the transverse orientation is best shown by Koester et al., 2008 (Figure 3.13a).

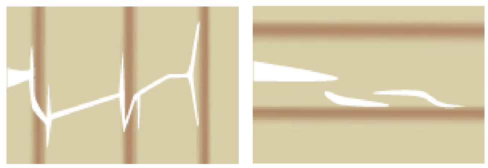

(a) (b)

Figure 3.13 *Pictorial representation of transverse crack propagation through osteons, with crack deflections in the longitudinal direction (a), and crack bridging (b). Figure adapted from Koester et al., 2008.*

Interestingly, in Figure 3.11 (left, column 1) the 1-day old specimen showed this type of crack propagation along the line of maximum principal stress. The failure description provided by Cheong et al., 2008 provides evidence to support that while the spiral fracture depicted in the figure is generated primarily because of failure under tension due to the angled failure, that there are clear signs that transverse shear is also a contributing factor to this spiral fracture pattern.

When bone is weak in the longitudinal direction, microcracks are produced along the osteons, creating crack bridges as shown by Koester et al., 2008 (Figure 3.13b). Agreeing with Turner et al., 2001, and as seen in Figure 3.11 (right, column 3) and 2.12b, the longitudinal shear direction is weak. The weakening of the cement lining observed in Figures 3.5 and 3.6 is most likely the result of Haversian remodeling, which as Norman et al., 1996 has noted reduces bone strength, perhaps primarily longitudinal shear strength.

The current literature has contradicting data on torsional failure for immature long bones. Like the studies of Chapter 2, Cheong et al., 2008, and Taylor et al., 2003, have also noted longitudinal fracture components (Table 1). Additionally, as in the Chapter 2, Theobald et al., 2012 finds that high rate tests produce lower angle fractures (higher ratios) than those in low-rate tests (low ratios), when measured from the long-axis. Contradictory to the Chapter 2 and to that of Theobald et al., 2012, Cheong et al., 2008 produces composite fracture angles that are lower at higher rotational rates. Additionally, Taylor et al., 2003, reports a large-angle fracture under cyclic fatigue, which for the purposes of comparison, can be considered a very low rate test. Based upon this study of Chapter 3, the varying results of the literature may be explained when considering specimen age as it relates to the intrinsic material property values. For example, as specimen age was not reported by Taylor et al., 2003, it is possible that young and old specimens were mixed in the test population. This would explain why one photo reported in the study is of a 55-degree tensile failure (a suspected younger specimen), while another photo in the study has tensile and longitudinal components of fracture (a suspected older specimen).

In summary the current study attempted to document which mechanical properties were dependent on specimen age and loading rate using the immature porcine femoral model, and its potential effect on the torsional fracture ratio. The study has documented that alternating transverse and longitudinal shear properties may help to provide a mechanical reasoning for interpreting changes in the helical fracture pattern under torsional loading. As may be shown by

Figures 3.5 and 3.6, it is speculated that combined tensile and transverse shear failure results in lower fracture ratios under torsional loading (high fracture angles from long-axis), which can be a result of either young specimen age, and/or a low rate of twist. In turn, combined tensile and longitudinal shear failure results in higher fracture ratios under torsional loading (low fracture angles from long-axis), which can be attributed to an older specimen or a younger specimen failed at a high rate of twist. The current study is limited and could easily be expanded upon for future work. A wide spectrum of test ages from immature to mature bone can provide a better understanding of how bone properties change during maturation and development. Additionally, multiple displacement rates should be stratified like in the work of Theobald et al., 2012. Such an effect would have more clinical relevance if ever transitioned into a human study. Furthermore, this study neglected curvature effects of the bone specimen. A larger bone model such as from an ovine or bovine femur would eliminate this issue and would be closer to a human surrogate model. However, while the current study is limited in scope, it may still provide useful ‘ground-truth’ data from which immature bone failure mechanisms can be better understood.

APPENDIX

Table 3.1. *Summary table of immature torsional data in the literature*

study	low rate (deg/sec)	composite fracture angle (deg)	fracture pattern	high rate (deg/sec)	composite fracture angle (deg)	fracture pattern	specimen age	specimen tested
Theobald	0.5	43	angled segment	90	31	angled segment	7 days	Bovine
Cheong	19.6	34.5	angled & vertical segments	196	41.5	angled segments & comminution	5 months	Ovine
Bertocci	0.17	x	x	90	x	x	3 months	Porcine
Taylor	cyclic failure (3 Hz)	55	angled & vertical segments	x	x	x	x	Bovine
Current Study	3	45.1	angled segment	90	31.67	angled segment	2 days	Porcine
Current Study	3	36.87	angled & vertical segments	90	30	angled segments & comminution	14 days	Porcine
Current Study	3	35.47	angled & vertical segments	90	28.93	angled segments & comminution	22 days	Porcine

REFERENCES

REFERENCES

Bertocci G, Thompson A, and Pierce MC. Femur fracture biomechanics and morphology associated with torsional and bending loading conditions in an in vitro immature porcine model. *J Forensic Leg.* 2017; 52:5-11.

Carty HM. Fractures caused by child abuse, *J Bone Joint Surg Br*. 75(6) (1993) 849-57.

Cheong VS, Karunaratne A, Amis AA, and Bull AMJ. Strain rate dependency of fractures of immature bone. *J Mech Behav Biomed Mater*. 2017; 66:68-76.

Katsamenis OL, Andriotis OG, and Thurner P. Load-bearing in cortical bone microstructure: Selective stiffening and the heterogenoeus strain distribution at the lamellar level. *J Mech Behav Biomed Mater*. 2012; 17:152-165.

Koester KJ, Ager JW, and Ritchie RO. The true toughness of human cortical bone measured with realistically short cracks. *Nat Mater*. 2008; 7:672-677.

Kress TA. Impact biomechanics of the human body [dissertation]. Knoxville (TN): Univ. of Tennessee, 1996.

Nalla RK, Stölken JS, Kinney JH, and Ritchie RO. Fracture in human cortical bone: local fracture criteria and toughening mechanisms. *J Biomech*. 2005; 38:1517-1525.

Norman TL, Nivargikar SV, and Burr DB. Resistance to crack growth in human cortical bone is greater in shear than in tension, *J Biomech* 29(8) (1996) 1023-31.

Pierce MC, Bertocci GE, Vogeley E, and Moreland MS. Evaluationg long bone fractures in children: a biomechanical approach with illustrative cases. *Child Abuse Negl*. 2004; 28(5):505-24.

Porta D.J. (2005) Biomechanics of Impact Injury. In: Rich J., Dean D.E., Powers R.H. (eds) Forensic Medicine of the Lower Extremity. *Forensic Science and Medicine*. Humana Press
Shukla A, and Dally JM. 2014. Experimental solid mechanics.

Tadano S, and Giri B. X-ray diffraction as a promising tool to characterize bone nanocomposites. *Sci. Technol. Adv. Mater*. 2011; 12(064708): 1-11.

Taylor D, Reilly PO, Vallet L, and Lee TC. The fatigue strength of compact bone in torsion. *J Biomech*. 2003; 36:1103-1109.

Theobald PS, Qureshi A, Jones MD. Biomechanical investigation into the torsional failure of immature long bone, *J Clin Orthop Trauma.* 3(1) (2012) 24-7.

Turner CH, Wang T, Burr DB. Shear strength and fatigue properties of human cortical bone determined from pure shear tests, *Calcif Tissue Int.* 69(6) (2001) 373-8.

Vashishth WT. Damage mechanisms and failure modes of cortical bone under components of physiological loading. *J. Orthop. Res*. 2005; 23:1047-1053.

CHAPTER FOUR: AGE EFFECTS ON BENDING FRACTURE PATTERNS IN OVINE FEMORA UNDER CONCENTRATED FOUR-POINT BENDING

ABSTRACT

Most research regarding bending of long bones focuses on a 3-point bending model. Under 3-point bending the bone typically fails directly under the point of loading, initiating as a transverse crack on the tensile surface of the bone. This transverse crack then branches out into a Y-shape pattern at approximately the midline of the bone with the two-branching fracture lines reaching out to either side of the loading point on the compressive side of the bone. This so-called tensile wedge is so prevalent that forensic practitioners commonly cite this fracture pattern as an indication of impact direction. The practice is problematic, however, as there appears to be a sub-class of bending that can produce reverse tensile wedges (compression wedges). Martens et al., 1986 performed a four-point loading test configuration where the lower supports are set to 60% of the bone length, and the inner-loading probes are set to 10% of the bone length. This is considered a concentrated loading scenario, as the inner loading probes under four-point bending are typically set between 40-50% of the bone length (Diab et al., 2006, Lanyon et al., 1979, and Quinn et al., 2009). Under these concentrated conditions Martens et al., 1986 documented that 85% of the human femora tested failed in the middle of the bone in a Y-shape. However, the Y-shape fracture pattern possessed a transverse fracture on the loading side of the bone, with the branching fractures connecting to the non-loading side of the bone, which is opposite to that produced and most commonly reported under a three-point bending configuration. The current study tested twenty ovine femora with (n=10) femora classified as mature (1-2 years of age) and another group (n=10) femora classified as immature (1 day – 1 week old). Within the mature testing group 7 specimens were tested at low rate and 3 were tested at high rate. All young

specimens were tested at a low rate. In general, old specimens under the Martens et al., 1986 loading conditions produced near-exclusive reverse tensile wedge fractures, while younger specimen commonly produced transverse fractures. Additionally, stress distributions were created for specimen-specific models from the young and old ovine femur groups. This was done by rendering a volumetric model from CT-scans, in mimics, and then applying experimentally-defined loading and boundary conditions to the model in Abaqus. The two models produced reasonable stress distributions that might help explain the fracture patterns generated in these experiments. The study demonstrated that specimen age affects the resultant fracture pattern under a concentrated, four-point bending test, and attempts to provide an explanation for the patterns using a basic finite element approach.

INTRODUCTION

Most research in forensic biomechanics of long bones is based on a 3-point bending model. The side of the bone that undergoes loading generates compressive stresses while the opposite side of the bone is in tension (Pierce et al.,2004, Gardener et al., 2010). Under 3-point bending the bone typically fails directly under the point of loading where the bending moment is highest, initiating as a transverse crack on the tensile surface of the bone. This transverse crack then branches out into a Y-shape pattern at approximately the midline of the bone, with the two-branching fracture lines reaching out to either side of the loading point on the compressive surface of the bone (Reber and Simmons, 2015). This wedge-shaped pattern of fracture is described as shear failure of the bone on its compressive side (Ebacher et al., 2007)

In forensic terminology these wedge-shaped fracture patterns are known as butterfly fractures. The tensile wedge is commonly used by forensic practitioners as an indication of impact direction (Kress et al., 1996, Porta et al., 2005, and Isa et al., 2015). This practice is problematic, however, as there are cases, and studies where reverse tensile wedges (also known in the literature as compression wedges) are produced. Reverse tensile wedges are defined as a transverse fracture on the compressive side of the bone with branching failure on the tensile side of the bone. In 1986, Levine et al. first noted these types of wedge fractures as common in automobile accidents where impacts to the tibia by car bumpers often produced reverse wedges in the fractured long bone. Kress et al., 1996, whom first recommended tensile wedges to be good indicators of impact direction, also noted reverse tensile wedges in some leg impact studies, deeming the pattern “an extremely uncommon pattern for long bones”, and one to be generally ignored. However, Martens et al., 1986 demonstrated nearly exclusive reverse tensile wedge fractures when loading human femur bones at a low rate, under a rather concentrated four-point bending scenario. More recently Reber and Simmons, 2015 report 40% complete wedge patterns as reverse tensile wedges using the sheep femur. It has therefore become clear in the literature that the reverse tensile wedge is not a failure mode to be ignored, but its mechanism has not been well studied.

As stated by Passalacqua and Fenton et al., 2012, it is imperative that forensic practitioners “move beyond our reliance on experience as the only way to inform us in the analysis of trauma”, and that there is a great “need to establish baseline parameters on how bones break in numerous scenarios”, moving towards a “science of trauma that involves hypothesis testing”. It is therefore forensically relevant to determine how this reverse tensile wedge might have been consistently produced under a Martens-type concentrated 4-point loading configuration.

Vaughan et al., 2016 has recently demonstrated in torsion tests on long bones that there are age and rate of loading effects influencing the generated spiral fracture patterns. It may therefore be important to determine what effects, if any, specimen age and rate of loading may have on the production of potential reverse tensile wedge produced under the 4-pt test configuration of Martens et al., 1986.

In the current study mature and immature ovine femurs were used to study the effects of age and rate of loading on the generation of reverse tensile wedges. The objectives of the study were to execute controlled, concentrated Martens-type 4-point bending tests on ovine femora to identify fracture patterns in association with specimen age and rate of loading. Furthermore, a simplified finite element (FE) modeling effort was conducted to understand the mechanism of reverse tensile wedges types of long bone fracture versus tensile wedges (Vaughan et al., 2017).

METHODS

Twenty ovine femora were tested with (n=10) femora classified as mature (1-2 years of age), and another group (n=10) of immature (1 day – 1 week old) femora. The specimens were collected by Colorado State University, dissected and cleaned of excess soft tissues, immediately wrapped in saline-soaked gauze to prevent dry-out of the bone (Wieberg et al., 2008), and frozen at -20°C before being shipped on ice from Colorado State to Michigan State University. Once received, specimens were immediately transferred to a freezer at a temperature of -20°C. All specimens for this study were from animals sacrificed for another research study.

A custom-built four-point bending fixture (Figures 4.1 and 4.2) was used to test freely supported ovine femora under a Martens-type concentrated 4-point bending configuration. In this test the two outer supports were set to 60% of the specimen bone length, and the testing distance of the inner loading-probes was set to 10% of the specimen length (Figure 4.1). It was important for both loading points to contact the bone at the same time to produce accurate results (Beaupied et al., 2007). To achieve this, the load fulcrum was set in place with a pin. A small pre-load of approximately 2 Newtons was applied to the bone to ensure initial contact of the loading probes with the bone shaft. Furthermore, specimen supports needed to be fairly-smooth and rounded to minimize stress concentrations at the point of contact (Beaupied et al., 2007). This was achieved by setting an external diameter to the inner probes of 6.4 mm and 5.40 mm (Figure 4.1 and 4.2 respectively), and by setting a smooth inner groove to the free-rotating supports of 11mm length, 2.60 mm width, and a 2 mm radial depth at its deepest (Figure 4.1). The free-rotating supports for the fixture in Figure 4.2 were set to a 5mm width, and a 1.8mm radial depth at its deepest.

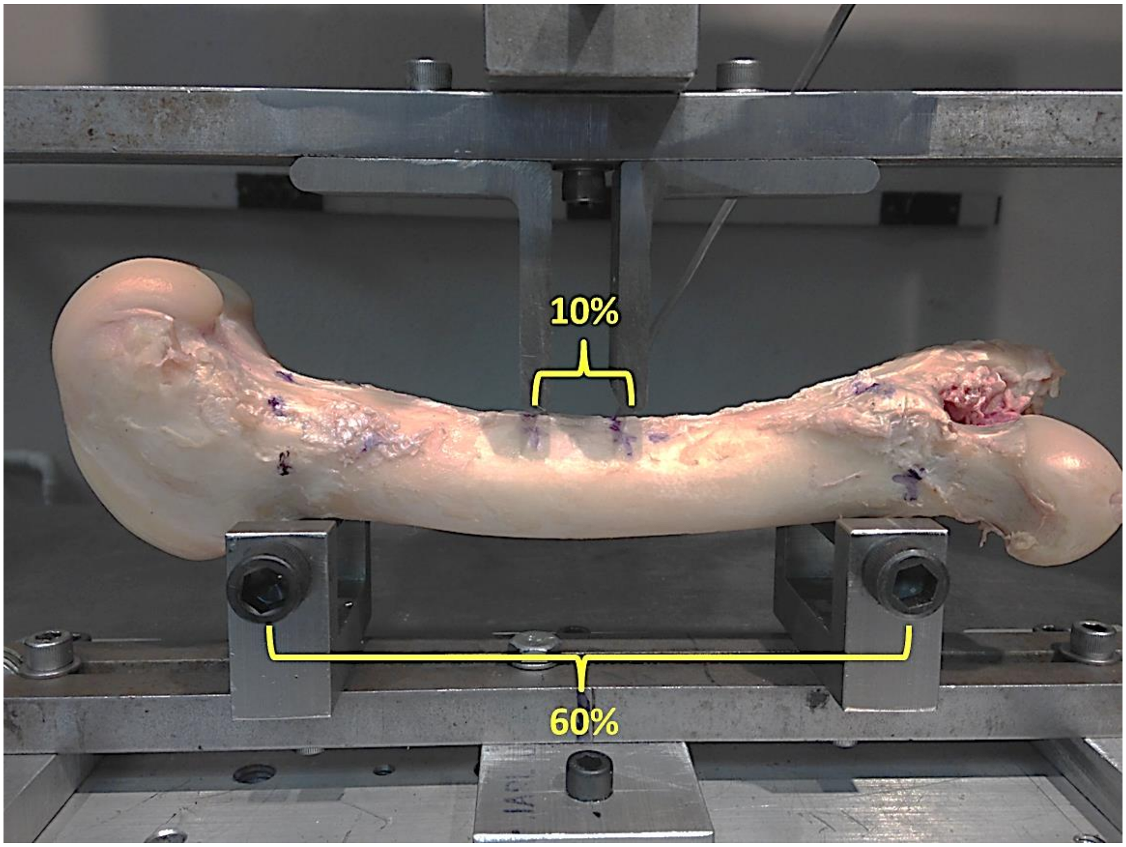

Figure 4.1 *Photograph of the concentrated four-point bending configuration based on the previous study by Martens et al., 1986 for old specimens.*

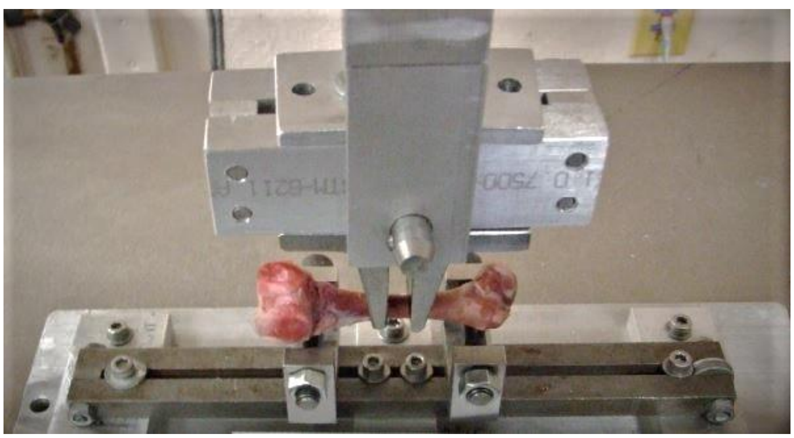

Figure 4.2 *Photograph of the concentrated four-point bending configuration based on Martens et al., 1986, for young specimens.*

Each specimen was loaded until failure in a servo-hydraulic testing machine (model 1331, Instron Corporation; Norwood, MA). All specimens were failed at a rate of 2 Hz with a 5 mm haversine wave, except for three of the old specimens which were used as a pilot study for these experiments and loaded at a rate of 2 Hz with a 20 mm haversine wave. Force-time data was collected using a 500-lb force transducer (model 1010AF-500, Interface; Scottsdale, AZ) for young specimens. For old specimens a 2500-lb load cell (model 1010-AF-2.5K-B, Interface; Scottsdale, AZ) was utilized. All bones were loaded on the posterior side of the bone (Figure 4.2). The experiments were filmed with a high-speed camera at 40,000 fps to capture the fracture initiation and propagation. After fracture, they were photographed to document gross fracture morphology.

Prior to mechanical tests a whole-bone CT scan was taken of one bone specimen from each of the old and young groups. These 3D images were processed using volumetric techniques in Mimics (Mimic Technologies Inc., Seattle WA) (Figure 4.3), given a tetrahedral mesh in 3-matic (Materialise, Leuven, Belgium) (Figure 4.4), and imported into ABAQUS 6.11 (Dassault Systemes, Waltham, MA) where loads and boundary conditions were applied to simulate the above-mentioned 4-point bending tests (Figure 4.5). A representative bone specimen was selected for both the young and old groups, and material property values were set to those determined from the current experiments, as described below and given in Table 1. A basic impact was simulated by placing vertical displacement constraints at the supports, static-loading at the loading points, and preventing out-of-plane motion (Figure 4.5).

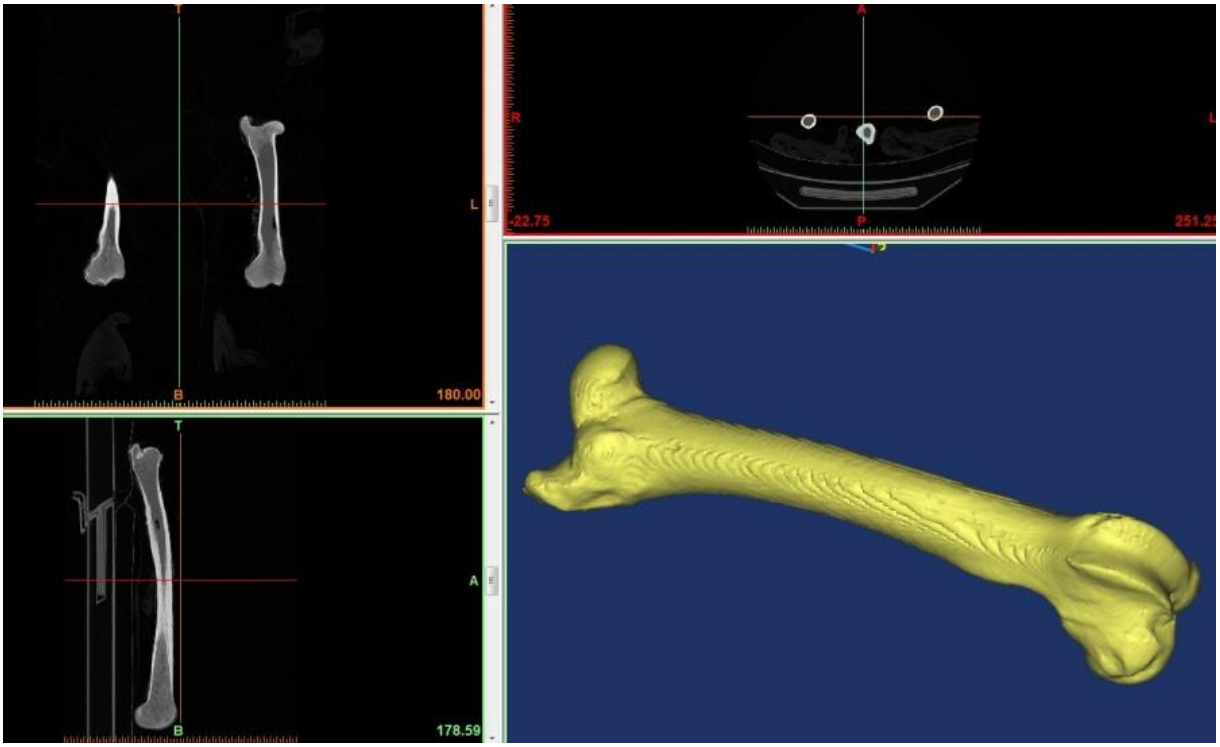

Figure 4.3 *Screen capture of 3D image reprocessing in Mimics.*

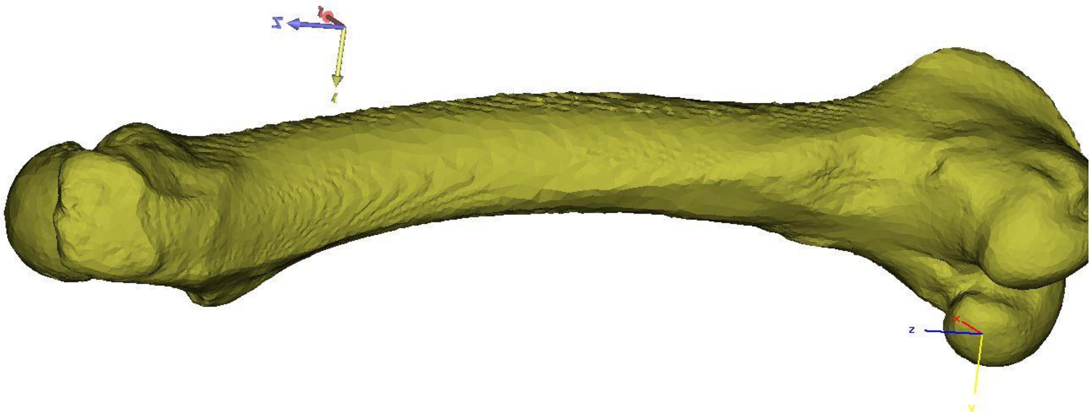

Figure 4.4 *Screen capture of volumetric meshing of bone in 3-matic.*

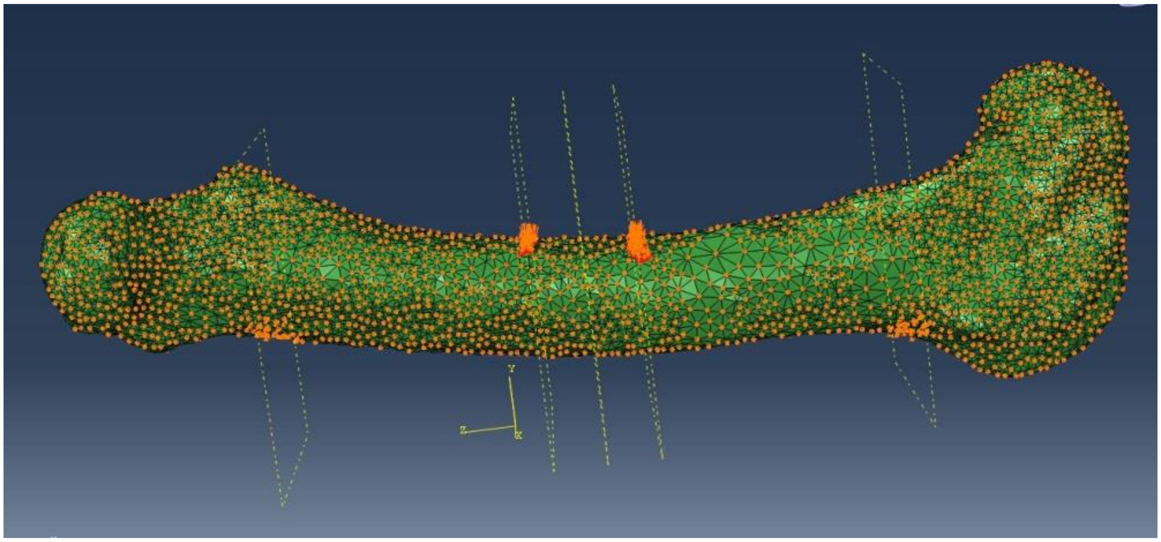

Figure 4.5 *Screen capture of loads and boundary condition applied to the model in Abaqus.*

Classical beam theory was utilized in the study to determine the material bone properties of representative young and old specimens (Rusme 1998). Under generalized four-point bending theory it is assumed that between the point loads there is a constant applied bending moment, with no developed shear stresses. Between the outer supports and the inner probes, the bending moment gradually increases and there are shear stresses developed (Figure 4.6). While Martens-type concentrated four-point bending has of yet no standardized mechanical description, the generalized case will be utilized to obtain approximated values.

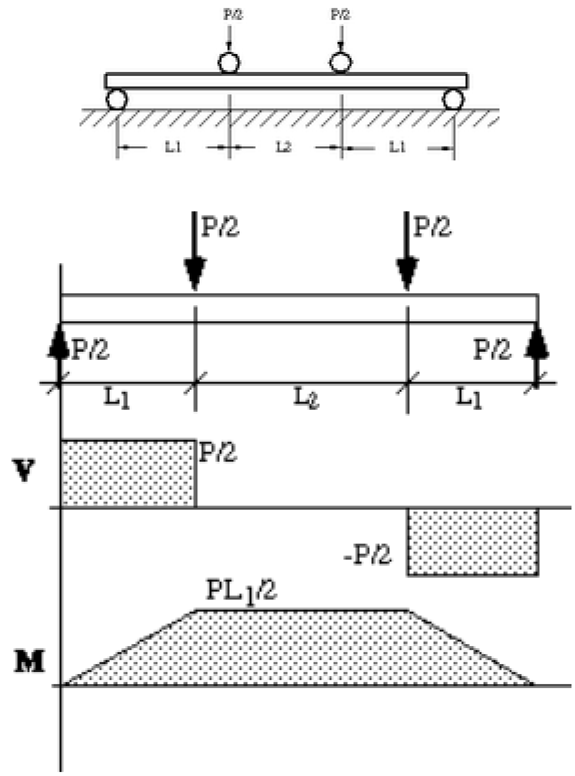

Figure 4.6 *Graphical representation of a standard four-point bending test, taken from Rusmee 1998.*

The bending moment of inertia for each bone was assumed to be elliptical and was calculated using the expression

$$I = \frac{\pi}{4}\left(a_o {b_o}^3\right) - \frac{\pi}{4}\left(a_i {b_i}^3\right) \tag{4.1}$$

where I is the bending moment of inertia in millimeters to the fourth power, a_o is the average anterior-posterior outer diameter in millimeters, b_o is the average medial-lateral outer diameter in millimeters, a_i is the average anterior-posterior inner diameter in millimeters, and b_i is the average medial-lateral inner diameter in millimeters. The moment arm was defined using the expression

$$x_m = \frac{L_o - L_i}{2} \tag{4.2}$$

where x_m is the moment arm in millimeters, L_o is the distance between outer supports in millimeters, and L_i is the distance between loading points in millimeters. The maximum bending moment is given as

$$M = \frac{F_{max\ elastic}}{2} * x_m \tag{4.3}$$

where M is the maximum bending moment in Newton-millimeter, $F_{max\ elastic}$ is the maximum elastic force in Newtons based on the linear regression, and x_m has been previously defined. The estimated bone tensile elastic modulus was calculated with the expression (Christoforo et al., 2012)

$$E = \frac{F_{max\ elastic} * (3 * {L_o}^2 - 4 * {L_i}^2) * L_i}{\Delta x * 4 * I} \tag{4.4}$$

where E is the estimated bone tensile elastic modulus in megapascals, Δx is the displacement of the bone based on the displacement recorded from the machine actuator in millimeters, $F_{max\ elastic}$ is the maximum elastic force in Newtons based on the linear regression, and all other terms have been previously defined. The bending failure stress was calculated by the expression

$$\sigma_{bending} = \frac{F_{max\ elastic} * x_m * a_o}{2 * I} \tag{4.5}$$

where $\sigma_{bending}$ is bending stress in megapascals, and all other terms have been previously defined. The energy absorbed by the bone to failure was expressed as

$$E_{input} = \frac{F_{max\ elastic}}{2} * \Delta x \tag{4.6}$$

where E is the energy of the bone in Joules after converting the displacement (Δx) from millimeters to meters. The initial stiffness of the bone is expressed as

$$k = \frac{F_{max\ elastic}}{\Delta x} \tag{4.7}$$

where k is the initial stiffness of the bone in Newton/millimeters, $F_{max\ elastic}$ is the force change in the elastic regime of the bone, and Δx is the displacement of the beam at the inner probe. Elastic modulus values and initial stiffness values were taken as linear regression over the elastic region of the plots of stress/strain and force/displacement respectively (Figure 4.7). It is important to note that the initial non-linear region in the data, below about 1.5% strain and below approximately 0.5mm displacement (Figure 4.7), is a result of the loading points adjusting themselves with the pivoting fulcrum to the bone's asymmetric surface for equal loading. The fulcrum prior to testing was visually lowered to the bones surface for alignment purposes, and the small 2N pre-load was applied to prevent slipping of the bone on the point supports during testing. Once the test initiated, the fulcrum initially adjusted, and this action coincided with the initial non-linear section of the data. Once there was an equal load under each of the points, the bone responded linearly, and this explains why the initial section of the data is excluded from the elastic linear regression fitting. For the most part this action was hypothesized and not experimentally validated in the current study.

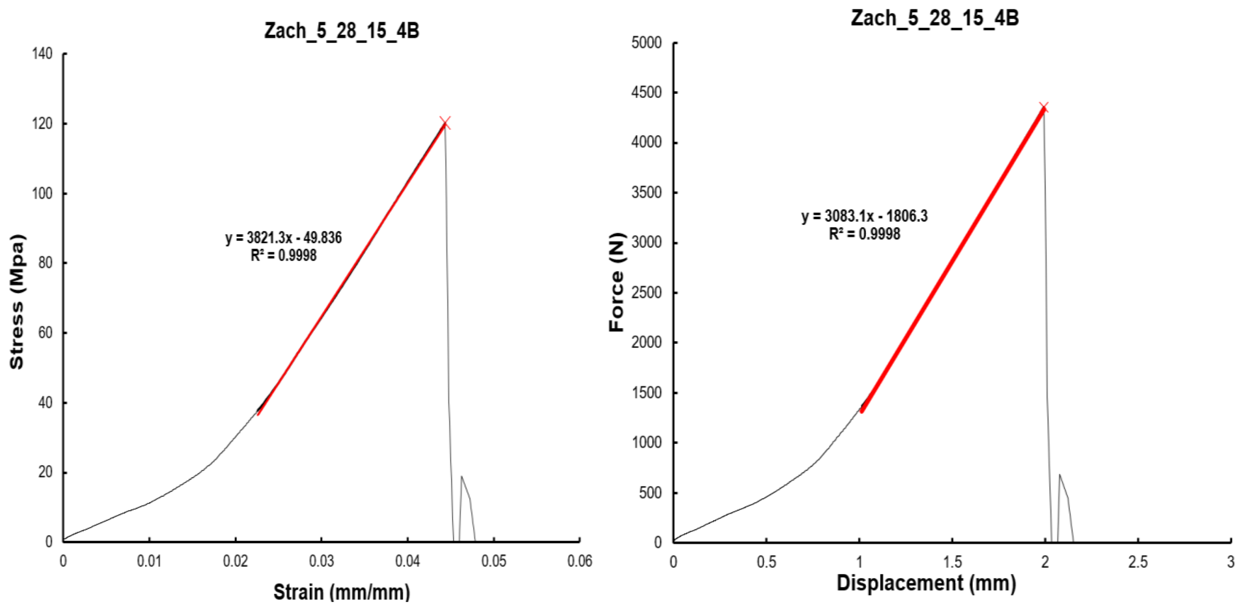

Figure 4.7 *Graphical determination of elastic modulus (left) and initial stiffness values (right).*

STATISTICAL METHODS

A general linear ANOVA was performed in Minitab 18 (State College, PA) to compare the effect of initial bone stiffness, elastic modulus, bone displacement to failure, and failure forces against specimen age (young/old). All statistical analyses used an alpha-criterion of 0.05.

RESULTS

Twenty ovine femora were tested with (n=10) femora classified as mature (1-2 years of age), and (n=10) femora classified as immature (1 day – 1 week old). Within the mature testing group, 7 specimens were tested at low rate and 3 were tested at high rate. All young specimens were tested at a low rate. Of the old specimens tested at a low rate, 6/7 produced a reverse tensile wedge pattern, while 1/7 produced an oblique pattern (Appendix 1). In the group of old specimens tested at a high rate 1/3 produced a tensile wedge pattern, and 2/3 produced oblique patterns. In the young group of specimens 6/10 produced transverse fractures, while 4/10 produced partial tensile wedges (Appendix 1).

The stiffness's of the three groups of bones (old high rate, old low rate, and young low rate) were significantly different ($p=0.0001$), with the old high rate specimens having the greatest initial stiffness at 3404 ± 895 N/mm, the old low rate specimens generating an initial bone stiffness of 2771 ± 269 N/mm, and the young low rate specimens generating an initial bone stiffness of 230.30 ± 111.30 N/mm. The elastic modulus based on the terminal linear range of response, was also a statistically significant parameter ($p=0.0001$). The older specimens were not statistically different from one another between test rates, however, the older specimens had a significantly higher modulus value of 3.41 ± 0.71 GPa compared to that of the young low-rate test specimens 0.77 ± 0.31 GPa. The failure strength of the bone was not statistically different between the young and old test groups. The bone's failure strength under bending was 107.85 ± 26.47 MPa.

In the old group of specimens, reverse tensile wedge fractures were captured on a high-speed camera. The fracture was shown to initiate on the non-loading (tensile side) of the bone with fracture initiation generated simultaneously in the areas between the loading point and support point at an angle theta. The fracture then propagated along the long-axis of the bone, meeting and finally propagating as a transverse crack on the loading side (compressive side) of the bone (Figure 4.8).

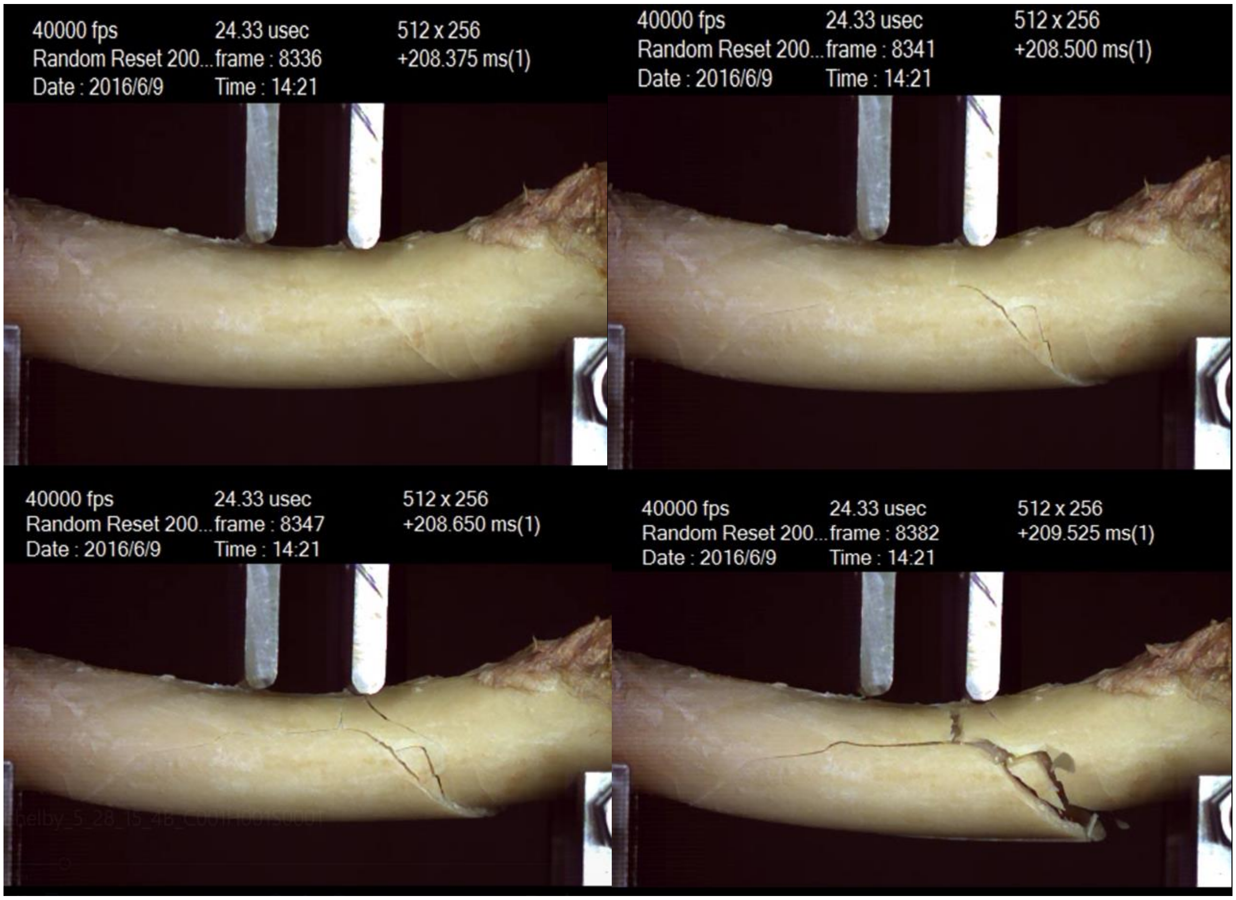

Figure 4.8 *High-speed capture of specimen Shelby_5_28_15_4B, showing fracture initiation (top left) on the tensile side of the bone, to fracture propagation (bottom right) on the compressive side of the bone.*

The oblique fractures were also captured using the high-speed camera. It was shown again that these fractures initiated at approximately the outer support on the distal end of the bone and propagated towards the loading probe. Interestingly, a fracture line along the long-axis of the bone was recorded, like that seen in the compressive wedge failure (Figure 4.9).

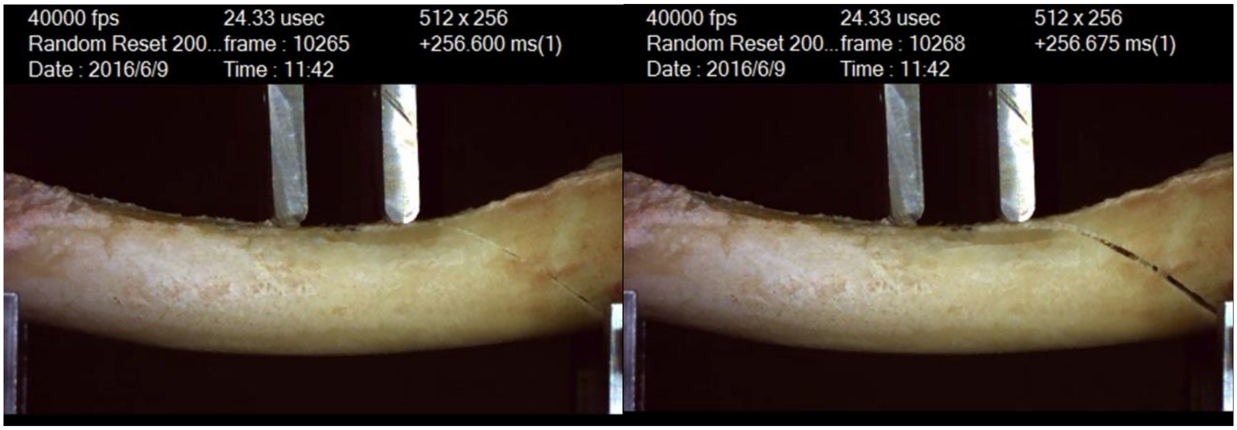

Figure 4.9 *High-speed capture of specimen Zach_5_28_15_4B, showing fracture initiation (left) and fracture propagation (right).*

In the young group of specimens, transverse failure and partial tensile wedge fractures were generated in these experiments. The transverse failure was shown to initiate on the tensile side of the bone directly between the two loading points, with the fracture propagating up towards one of the loading points (Figure 4.10). The partial tensile wedge failure pattern was shown to initiate between the two loading points, branching into a typical Y-pattern. However, only one side of the branch connected to the compressive side of the bone (Figure 4.11).

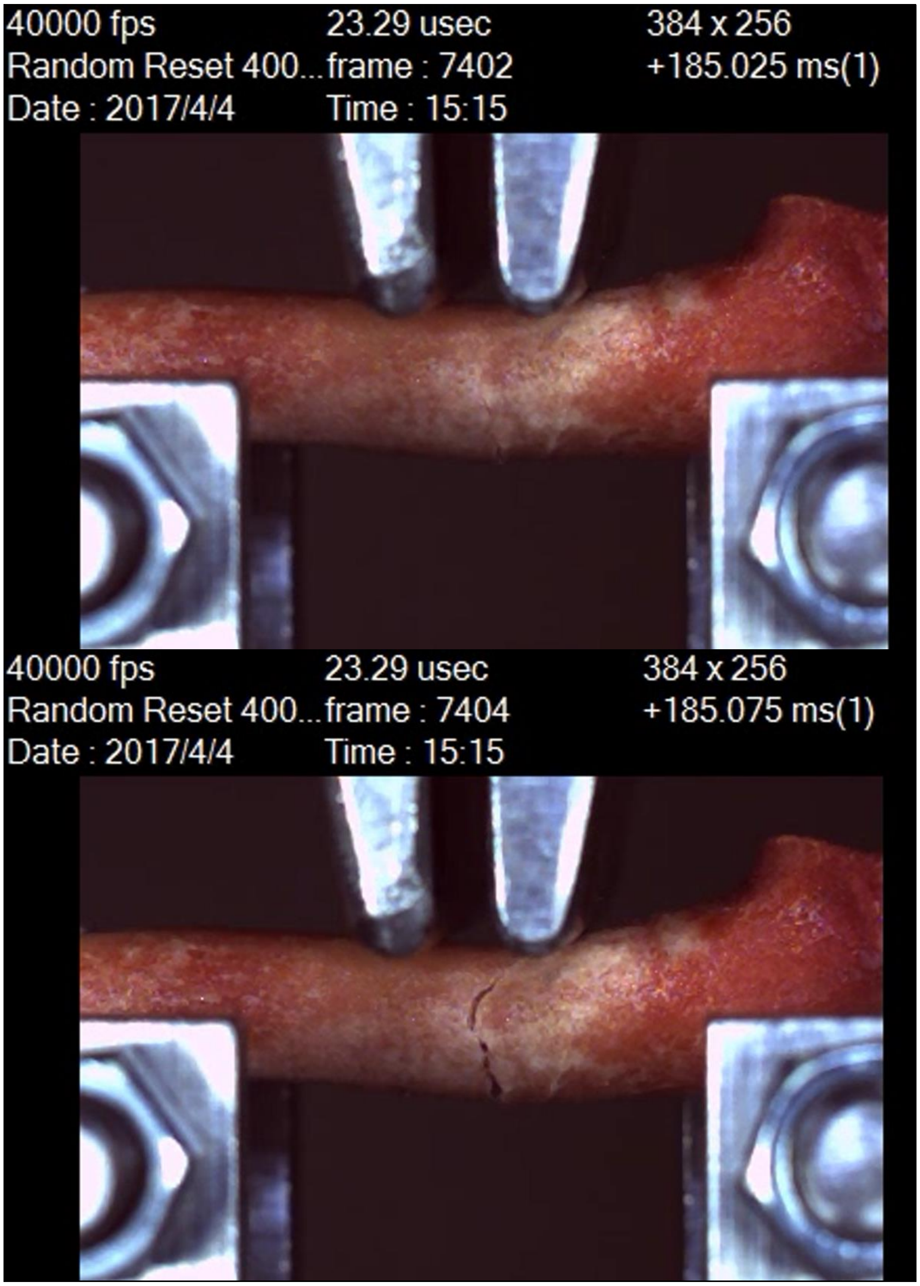

Figure 4.10 *High-speed capture of specimen SF3R4B, showing fracture initiation (top) and fracture propagation (bottom).*

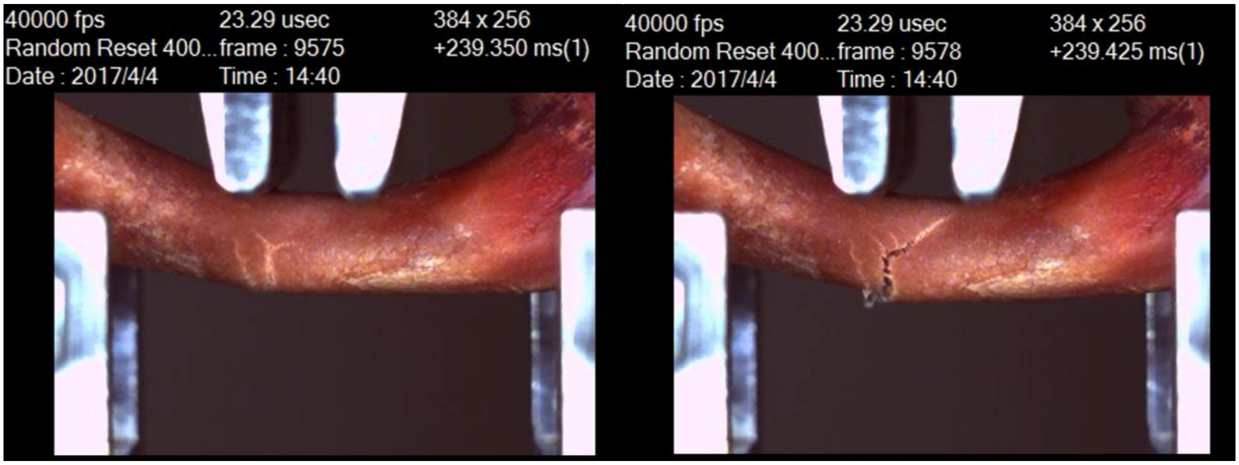

Figure 4.11 *High-speed capture of specimen SF5R4B, showing fracture initiation (left) and fracture propagation (right).*

Analysis of the specimen-specific maximum principal stresses under finite element modeling showed the potential stress distribution observed over the bones surface when loaded under a Martens-type configuration. The old group of specimens was represented by *Shelby_5_28_15_4B.* The model showed high tensile stresses near the support points which were shown to exist at some angle theta. Interestingly, there was a mixture of large compressive and tensile stresses generated directly under the applied loading points. These longitudinally-oriented tensile stresses under the loading points may explain the generation of a transverse fracture on the loading surface. Under the assumption that fracture lines are generated perpendicular to high principal (tensile) stresses (Chen, 2007), the experimental results appear to be comparable to the stress distribution generated under FE modeling (Figure 4.12). It is important to note however, that the data generated under FE modeling was only intended to illustrate what a relative stress distribution under these experimental loading conditions may look like prior to actual bone fracture.

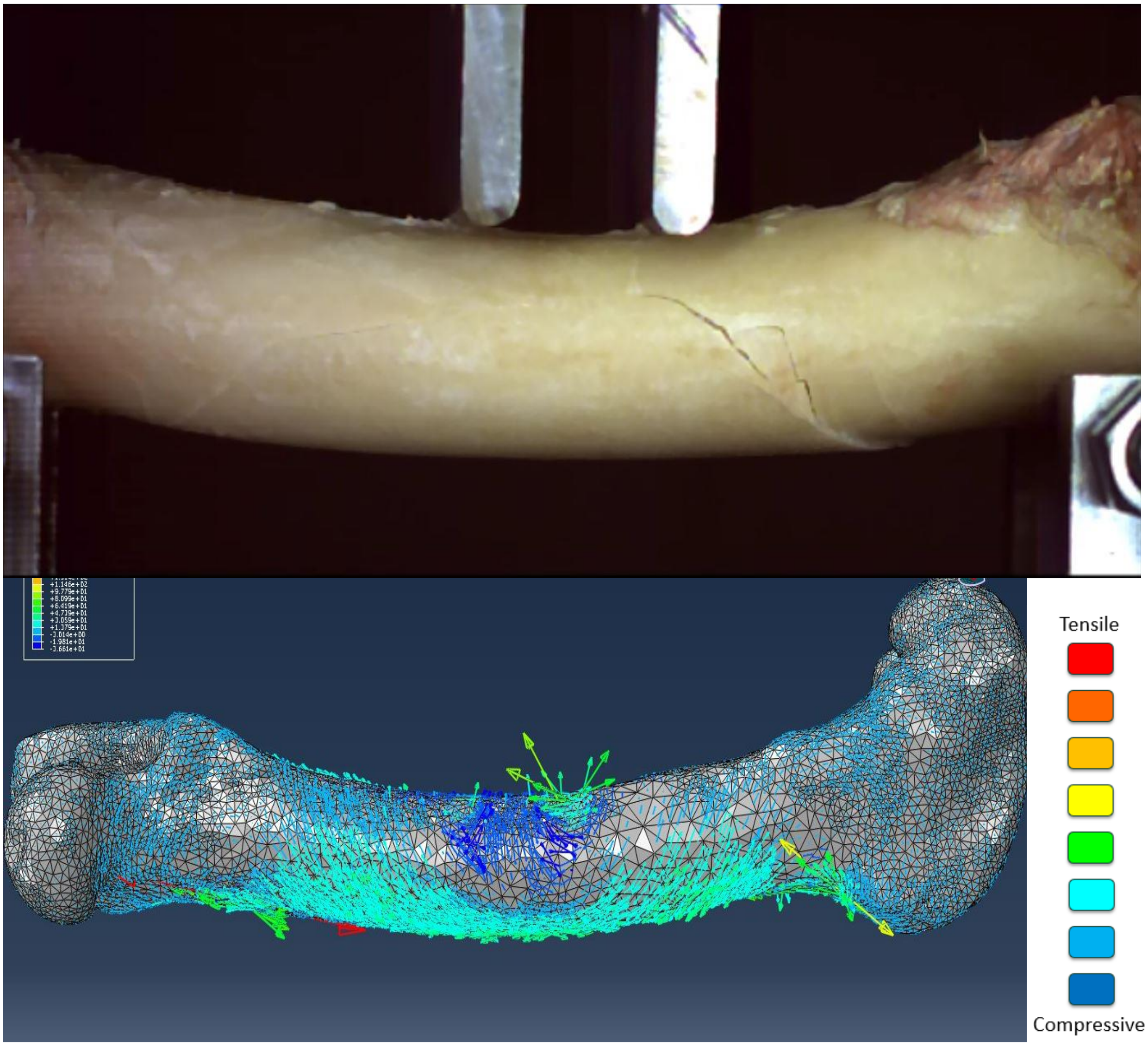

Figure 4.12 *Experimental high-speed capture (top) and maximum principal stress distribution, generated with FE modeling (bottom).*

The young group was represented by specimen *SF3L4B.* The model showed high tensile stresses generated within the loading region, with high compressive stresses generated at the loading surface. Under the assumption that fracture lines are generated perpendicular to high principal (tensile) stresses (Chen, 2007), the experimental results appear to be comparable to the stress distribution generated under FE modeling (Figure 4.13). It is important to note as before, that the data generated under FE modeling was only intended to illustrate what a relative stress distribution under these experimental loading conditions may look like prior to actual bone fracture.

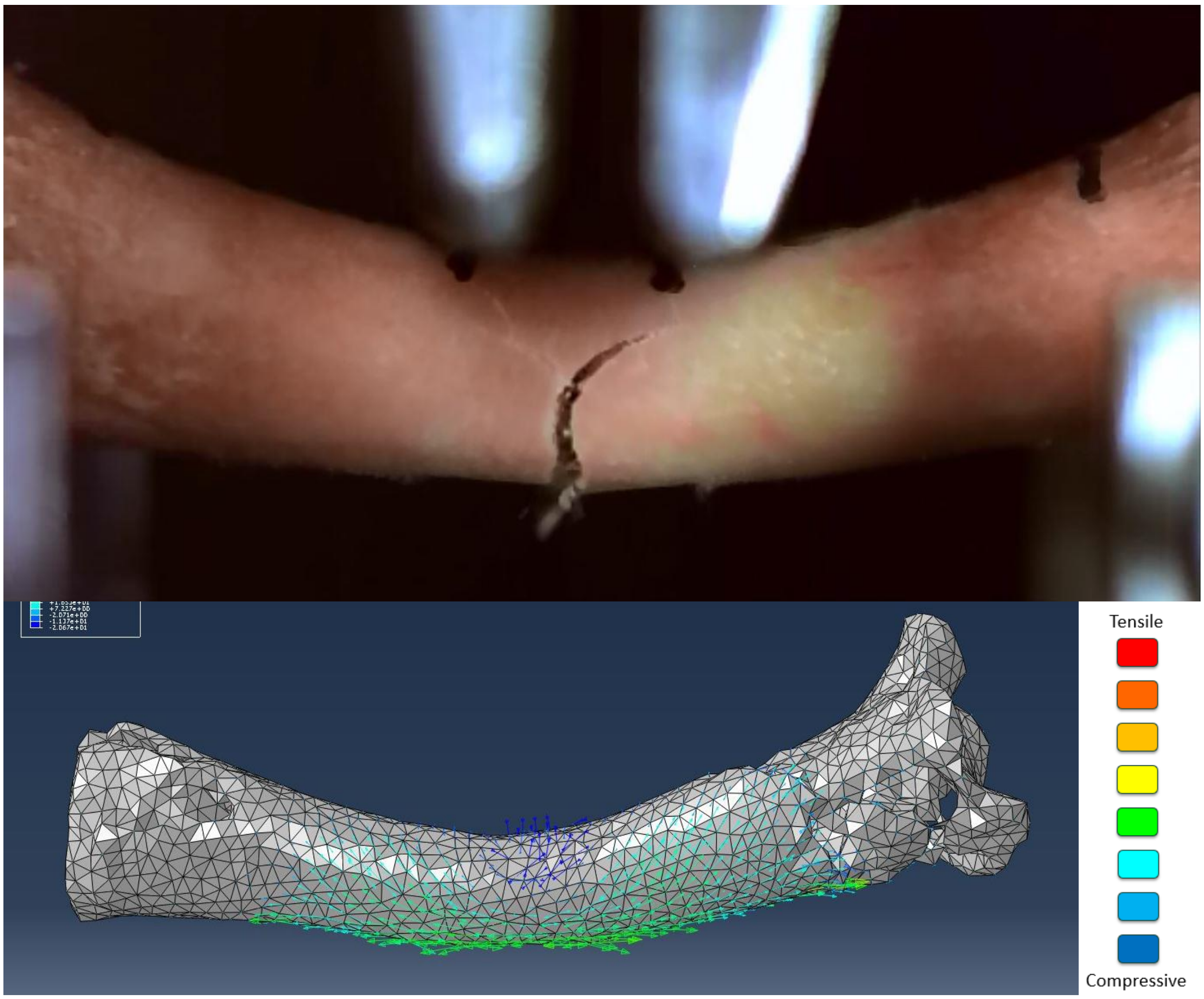

Figure 4.13 *Experimental high-speed capture (top) and maximum principal stress distribution, generated with FE modeling (bottom).*

DISCUSSION

The aim of the current study was to perform a Martens-type 4-point bending test on both young and old specimens, to evaluate if the resultant fracture pattern differed with specimen age. Biomechanical data was generated, demonstrating that the fracture pattern was significantly different between the young and old testing group. The second aim of the study was to investigate what the potential principal (tensile) stress distribution looked like under the experimentally tested Martens-type loading. For comparison purposes models were also generated for a typical 3-point bending configuration and under a typical 4-point bending configuration.

In Appendix 1, finite element models were generated under the two typically reported loading scenarios in the forensic literature of three-point bending and four-point bending (with a loading point at midpoint of the bone, and loading-points oriented at 40% of the bone length respectively), and under the Martens-type configurations using the mature bone model Shelby_5_28_15_4B. All parameters were kept the same between models. As seen in Figure 4.19 of Appendix 1, under three-point loading high tensile stresses were generated directly under the point of impact on the non-loading side of the bone, with large compressive and some tensile stresses generated directly under the loading point on the loading side of the bone. Under typical three-point bending, a tensile wedge pattern of fracture is expected under such a stress-distribution. It is currently believed that the tensile wedge pattern is formed because a transverse fracture results from the high tensile stresses, and then two branching shear failures are then formed within the zone of compression. This result parallels with the forensic literature (Kress et al., 1996, Porta, 2005, and Isa et al., 2015). As seen in Figure 4.20 in Appendix 1, under typical four-point bending large tensile stresses are seen at both the supports on the non-loading side, and just outside the loading points on the loading side. Visually mapping fracture patterns as normal to the maximum tensile stresses, two sets of almost cubic-shaped fracture patterns are generated. In the forensic literature, typical four-point bending is associated with a segmented fracture pattern (Turek, 1994, and Kress et al., 1996), and this pattern tends to agree with the stress-distribution generated by the model. Martens-type loading then appears to be a special combination of both the three-point and four-point loading models. As seen in Appendix 1, Figure 4.21, large tensile stresses are generated between the supporting points and the loading points at some angle theta, like what is generated under the four-point model. However, as the loading points are concentrated at only 10% of the bone length, directly under the loading points there is a large concentration of compressive stress, like what is seen in the three-point bending model, with some local tensile stresses also generated directly underneath the right loading point. These large compressive stresses appear to act as a barrier against transverse crack propagation, and instead allow the fracture to propagate longitudinally along the cement line of the bone, which is known to be a weak crack path (Zimmerman et al, 2009 and Nalla et al., 2005), and is also the path that appears to be dictated by the tensile stress distribution. Interestingly, this path may also be dictated by longitudinal shear stress within the zone of compression. Finally, once the two opposing crack lines meet longitudinally, the pattern completes with a transverse fracture at an area of high tensile stress, generated directly underneath the right loading point in this instance.

As reverse tension wedges (compression wedges), require a large concentrated load spanning approximately 10% of the specimen length, this may explain why reverse tension wedges have previously not been consistently produced within the forensic literature. The most common loading-scenario tested, three-point bending, is too small of a concentrated load to produce the reverse tension wedge (compression wedge) pattern, and the typical four-point bending scenario has loads so widely dispersed, that they tend to act as two individual and simultaneous impacts, as opposed to a singular concentrated impact. This line of reasoning may then explain why the experiments of Reber and Simmons, 2015, generated a reverse tension wedge pattern while impacting bone with a large flat plate (Figure 4.14), and why Kress et al. managed to produce the pattern while impacting with a 10-cm steel impact pipe (Figure 4.15). Inadvertently, these experiments may have generated a large concentrated loading scenario, like what would be generated under Martens-type four-point bending. Further indicating that this fracture pattern may be more common than previously thought, as large flat impacts, or impacts by a curved surface could be representative of impacts by the bumper of a car, as first suggested by Levine et al., 1986 on tibial impacts by a car's bumper.

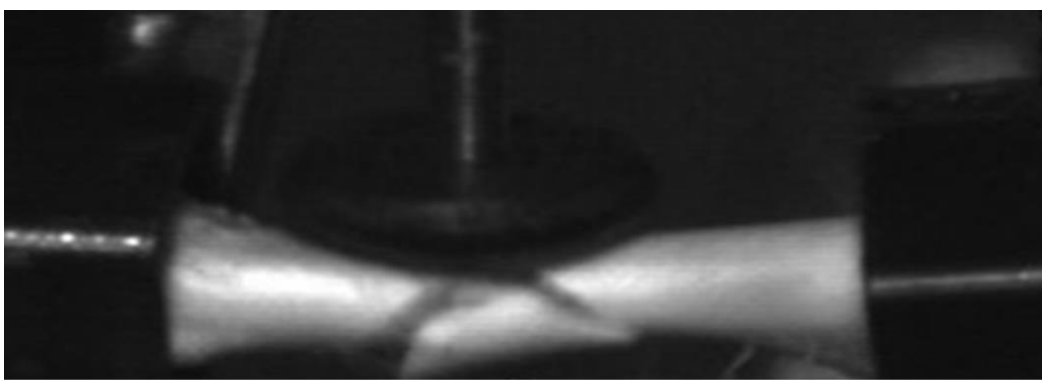

Figure 4.14 *Photograph of an impact scenario which produces reverse tensile wedges, taken from Reber and Simmons 2015.*

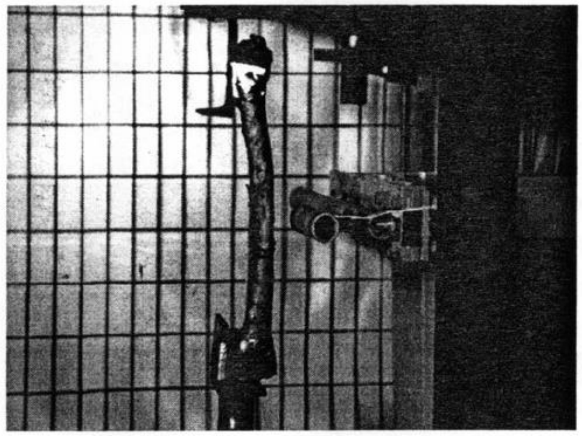

Figure 4.15 *Photograph of an impact scenario which produces reverse tensile wedges, taken from Kress et al., 1996.*

Interestingly, the reverse tensile wedge pattern was not generated for young specimen tested in the study. Instead, 60% of the specimen generated transverse fractures under low-speed conditions, with 40% of specimen tested generating incipient tensile wedge patterns as indicated in Figure 4.13 (top). These results appear to agree with a study by Cheong et al., 2017, whom investigated the effects of low, medium, and fast rates of loading on immature 5-month-old lamb tibiae using a 4-point bending configuration. The authors produced transverse failures in 100% of low-rate testing, with 3/8 transverse fractures produced in medium and high rate testing, 4/8 oblique fractures in the medium and high-rate tests, and 1/8 tensile wedge failure in the medium and high rate tests (Cheong et al., 2017). However, it is unclear what percentage of the specimen length the supports and loading points were held in the Cheong et al., 2017 study. Therefore, it is not clear if the results of the study are comparable to those performed using the concentrated, four-point Martens-type loading scenario of this current study.

A potential explanation for the transverse fracture generated under four-point bending at younger ages, is that as noted by Gosman et al., 2013, bone possesses a relatively circular geometry at younger ages, and becomes increasingly asymmetric at older ages. As is suggested by the stress distribution of the three-point bending model of old bone (Figure 4.19 in Appendix 1), and by the four-point bending model of young bone (Figure 4.13 (bottom)), the bones relatively uniform and circular geometry at younger ages may influence the uniformity of tensile stresses generated on the non-loading side of the bone. Uniformly generated tensile stresses of the young group may in turn allow for transverse fractures to be easily produced, due to the large propensity for fracture transversely across the bone. Conversely, due to the asymmetric geometry of the bone at older ages under concentrated four-point bending (Appendix 1, Figure 4.21), less uniformly distributed tensile stresses are generated under the loading points on the non-loading side of the bone, allowing for greater tensile stresses to be built up on the outer more curved sections of the bone by the supports. Thus, producing the reverse tensile wedge generated in the current study.

While more testing needs to be performed to verify potential rate effects under Martens-type four-point loading, it may be suggested from the Cheong et al., 2017 study, and from the old specimen tested here at a high loading rate, that tensile wedge fracture patterns may be produced at higher loading rates under Martens-type conditions. The reverse tensile wedge pattern produced here, may only be representative of low rate loading. This potential rate-effect will need to be investigated further in future work.

APPENDIX

Figure 4.16 *Photographs of specimen representative of variations in the fracture patterns, tested at a high rate of 2 Hz over a 20mm haversine displacement (from left to right; AbeL12_10_14_4B_HighRate, AbeR12_10_14_4B_HighRate, and ClaudeL12_10_14_4B_HighRate).*

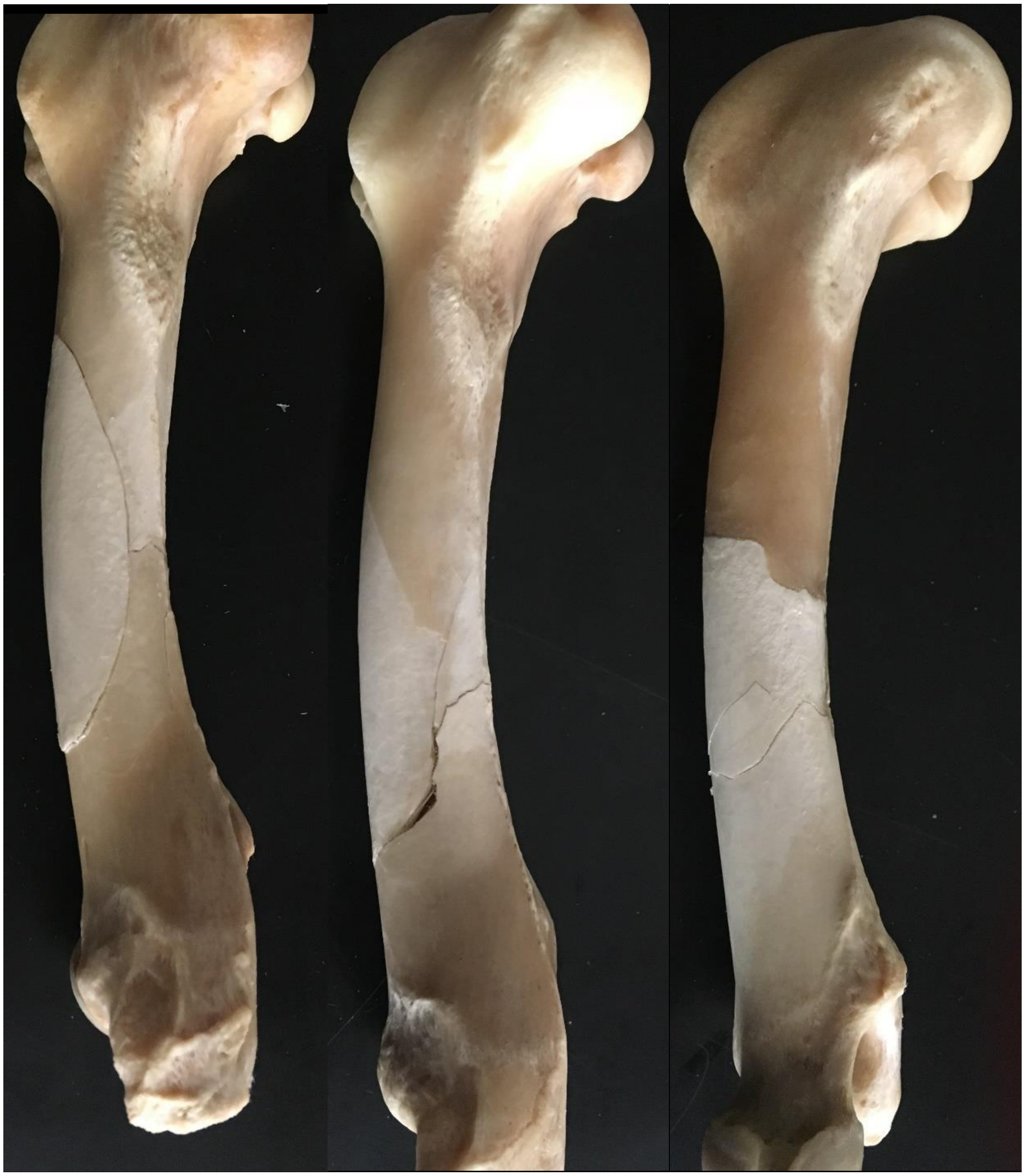

Figure 4.17 *Photographs of specimen representative of variations in the reverse tensile wedge pattern, tested at a low rate of 2 Hz over a 5mm haversine displacement (from left to right; Shelby_5_28_15_4B, Ryan_5_28_15_4B, and Lindy_5_28_15_4B).*

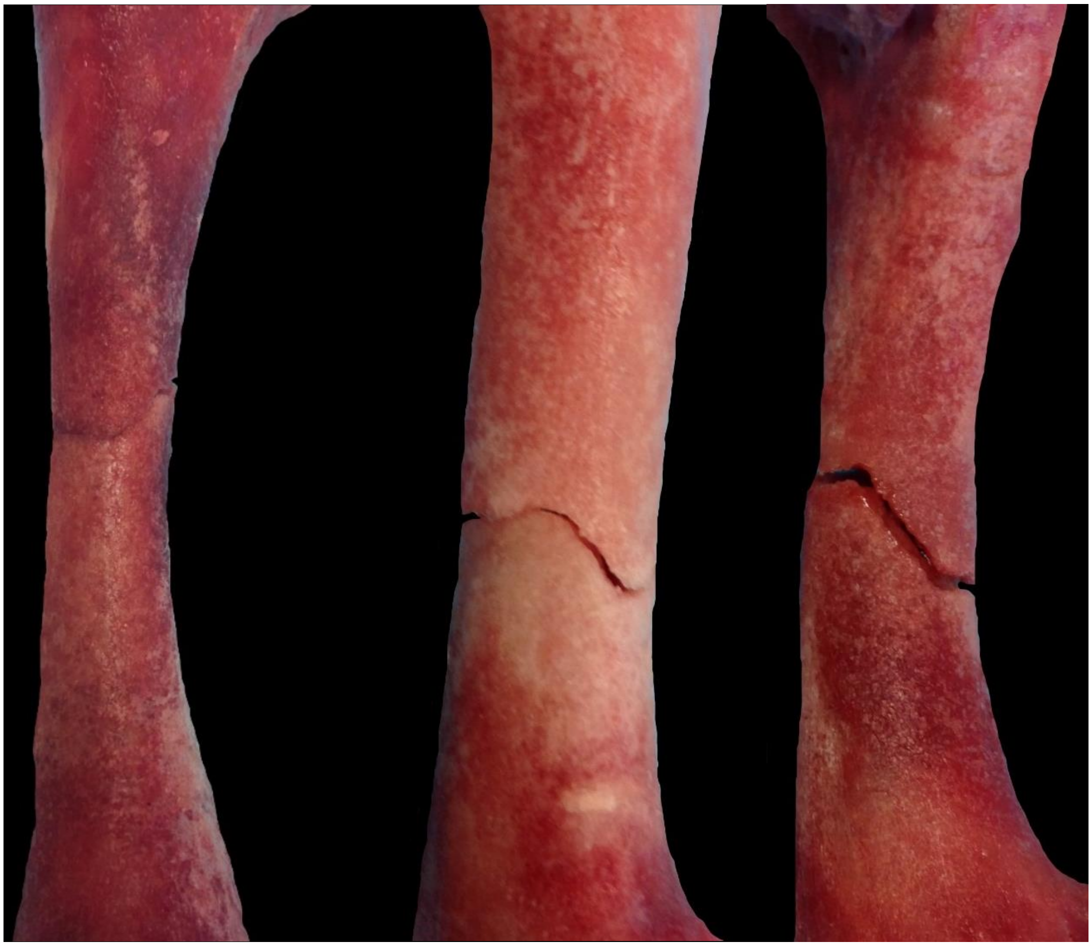

Figure 4.18 *Photographs of specimen representative of variations in the young bone fracture pattern, tested at a low rate of 2 Hz over a 5mm haversine displacement (from left to right; SF1R4B, SF2R4B, and SF5R4B).*

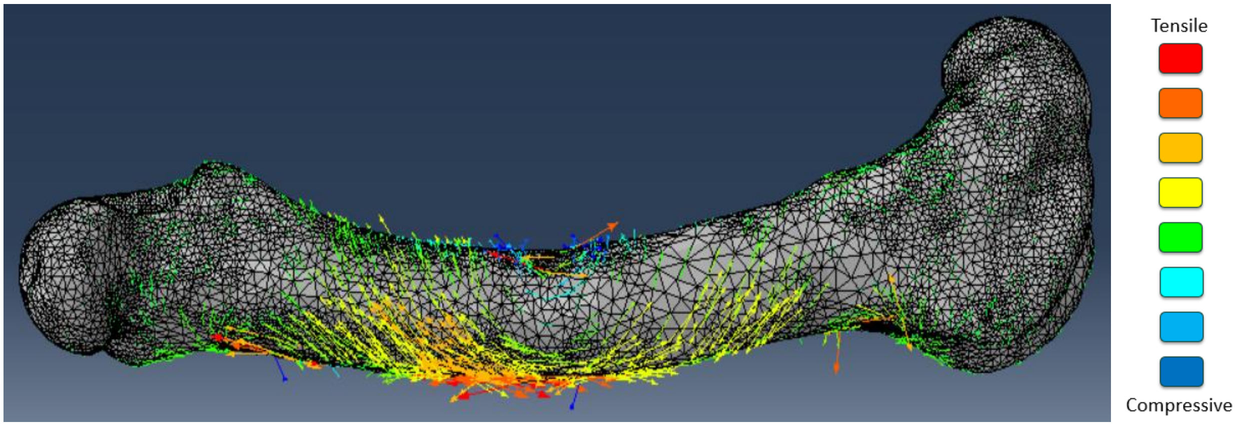

Figure 4.19 *Maximum principal stress distribution, typical 3-point bending*

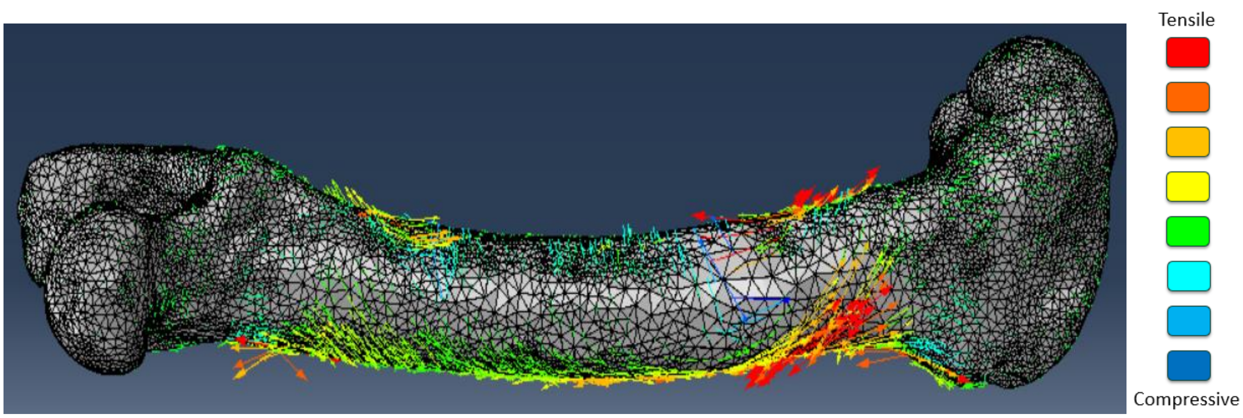

Figure 4.20 *Maximum principal stress distribution, typical 4-point bending.*

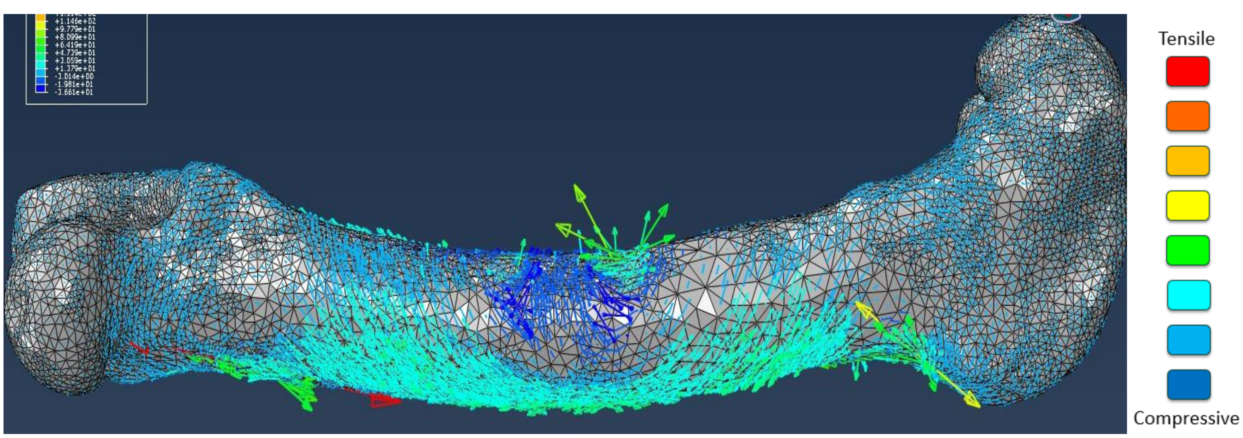

Figure 4.21 *Maximum principal stress distribution, Martens-type 4-point bending.*

Table 4.1. *Summary table of raw experimental data*

Specimen Name	Group	Wedge Type	Bone Length	Inner Length (Li)	outter length (Lo)	Innertia	Max Load	Displacement	Input Energy	Initial Stiffness	Failure Stress	Elastic Modulus	ML OD	AP OD	ML ID	AP ID	ML Thickness	AP Thickness
Units	*young/old*	*fracture pattern*	*mm*	*mm*	*mm*	*mm^4*	*N*	*mm*	*mJ*	*N/mm*	*Mpa*	*Gpa*	*mm*	*mm*	*mm*	*mm*	*mm*	*mm*
SF1L4B	young	Tensile	106.17	10.62	63.70	4678	410	3.64	1038	171	99	0.75	9.55	9.13	6.63	6.85	1.46	1.14
SF2L4B	young	Transverse	82.77	8.28	49.66	4149	865	2.72	1310	339	140	1.13	8.73	9.67	5.59	6.59	1.57	1.54
SF3L4B	young	Tensile	94.57	9.46	56.74	4410	777	3.10	1610	373	147	1.25	8.85	9.07	4.97	5.47	1.94	1.80
SF4L4B	young	Transverse	103.14	10.31	61.88	5934	369	4.39	877	87	63	0.40	9.99	9.95	7.05	6.75	1.47	1.60
SF5L4B	young	Tensile	90.76	9.08	54.46	4664	575	4.87	1695	211	87	0.49	9.01	10.30	6.15	6.86	1.43	1.72
SF1R4B	young	Transverse	107.00	10.70	64.20	4007	465	3.80	1149	160	110	0.97	8.89	8.83	5.95	5.23	1.47	1.80
SF2R4B	young	Transverse	75.27	7.53	45.16	5088	795	2.32	937	369	105	0.75	8.96	10.00	5.16	5.20	1.90	2.40
SF3R4B	young	Transverse	94.10	9.41	56.46	4771	723	3.16	1423	332	129	1.04	9.02	9.33	5.62	4.35	1.70	2.49
SF4R4B	young	Transverse	104.37	10.44	62.62	5314	408	4.23	1163	142	75	0.54	9.41	9.72	6.05	6.02	1.68	1.85
SF5R4B	young	Tensile	94.10	9.41	56.46	5936	463	4.09	1074	119	69	0.41	9.36	10.28	5.42	5.48	1.97	2.40
Young Bone Low Rate Means	***young***	**-**	***95.23***	***9.52***	***57.14***	***4915***	***585***	***3.63***	***1228***	***230***	***102***	***0.74***	***9.18***	***9.63***	***5.86***	***5.88***	***1.66***	***1.87***
AbeL12_10_14_4B_High Rate	old	oblique	207.15	20.72	124.29	179009	4290	1.46	2675	3433	91	3.79	22.9	24.72	15.56	18.3	3.67	3.21
AbeR12_10_14_4B_High Rate	old	Tensile	207.23	20.72	124.34	167422	3958	1.24	1449	4284	144	4.41	22.62	24.19	15.52	17.87	3.55	3.16
ClaudeL12_10_14_4B_High Rate	old	oblique	205.23	20.52	123.14	172367	3595	2.39	3231	2495	68	1.96	22.29	26.94	15.63	20.66	3.33	3.14
Old Bone High Rate Means	***old***	**-**	***206.54***	***20.65***	***123.92***	***173162***	***3948***	***1.70***	***2452***	***3404***	***101***	***3.08***	***22.60***	***25.28***	***15.57***	***18.94***	***3.52***	***3.17***
BettyL12_10_4B	old	Reverse Tensile	219.00	21.90	131.40	164953	3649	1.86	3090	2447	110	3.25	22.9	23.93	16.34	17.73	3.28	3.1
DorisL12_10_14_4B	old	Reverse Tensile	222.00	22.20	133.20	163700	4054	1.82	3215	2601	116	3.87	22.31	24.72	15.33	18.34	3.49	3.19
ErnestL12_10_14	old	Reverse Tensile	232.00	23.20	139.20	204692	5073	2.85	5524	2557	142	2.82	24.37	25.12	17.57	18.98	3.4	3.07
Lindy_5_28_15_4B	old	Reverse Tensile	209.15	20.92	125.49	190617	5280	2.07	5863	3040	128	3.18	23.63	25.23	17.09	18.07	3.27	3.58
Ryan_5_28_15_4B	old	Reverse Tensile	208.89	20.89	125.33	135157	3399	1.47	2291	2638	116	4.05	22.08	22.9	16.22	17.44	2.93	2.73
Shelby_5_28_15_4B	old	Reverse Tensile	208.85	20.89	125.31	177877	3469	1.25	2095	3029	98	3.70	23.81	24.76	17.77	19.2	3.02	2.78
Zach_5_28_15_4B	old	oblique	208.63	20.86	125.18	168015	4354	1.99	3325	3083	120	3.07	22.91	24.22	16.31	17.82	3.3	3.2
Old Bone Low Rate Means	***old***	**-**	***215.50***	***21.55***	***129.30***	***171484***	***4183***	***1.90***	***3629***	***2771***	***119***	***3.34***	***23.14***	***24.41***	***16.66***	***18.23***	***3.24***	***3.09***

REFERENCES

REFERENCES

Beaupied H, Lespessailles E, and Benhamou C. Evaluation of macrostructural bone biomechanics. *Joint Bone Spine*. 2007; 74:233-239.

Chen W. Plasticity in reinforced concrete. J. Ross Publishing, 2007. ISBN 1932159746.

Cheong VS, Karunaratne A, Amis AA, and Bull AMJ. Strain rate dependency of fractures of immature bone. *J Mech Behav Biomed Mater*. 2017; 66:68-76.

Christoforo AL, Lahr FAR, Morales EAM, Panzera TH, and Borges PHR. Numerical evaluation of longitudinal modulus of elasticity of eucalyptis grandis timber beams. *J Agric For*. 2012; 2(4):166-170.

Diab T, Condon KW, Burr DB, and Vashishth D. Age-related change in the damage morphology of human cortical bone and its role in bone fragility. *Bone*. 2006; 38:427-431.

Ebacher V, Tang C, McKay H, Oxland TR, Guy P, and Wang R. Strain redistribution and cracking behavior of human bone during bending. *Bone*. 2007; 40:1265-1275.

Gardener MP, Chong ACM, Pollock AG, and Wooley PH. Mechanical evaluation of large-size fourth-generation composite femur and tibia. *Ann Biomed Eng*. 2010; 38(3):613-620.

Gosman JH, and Shaw CN. Development of cortical bone geometry in the human femoral and tibial diaphysis. *Anat Rec*. 2013; 296:774-787.

Isa M, Fenton TW, Deland T, and Haut RC. Fracture characteristics of fresh human femora under controlled three-point bending. Proceedings of the American Academy of Forensic Sciences, 67th Annual Scientific Meeting, Orlando, FL. 2015.

Kress TA. Impact biomechanics of the human body [dissertation]. Knoxville (TN): Univ. of Tennessee, 1996.

Lanyon LE, Magee PT, and Baggott DG. The relationship of functional stress and strain to the processes of bone remodeling. An experimental study on the sheep radius. *J. Biomech*. 1979; 12:593-600.

Levine RS. An introduction to lower limb injuries. In: biomechanics and medical aspects of lower limb injuries. Warrendale, Pa: *Society of Automotive Engineers*, Inc; 1986:23-32.

Martens M, Van Audekercke R, De Meester P, and Mulier JC. Mechanical behavior of femoral bones in bending loading. *J Biomechanics*. 1986; 19(6):443-454.

Nalla RK, Stölken JS, Kinney JH, and Ritchie RO. Fracture in human cortical bone: local fracture criteria and toughening mechanisms. *J Biomech*. 2005; 38:1517-1525.

Passalacqua NV, and Fenton TW. Developments in skeletal trauma: blunt-force trauma. In: Dirkmaat D, editor. A companion to forensic anthropology. Chichester, West Sussex, U.K.: John Wiley & Sons Ltd, 2012;400–12.

Pierce MC, Bertocci GE, Vogeley E, and Moreland MS. Evaluationg long bone fractures in children: a biomechanical approach with illustrative cases. *Child Abuse Negl*. 2004; 28(5):505-24.

Porta D (2005). Biomechanics of impact injury. In forensic medicine of the lower extremity, J. Rich, D. Dean, and R. Powers (Eds.), pp. 279-310.

Quinn GD, Sparenburg BT, Koshy P, Ives LK, Jahanmir S, and Arola DD. Flexural strength of ceramic and glass rods. *J Test Eval*. 2009; 37(3):1-23.

Reber SL, and Simmons T. Interpreting injury mechanisms of blunt force trauma from butterfly fracture formation. *J Forensic Sci*. 2015; 60(6):1401-1411.

Rusmee P. High Strength Composites 1998-2005, webpage University of Utah, Department of Mechanical Engineering: http://www.mech.utah.edu/~rusmeeha/labNotes/composites.html

Turek, Samuel L. Turek's Orthopaedics : Principles and Their Application. Philadelphia :Lippincott, 1994.

Vaughan PE, Wei F, and Haut RC. Age effects on bending fracture patterns in ovine femora. Proceedings of the American Academy of Forensic Sciences, 69th Annual Scientific Meeting, New Orleans, LA. 2017.

Vaughan PE, Wei F, and Haut RC. Specimen age affects the fracture pattern of immature porcine femurs under torsional loading. Proceedings of the American Academy of Forensic Sciences, 68th Annual Scientific Meeting, Los Vegas, NV. 2016.

Wieberg D, and Wescott DJ. Estimating the timing of long bone fractures: correlation between the postmortem interval, bone moisture content, and blunt force trauma fracture characteristics. *J Forensic Sci*. 2008; 53(5):1028-1034

Zimmerman E, Launey ME, Barth HD, and Rithcie RO. Mixed-mode fracture of human cortical bone. *Biomaterials*. 2009; 30:5877-5884.

CHAPTER FIVE: CONCLUSIONS

OVERVIEW

From the study of Murphy et al., 2015, questions arose regarding the authors proposed fracture ratio as a means of interpreting the spiral fracture pattern under abusive and accidental-type injury scenarios. It became evident that the authors case-based study may have been indirectly influenced by specimen age. In the case-based study of Murphy et al., 2015 the mean age for abuse victims was, on average, lower than the mean age of the accidental victims. While noted in the study, however, age was not a statistically significant factor. The work of Theobald et al., 2012 also raised further questions about the Murphy et al., 2015 study, as the authors demonstrated that an increased loading rate significantly decreased the spiral fracture angle. While the Theobald et al., 2012 study did not consider varying specimen age, it provided a significant indicator that the Murphy et al., 2015 study may have been biased due to the types of loading scenarios classified as accidental and abuse. A correspondence with the authors in the Murphy et al., 2015 study uncovered that many accidental injuries of the femur were the result of motor-vehicle accidents or falls from heights, which likely produce high rates of loading scenarios. Experimental results using the porcine femora under torsion in the current study have demonstrated that both specimen age and loading rate are influential factors on the fracture ratio. Therefore, in future work, it is paramount that these factors be considered when evaluating spiral fracture patterns.

Potential age and rate effects were not just limited to torsional fracture patterns, but also appeared to influence bending fracture patterns in the literature as well. Martens et al., 1986 demonstrate near-exclusive reverse tensile wedge patterns (compressive wedge patterns) in studies using the human femur. Cheong et al., 2017, while not testing under Martens-type loading conditions, was able to produce exclusive transverse fractures under typical four-point bending in 5-month-old sheep. Interestingly, as the loading rate was increased in the study, the pattern of fracture changed into the oblique fracture pattern, and even a tensile wedge pattern was produced for younger aged specimens. It therefore became forensically relevant not only to test how/why the compression wedge was produced under Martens-type loading of long bones, but also to see what effects, if any, specimen age and loading rate might have under this special loading configuration.

The first hypothesis of this thesis work was that material parameters would change with developmental age in the porcine model, and that these will in turn influence the resultant fracture pattern in the femur. This was investigated by performing direction-specific tensile and shear tests over a range of immature specimens. Testing of these parameters against development in days was performed to demonstrate how the longitudinal and transverse parameters change throughout early development of the immature, porcine femur. The goal was to utilize these aggregate material parameters to aid in an interpretation at the mechanical level, addressing the question of why the gross-scale fracture pattern was altered with specimen age under torsional loading, when tested at the whole-bone level using the immature porcine model.

The second hypothesis of the current research was to address how the material properties are impacted by loading rate in the transverse and longitudinal directions. The goal once more was to utilize these aggregate material parameters to aid in the interpretation at the mechanical level, addressing the question of why the gross-scale fracture pattern is altering with loading rate under torsion, when tested at the whole-bone level using the immature porcine model.

The final hypothesis of the current research was that Martens-type loading is a special loading scenario that also is influenced by specimen age and loading rate. The goal of this study was to provide pilot work demonstrating that under Martens-type loading, young specimens would not generate compression wedge failures, and that the compressive wedge pattern would be produced under low-rate loading in mature specimen.

CHAPTER 2

Chapter 2 was an experimental study which tested whole, intact immature porcine femora of varying developmental age under rate-controlled torsional loading. The purpose of this study was to test the validity of the fracture ratio proposed by Murphy et al., 2015, while additionally addressing what effects developmental age and loading rate may have on the fracture pattern (fracture ratio). Results of this study showed that both specimen age and rate of twist were significant factors influencing fracture ratio in immature specimen. Interestingly, at lower rates, the pattern of fracture transitioned from a high-angle fracture in the young group, to a combination of both low-angle and horizontal failure segments in the older group when measured from the longitudinal axis. At higher rates the fracture pattern rapidly transitioned from low-angle failure, to very low angle tensile failure, with horizontal elements and increased comminution as specimen age increased. In summary, the study documented that fracture ratio was significantly dependent on both specimen age and rate of twist, using the infant porcine femur model, with low rates of twist consistently producing lower fracture ratios than those shown under high rates of twist. While both an accidental and abusive act may produce spiral fractures, the results of the current study would not help determine intent. This study does, however, provide experimental 'ground-truth' data that may help forensic biomechanists and anthropologists draw conclusions surrounding the circumstances of an injury, which in turn may help in the evaluation of 'truth of testimony' during criminal litigations. As such the current study, while limited to using the infant porcine model, might suggest additional clinical studies utilizing more specimens over a pediatric age range with a stratification by loading rate, may be needed before fracture ratio alone should be utilized for the determination of accidental versus abusive pediatric trauma.

CHAPTER 3

Chapter 3 was an experimental study which tested cortical bone segments of the immature porcine femur, shaped into notched and dog-bone specimens oriented in the longitudinal and transverse directions along the bone. The purpose of this study was to test the effects of specimen age and loading rate against calculated material parameters under tensile and shear testing. Results of the study indicated that at both low and high rates of loading, the longitudinal shear strength decreased with specimen age. Interestingly, the longitudinal shear strength from birth was initially stronger than the transverse shear strength, becoming weaker than the transverse shear strength at a critical age of approximately 7 days of development for low rate tests, and approximately 4.5 days of development for high rate tests. Prior to this critical age in development, the transverse shear strength is weaker than the longitudinal shear strength, allowing for deviations from the mechanically preferred mode of failure under tension, allowing energy to be dissipated via crack failure through osteons (resulting in a low fracture ratio/high fracture angle). After this critical age the longitudinal shear strength became weaker than the transverse shear strength, allowing for deviations from the mechanically preferred mode of failure under tension, by allowing energy to be dissipated by crack failure along the cement interface between osteon, longitudinally (resulting in a high fracture ratio/low fracture angle). This information supported the notion that three are three types of spiral fracture modes. Below the critical age, a combined transverse shear and tensile failure mode, within the critical age, a purely tensile mode of failure due to equal parts longitudinal and transverse shear failure along the line of maximum principal stress, and after the critical region, a combined tensile and longitudinal mode of failure. Future work towards mechanistically explaining why the torsional spiral fracture pattern changes with specimen age and rate first and foremost should utilize a larger bone model, as curvature effects with specimen age may have influenced the results of the study. Furthermore, biological studies such as osteon population density and mineral density should be studied in comparison with specimen age, as these parameters influence the basic structural characteristics of bone as it develops into a maturity. Finally, tensile tests should be conducted at incremental angles from 0 to 90 degrees to test if the weakest composite plane in tension is altering with specimen age and loading rate. It would be useful to create a theoretical model using equations from linear elasticity to validate such work.

CHAPTER 4

Chapter 4 was an experimental study which tested whole and intact sheep femora under concentrated four-point bending to simulate the loading conditions of Martens et al., 2015 using mature and immature specimens. Additionally, a basic finite element model was developed to investigate what the potential principal (tensile) stress distribution looks like under the experimentally tested Martens-type loading, compared to the stress distributions formed under a typical 3-point bending configuration and under a typical 4-point bending configuration. Computational models were generated to match specimen geometry by creating volumetric meshes based on CT images of a young and older test specimen. The two-fold purpose of this work was to first, to determine the effect of age on the pattern of femur fracture using a Martens-type loading configuration. Secondly the study was to investigate how the stress distribution generated under the Martens-type loading condition differed from the traditional 3-point and 4-point bending tests used in traditional studies in the biomechanical and forensic fields. Results of the study indicated that in mature specimens tested under a Martens-type bending configuration, there is a near-exclusive production of compression wedge fracture patterns when tested at low rates. Furthermore, immature specimens tested at low rates under a Martens-type configuration appeared to commonly produce transverse fracture patterns, or incipient tensile wedge patterns. Interestingly, in this pilot study the preliminary results from mature bone specimens tested under Martens-type loading at high rates demonstrated that non-compressive wedge patterns (oblique and tensile wedge patterns) can be produced. These data suggested that the compressive-wedge pattern may be rate-sensitive, as well as age-sensitive. The experimental portion of this study demonstrated that specimen age does indeed affect the resultant fracture pattern under concentrated, four-point bending, and provides preliminary framework indicating that loading rate may also influence the fracture pattern under Martens-type conditions.

From the computational work of this study, specimen-specific models appeared to correspond well with their experimental counterparts for both young and old specimens. Interestingly, when testing mature bones at low loading rates the stress distribution was shown to markedly change between 3-point bending, 4-point bending, and Martens-type bending scenarios. These modeling studies demonstrated that each loading type generated unique stress patterns. Typical 3-point bending produced high tensile stresses under the point of impact on the non-loading side of the bone, in addition to large compressive stress on the loading side of the bone, correlating well with the typical tensile wedge fracture pattern, assuming wedge fractures due to shear in the compression side of the bone as suggested in the biomechanical literature. Typical 4-point bending produced large tensile stresses just outside each of the loading points on the loading side of the bone, in addition to large tensile stresses observed just outside each of the supports on the non-loading side of the bone. This stress distribution indicated possibly two zones of failure that likely may correlate well to the typical segmental fragment pattern associated with standard 4-point bending. Most notedly, the Martens-type loading appeared to act as a unique, and novel combination of both 4-point and 3-point bending stress distributions. For Martens-type bending, large tensile stresses were noted just outside the outer supports like that shown in typical 4-point bending, with large compressive stresses generated under the inner loading probes, typical to that observed under three-point bending. Interestingly, there are also small tensile stresses generated underneath the inner probe loading points on the surface of the bone. The stress distribution appeared to correlate well with the compression wedge fracture pattern.

While more testing needs to be performed to verify potential rate effects under Martens-type four-point loading, it may be suggested from the Cheong et al., 2017 study of immature specimen, and from the limited number of mature specimen tested in the current work under a high loading rate, that both younger and older specimens may be more inclined to produce the typical tensile wedge fracture pattern under Martens-type loading. In future work it should be paramount to stratify the four standardized fracture patterns of tensile/compression wedges, segmental fragments, and transverse fractures by developmental age of occurrence, under what loading speeds they can be generated, and at what percentage of loaded bone length the four patterns can be generated under four-point bending and/or 3-point bending.

APPENDIX

PUBLICATIONS

Vaughan P, Vogelsberg C, Vollner J, Fenton, Haut R: The Role of Interface Shape on the Impact Characteristics and Cranial Fracture Patterns Using the Immature Porcine Head Model. J Forensic Sci 2016; 61(5)1190-7

Vaughan P, Orth MW, Haut RC, Karcher DM: A method of determining bending properties of poultry long bones using beam analysis and micro-CT data. J Poultry Sciences 2016; 95(1):207-12

Vaughan P, Wei F, Haut R: The Effect of Specimen Age and Speed of Torsion on Fracture Patterns of the Immature Porcine Femur. J Biomech Eng, In Review

PRESENTATIONS

Vaughan P, Wei F, and Haut R: Age effects on bending fracture patterns in ovine femora. Proceedings of the 69th annual scientific meeting of the American Academy of Forensic Sciences, New Orleans, Louisiana, D3:629, 2017

Vaughan P, Wei F, and Haut R: Specimen age affects the fracture pattern of immature porcine femurs under torsional loading. Proceedings of the 68th annual scientific meeting of the American Academy of Forensic Sciences, Las Vegas, Nevada, D3:453, 2016

ABSTRACTS

Goots A, Isa M, Fenton TW, Watson E, **Vaughan P**, Wei F, and Haut R: Estimating points of impact in multiple blunt force cranial trauma: lessons from experimental impacts. Proceedings of the 70th annual scientific meeting of the American Academy of Forensic Sciences, Seattle, Washington, 2018, In Review

Isa M, Fenton TW, Goots A, Watson E, **Vaughan P**, Wei F, and Haut R: Initiation and propagation of fractures in blunt impacts to minimally-constrained human cadaver heads. Proceedings of the 70th annual scientific meeting of the American Academy of Forensic Sciences, Seattle, Washington, 2018, In Review

Watson E, Fenton TW, Isa M, Goots A, Watson E, **Vaughan P**, Wei F, and Haut R: The influence of implement shape on fracture pattern and defect size in experimental blunt cranial impacts. Proceedings of the 70th annual scientific meeting of the American Academy of Forensic Sciences, Seattle, Washington, 2018, In Review

Isa M, Fenton TW, **Vaughan P**, and Haut R: Understanding the role of contact area in adult cranial fracture variation. Proceedings of the 68th annual scientific meeting of the American Academy of Forensic Sciences, Las Vegas, Nevada, A78:131, 2016

Vollner J, Vogelsberg CM, **Vaughan P**, Fenton TW, Clark SC, and Haut R: The interpretation of human pediatric cranial fracture patterns using experimentally generated porcine ground-truth data. Proceedings of the 68th annual scientific meeting of the American Academy of Forensic Sciences, Las Vegas, Nevada, A76:128, 2016

Fenton TW, Isa M, **Vaughan P**, and Haut R: Experimental and computational validations of the initiation and propagation of cranial fractures in the adult skull. Proceedings of the 67th annual scientific meeting of the American Academy of Forensic Sciences, Orlando, Florida, A100:180, 2015

Vogelsberg CM, **Vaughan P**, Fenton TW, and Haut R: A forensic pathology tool to predict pediatric skull fracture patterns: Part V. Proceedings of the 67th annual scientific meeting of the American Academy of Forensic Sciences, Orlando, Florida, A99:178, 2015